# *The*
# PHILOSOPHICAL MAGAZINE

FIRST PUBLISHED IN 1798

L. 46 SEVENTH SERIES No. 379 August 1955

## *A Journal of Theoretical Experimental and Applied Physics*

UNIVERSITY OF HAWAII
LIBRARY
SEP 30

EDITOR
PROFESSOR N. F. MOTT, M.A., D.Sc., F.R.S.

EDITORIAL BOARD
SIR LAWRENCE BRAGG, O.B.E., M.C., M.A., D.Sc., F.R.S.
SIR GEORGE THOMSON, M.A., D.Sc., F.R.S.
PROFESSOR A. M. TYNDALL, C.B.E., D.Sc., F.R.S.

PRICE 15s. 0d.
Annual Subscription £8 0s. 0d. payable in advance

D AND PUBLISHED BY TAYLOR & FRANCIS LTD., RED LION COURT, FLEET ST., LONDON, E.C.4

***New Journal Announcement***

JOURNAL OF

**ELECTRONICS**

A "PHILOSOPHICAL MAGAZINE" ASSOCIATED JOURNAL

*Editor:* J. THOMSON, M.A., D.Sc., M.I.E.E., F.Inst.P.
*Consultant Editor:* PROFESSOR N. F. MOTT, F.R.S.

CONTENTS—NO. 1, JULY 1955

On the Initial Space Charge Distribution in a Cylindrical Magnetron Diode. By R. Q. TWISS (*Services Electronics Research Laboratory, Baldock, Herts.*).

The Space Charge Distribution in the Pre-Oscillation Magnetron. By L. E. S. MATHIAS (*Services Electronics Research Laboratory, Baldock, Herts.*).

Theory of the Preoscillating Magnetron. By D. GABOR (*Imperial College, London*) and G. D. SIMS (*Imperial College and General Electric Company, Wembley*).

Factors in the Design of Power Amplifiers for Ultra High Frequencies. By J. DAIN (*English Electric Valve Co., Chelmsford, Essex*).

Some Experiments on a Cylindrical Electron Beam Constrained by a Magnetic Field. By J. D. LAWSON (*Atomic Energy Research Establishment, Harwell, Berks.*).

On the Solution of an Equation of Electron Optics. By B. MELTZER (*The Clock Tower House, Maidenhead Road, Windsor, Berks.*).

Note on Moving Striations. By V. D. FARRIS (*Physics Department, Queen's University, Belfast*).

A Review of the Structure and some Magnetic Properties of Ferrites. By L. C. F. BLACKMAN (*Services Electronics Research Laboratory, Ext., Harlow, Essex*).

Recent Research with an Experimental Mass Spectrometer. By G. P. BARNARD (*National Physical Laboratory, Teddington*).

6 parts per volume—£1-0-0 per part
Subscription price per volume £5-10 *post free*, payable in advance

*Publishers*
TAYLOR & FRANCIS, LTD
RED LION COURT, FLEET STREET, LONDON, E.C.4

# XCII. *Impurity Diffusion in Polar Crystals*

By A. B. Lidiard
Atomic Energy Research Establishment, Harwell Berks.*

[Received March 23, 1955]

## Abstract

A theoretical discussion of the diffusion of divalent impurities in polar crystals of the NaCl-type is given with the aid of the Stasiw–Teltow association model. It is shown how accurate measurements of the impurity diffusion coefficient can yield fundamental information about the existence and concentration of impurity–vacancy pairs (' complexes ') in a simple and direct manner. Such measurements would therefore provide a valuable addition to the studies of ionic crystals already made of their ionic conductivity, dielectric loss, etc. The main restriction of the present theory is that the impurity–vacancy complexes should have a mean lifetime which is long compared with the mean jump times which govern their changes of position and orientation.

## § 1. Introduction

A knowledge of the properties of defects in ionic solids is essential to the understanding of a wide range of physical and chemical phenomena (e.g. colour centres and oxidation of metals and alloys). The absence of complications such as electronic conductivity in crystals like NaCl and AgBr has permitted the extensive study of their lattice defects (cf. Seitz 1951, 1954), and the possibility of forming substitutional solutions with for example $CaCl_2$ has allowed the study of systems containing constant controlled numbers of vacancies present in much greater concentrations than the intrinsic or thermal defects. This useful fact results from the condition of electroneutrality, which requires that every $Ca^{2+}$ ion dissolving substitutionally in the NaCl lattice, be accompanied somewhere by a $Na^+$ vacancy. The solution of, say, $AlCl_3$ in a similar way would introduce two $Na^+$ vacancies for every $Al^{3+}$ ion.

Unfortunately, however, these solid solutions are not as simple as appears at first sight, owing to the long range Coulomb interactions existing between the unbalanced charges on the impurities and the vacancies. This system of impurities and vacancies dispersed throughout an otherwise perfect crystal forms a sort of electrolyte solution rather than an ideal mixture. For the statistical description of these systems one has available on the one hand the theories of ' strong ', i.e. totally

---

* Communicated by the Author.

dissociated, electrolytes (e.g. the Debye and Hückel (1923) theory; general references are Falkenhagen (1934) and Harned and Owen (1950)), and on the other the 'weak' electrolyte theories which describe the state of the system in terms of the numbers of opposite 'charges' (i.e. impurity and vacancy) which are associated into pairs. In the case of divalent impurity ions in 1 : 1 salts these pairs are electrically neutral and do not contribute to the ionic conductivity*.

The simplest form of the weak electrolyte theory, in its application to the present problem, was given by Stasiw and Teltow (1947); it neglects the long range interactions between the unassociated impurities and vacancies and in the limit of high temperatures goes over into the theory of an ideal solid solution. In effect, it treats the equilibrium existing between the associated pairs and the unassociated vacancies and impurities as an equilibrium for a reversible chemical reaction; the associated pairs, or complexes as they are often called, are treated like dissociating diatomic molecules. Detailed applications of this approach have been made among others by Teltow (1949, for $AgBr+CdBr_2$), Etzel and Maurer (1950, for $NaCl+CdCl_2$), Stasiw (1952, for silver halides$+Ag_2S$) and by Haven (1953, for $NaCl+CaCl_2$ and $MnCl_2$). An extension of the theory so as to include the effects of the long range interactions has been given and applied to the $NaCl+CdCl_2$ system (Lidiard 1954).

In general one would expect the association theory to give a better approximation to these crystal systems than the 'strong', i.e. totally dissociated, electrolyte theories. Thus it is known that salts such as KCl which are 'strong' electrolytes when dissolved in water (dielectric constant $\sim 80$), must be regarded as only 'weak' electrolytes when dissolved in solvents of much lower dielectric constant. We would therefore expect to find a similar situation existing within the solids themselves since their dielectric constants are not large.

Granted that appreciable association does occur between impurities and vacancies we must next consider how to obtain the *degree* of association from experimental data. This information can be obtained indirectly from studies of ionic conductivity (d.c.) as a function of temperature and impurity content. More immediate information can be obtained from alternating current studies since the dipolar nature of the complexes gives rise to a characteristic Debye-type loss proportional to their concentration (Haven 1953, Lidiard 1955). A third method which is discussed in the present paper is the study of the diffusion of the impurities themselves. For the case where the mean lifetime of the complexes is much greater than the mean times characterizing the re-orientation jumps, we show that measurements of impurity diffusion can provide direct information about the degree of association as function of impurity concentration and temperature. Indeed it would seem strange if this were not so, since the impurity ions are only in a position to move when there is a vacancy adjacent to them, i.e. when they are in an associated condition. However, when the lifetime of the complexes is relatively short the results are in general more complicated and appear difficult to apply at the present time.

---

* This would not be true in the case of a pair formed from a trivalent cation, e.g. $Fe^{3+}$ and a $Na^+$ vacancy since here the net charge is positive. Thus Kelting and Witt (1949) in their experiments on KCl found that $Ca^{2+}$ additions were not removed electrolytically although an appreciable fraction of the background impurity in the "pure" KCl crystals was removed in this way (presumably polyvalent ions).

A previous theoretical treatment of the subject of diffusion of impurities in simple polar crystals by Schöne, Stasiw and Teltow (1951), we believe to be incorrect. Our principal objections are to their use of a diffusion coefficient for *unassociated* impurity ions and to their neglect of the dynamical association–dissociation equilibrium between the complexes and the unassociated vacancies and impurities. As noted above it is obvious that at any instant the only impurity ions free to move are those which are associated with vacancies at that instant. Therefore provided we take adequate account of the dissociation–association ‘ reaction ’ and provided we correctly describe the motion of the complexes, we have the basis of a correct calculation.

In the present paper we derive our principal results in a plausible elementary manner (§ 2) and discuss their implications (§§ 3, 4). The dependence of the diffusion coefficient on temperature and concentration is shown both analytically and graphically. In a subsequent paper we shall supply the full rigorous kinetic derivation of the general equations.

## § 2. IMPURITY DIFFUSION COEFFICIENT, $D(c)$

In the following calculation we have a definite steady state situation in mind. We suppose that we have a mixed crystal, e.g. NaCl containing a mole fraction, $c$, of $CdCl_2$, set between a source and a sink of the impurity and across which there is a small steady gradient of impurity concentration, $dc/dx$. We further imagine that our crystal is in the shape of a right cylinder so that the problem is one-dimensional. Corresponding to the concentration gradient there will be small steady current of impurity ions $J$ (number of ions per cm² per sec) given by Fick's law

$$J=-D(c)\frac{d}{dx}(N_+c) \quad . \; . \; . \; . \; . \; . \; . \quad (2.1)$$

where $N_+$ is the number of cation sites per cm³. The diffusion constant $D(c)$ is a function of the crystal composition. By using the Stasiw and Teltow (1947) association theory we shall calculate $D(c)$ as a function of $c$ for the case of divalent additions. For definiteness we shall restrict ourselves to crystals of the NaCl type where the cation sublattice is face centred cubic.

When the molar impurity concentration is $c$ let the number of impurity ions per cm³ be $N_i$; then $N_i=N_+c$. Of these let $n$ be associated with vacancies. Since we shall assume sufficient impurity for the thermal defects to be negligible it follows that there are $N_i-n$ unassociated impurity ions and $N_i-n$ unassociated vacancies. If local equilibrium of the association–dissociation reaction is maintained then (Lidiard 1954)

$$\frac{N_+ n}{(N_i-n)^2}=12\exp(\Delta G/\boldsymbol{k}T), \quad . \quad . \quad . \quad . \quad . \quad . \quad (2.2)$$

where the factor 12 comes from the orientational entropy of the complexes. $\Delta G$ is the Gibbs free energy of association and $\boldsymbol{k}$ is Boltzmann's constant. We shall return to this equation later.

When we now consider the impurity diffusion we see at once that on the vacancy diffusion model the unassociated impurity ions are unable to move. Also the unassociated vacancies are prevented from diffusing to a region of lower impurity content by the Nernst diffusion potential which arises from the immobility of the oppositely charged impurity ions (see e.g. Denbigh 1951, especially § 5.3). Hence in calculating the impurity diffusion we need to consider only the independent, random motions of the complexes.

For simplicity let us study diffusion along a [100] direction in a cylindrical crystal of cross section 1 cm$^2$. (NaCl-type crystals, being cubic, display isotropic diffusion properties so our choice of the [100] direction will not restrict our results.) A single lattice plane perpendicular to the diffusion direction may then be regarded as occupying a volume $a$ cm$^3$ where $a$ is the smallest anion–cation separation. Hence this plane will contain $a\,n$ associated impurity ions, i.e. $a\,n$ complexes with the impurity end in the plane $x=0$. One-third of these will have the vacancy located in the forward neighbouring plane ($x=a$). At any instant only complexes with this orientation are in a position to contribute to the forward diffusion of impurities. Likewise the only complexes able to contribute to diffusion backwards into the plane $x=0$ are those with impurity at $x=a$ and vacancy at $x=0$.

Provided that the continued diffusion of the complexes is not hindered by a very slow motion of the attached vacancy around the impurity ion (see below) the diffusion coefficient can then be calculated very simply in the following manner. Let $w_2$ be the probability per unit time that an impurity ion will exchange places with its associated vacancy. Then the number of impurity ions crossing a mathematical plane set between the planes of atoms $x=0$ and $x=a$ is $a\,n(0)w_2/3$ per cm$^2$ per sec in the forward direction and $an(a)w_2/3$ per cm$^2$ per sec in the backward direction. The net number crossing is therefore

$$J=-\frac{a^2}{3}w_2\left(\frac{dn}{dx}\right)_0 \quad . \quad . \quad . \quad . \quad . \quad . \quad . \quad . \quad (2.3)$$

where we have replaced $n(a)-n(0)$ by $a(dn/dx)$ evaluated at $x=0$. Introducing the *degree* of association $p\equiv n/N_i$ and the fractional molar concentration $c$ we find that a comparison of (2.3) with (2.1) yields

$$D(c)=\tfrac{1}{3}a^2w_2\frac{d}{dc}(pc), \quad . \quad . \quad . \quad . \quad . \quad . \quad . \quad . \quad (2.4)$$

where $p$ is determined as a function of $c$ by (2.2).

Before proceeding to discuss the dependence of $D$ on $c$ we may generalize the constant factor in (2.4). Our elementary discussion has overlooked one important feature of the process of diffusion via complexes; namely that in order to continue its forward diffusion the complex must go through a cycle of orientation changes. Each impurity–vacancy exchange must be followed by two successive forward jumps of the vacancy around the impurity as centre—as it were to reset the complex for a fresh forward jump of the impurity. Hence the probability occurring in (2.4) is the probability of impurity–vacancy exchange only if the speed of the diffusion is not limited by a slow motion of the vacancy around the impurity. The appropriate factor in intermediate cases can only be found rigorously by a full kinetic discussion; such a calculation shows, however, that it is also given correctly by the following plausible argument.

Fig. 1

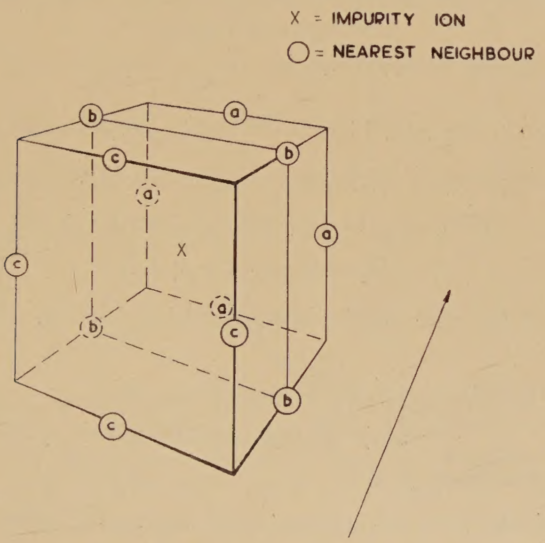

The twelve nearest cation neighbours to an impurity ion ($X$) in a NaCl-type lattice. If the impurity is part of a complex, one of these twelve sites will be vacant. When the diffusion direction defines the $x$-axis as shown, then $a$, $b$ and $c$ represent the planes $x=a$, $x=0$ and $x=-a$. The impurity ion lies at the centre of $x=0$.

We notice that if $w_1$ be the probability per unit time that an associated vacancy will jump from one attached position to another particular attached position, then $2w_1$ is the probability per unit time that an associated vacancy will make one of the necessary forward jumps (say $c$ to $b$ in fig. 1) since there are two distinct ways in which it can do so. Likewise $2w_1$ is the probability for executing the second forward jump necessary for completion of the cycle.

Now in general it is possible to associate with such probabilities a *mean* time which must elapse before the event occurs. Furthermore, the time required is the reciprocal of the corresponding probability. Thus the mean time required for the impurity–vacancy exchange is $w_2^{-1}$. Now it is reasonable to suppose that the mean time required for the performance of several steps is the sum of the mean times for the individual steps. Hence the mean time associated with the cycle of jumps necessary for the continued diffusion of the complexes will be $w_2^{-1}+(2w_1)^{-1}+(2w_1)^{-1}$. The corresponding mean probability is the inverse of this or $w_1w_2/(w_1+w_2)$. It is this mean probability which must be inserted in place of $w_2$ in (2.4), giving

$$D(c)=\frac{a^2}{3}\frac{w_1w_2}{(w_1+w_2)}\cdot\frac{d}{dc}(pc). \qquad . \quad . \quad . \quad . \quad . \quad . \quad (2.5)$$

We observe that when $w_1 \gg w_2$, (2.5) goes over into (2.4) as it must do.

## § 3. Dependence of $D(c)$ on $c$ According to the Stasiw–Teltow Association Theory

Equation (2.2) can be rewritten as

$$\frac{p}{(1-p)^2}=12c\exp(\Delta G/\boldsymbol{k}T)\equiv 12c\exp(-\Delta S/\boldsymbol{k})\,.\,\exp(\Delta H/\boldsymbol{k}T),$$

so that the dependence of $D(c)$ upon $c$ implicit in (2.5) can be expressed by

$$D(c)=D_0\{1-[1+48c\exp(\Delta G/\boldsymbol{k}T)]^{-1/2}\}, \qquad . \quad . \quad (3.1)$$

where

$$D_0=a^2w_1w_2/3(w_1+w_2). \qquad . \quad . \quad . \quad . \quad . \quad . \quad . \quad (3.2)$$

$D(c)$ depends on $c$ as shown graphically in fig. 2. We notice two limiting cases :

(i) $c\exp(\Delta G/\boldsymbol{k}T)\ll 1$, i.e. little association, then

$$D(c)=24D_0c\exp(\Delta G/\boldsymbol{k}T) \qquad . \quad . \quad . \quad . \quad . \quad . \quad (3.3)$$

i.e. $D(c)$ is proportional to $c$.

(ii) $c\exp(\Delta G/\boldsymbol{k}T)\gg 1$, i.e. almost total association, then

$$D(c)\rightarrow D_0,$$

i.e. $D(c)$ tends to a saturation value.

Naturally the practical attainment of saturation is easier at low temperatures, where $\exp(\Delta G/\boldsymbol{k}T)$ is large, than at high temperatures.

The matching of experimental isothermals to eqn. (3.1) is a matter of inferring the unknowns $D_0$ and $\Delta G$. This may be done by inserting into (3.1) corresponding values of $D(c)$ and $c$ at two points and solving the resulting equations for $D_0$ and $\exp(\Delta G/\boldsymbol{k}T)$. Alternatively if the experimental values at low concentrations are sufficiently accurate, in place of one of these equations we can use the simpler relation,

$$24D_0\exp(\Delta G/\boldsymbol{k}T)=\lim_{c\to 0}\frac{dD}{dc} \qquad \text{(cf. eqn. (3.3))}.$$

It is clear that given diffusion isotherms at a number of temperatures we can infer $D_0$ and $\Delta G$ as functions of temperature. Furthermore, since dielectric loss measurements can provide values for $w_1+w_2$ and since $D_0$ immediately enables $w_1w_2/(w_1+w_2)$ to be found, both $w_1$ and $w_2$ can be found separately. Simultaneous diffusion and alternating current studies can therefore in principle, yield $w_1$, $w_2$ and $\Delta G$, i.e. all the relevant parameters for tightly bound complexes.

Fig. 2

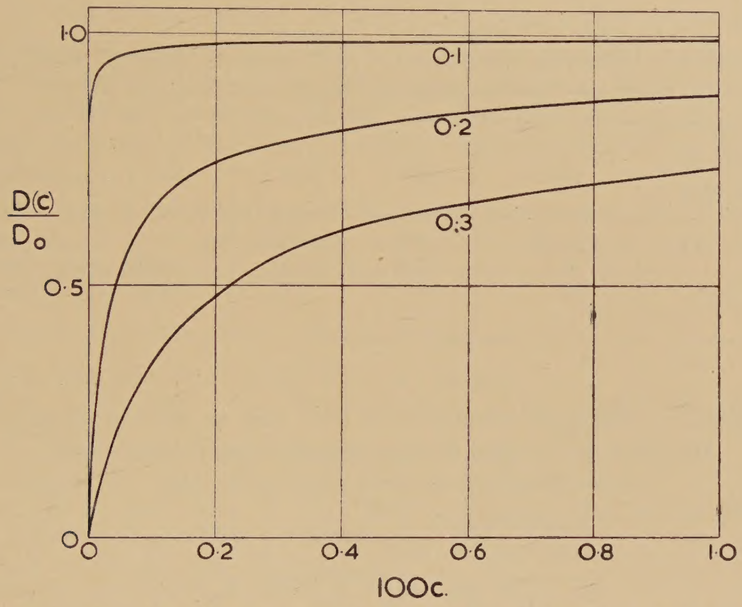

The divalent impurity diffusion coefficient $D(c)$ as a function of the impurity concentration (mole fraction) for three different temperatures. The numbers on the curves represent absolute temperature measured in units of $\Delta G/\boldsymbol{k}$. When $\Delta S=0$ and $\Delta H$ is a constant these numbers are proportional to $T$.

## § 4. AGREEMENT WITH EXPERIMENTAL RESULTS ON IMPURITY DIFFUSION

The only experimental results known to us on the kind of system we have considered are those obtained by Schöne, Stasiw and Teltow (1951) on AgBr containing $CdBr_2$ and $PbBr_2$. These measurements are unfortunately not very exact and are not susceptible to a detailed analysis. As may be seen from tables 1 and 2 the diffusion coefficients which have been obtained are averages over ranges of impurity content. Nevertheless, it is clear that the general trend of these values corresponds with the predictions of our theory, particularly the tendency to saturation at high impurity concentrations. If we interpret the highest $D$ value at each temperature as $D_0$ then we find that the five $D_0$ values for $Cd^{2+}$ can be roughly approximated by the following function of temperature

$$D_0 \sim 0{\cdot}21 \exp(-8300/T) \text{ cm}^2 \text{ sec}^{-1}. \quad . \quad . \quad . \quad (4.1)$$

If we suppose that the barrier height for the jump involving the impurity ion is great owing to its double charge then $w_2 \ll w_1$ and (4.1) and (3.2) give

$$w_2 \sim 7{\cdot}7 \times 10^{14} \exp(-8300/T) \text{ sec}^{-1}$$

for $Cd^{2+}$ in AgBr. However, this result is clearly very uncertain.

Table 1. Diffusion coefficient of $Cd^{2+}$ ions in AgBr in units of $10^{-7}$ cm$^2$ sec$^{-1}$ (after Schöne, Stasiw and Teltow 1951)

| Concentration Interval Mol. % | 400°c | 350°c | 300°c | 250°c | 200°c |
|---|---|---|---|---|---|
| 0 – 0·1 | 0·83 | 0·3 | 0·13 | — | — |
| 0·6 – 1 | 2·4 | 1·3 | 1·0 | 0·26 | 0·05 |
| 2 – 4 | 9 | 7 | 1·1 | 0·28 | 0·05 |

Table 2. Diffusion coefficient of $Pb^{2+}$ ions in AgBr in units of $10^{-7}$ cm$^2$ sec$^{-1}$ (after Schöne, Stasiw and Teltow 1951)

| Concentration Interval Mol. % | 350°c | 200°c |
|---|---|---|
| 0 – 0·1 | 0·2 | 0·1 |
| 0·6 – 1 | 1·0 | 0·1 |
| 2 – 4 | 1·2 | 0·1 |

## § 5. CONCLUSION

We have shown how measurements of the diffusion of divalent impurities in alkali halides, silver halides, etc. can yield direct information about the existence and concentration of the impurity–vacancy complexes employed in the Stasiw–Teltow association model. The dependence of the diffusion coefficient on impurity concentration and on the fundamental parameters of the complexes has been calculated for the case where the complexes are tightly bound, i.e. for the case where their mean lifetime is long compared with the mean jump times involved. This restriction will be removed in a subsequent paper, in which we shall give a full kinetic discussion. However, the results for the case where the complexes are only loosely bound are complicated and do not appear convenient for the quantitative analysis of experimental data.

## ACKNOWLEDGMENTS

This investigation was begun in the first instance at the suggestion of Professor F. Seitz, to whom I am very grateful for his interest and encouragement. Some of the results presented in this paper were obtained while I was at the University of California ; as such the research has enjoyed the partial support of the United States Office of Naval Research and the National Science Foundation.

### *Notes added in proof*

1. Dr. Teltow has pointed out that if the terms involving the diffusion coefficient of the unassociated impurity ions are removed from the Schöne, Stasiw and Teltow theory, the resulting equations are largely equivalent to the equations of the present paper. In particular their eqn. (8) becomes identical with eqn. (2.4) above (J. Teltow, communication to be published in *Phil. Mag.*).

2. The completed investigation of a system of complexes of arbitrary lifetime shows that provided $w_2 \ll w_1$ eqn. (2.4) remains true. In this case the diffusion isothermals are exactly as shown in fig. 2.

## REFERENCES

DEBYE, P., and HÜCKEL, E., 1923, *Phys. Z.*, **24**, 185.
DENBIGH, K. G., 1951, *The Thermodynamics of the Steady State* (London : Methuen).
ETZEL, H. W., and MAURER, R. J., 1950, *J. Chem. Phys.*, **18**, 1003.
FALKENHAGEN, H., 1934, *Electrolytes* (Oxford : University Press).
HARNED, H. S., and OWEN, B. B., 1950, *The Physical Chemistry of Electrolyte Solutions* (New York : Reinhold).
HAVEN, Y., 1953, *J. Chem. Phys.*, **21**, 171.
KELTING, H., and WITT, H., 1949, *Z. Phys.*, **126**, 697.
LIDIARD, A. B., 1954, *Phys. Rev.*, **94**, 29 ; 1955, *Report of the Conference on Defects in Crystalline Solids held at Bristol in July* 1954, p. 283.
SCHÖNE, E., STASIW, O., and TELTOW, J., 1951, *Z. Phys. Chem.*, **197**, 145.
SEITZ, F., 1951, *Rev. Mod. Phys.*, **23**, 328 ; 1954, *Ibid.*, **26**, 7.
STASIW, O., 1952, *Z. Phys.*, **134**, 106.
STASIW, O., and TELTOW, J., 1947, *Ann. Phys., Lpz.*, **1**, 261.
TELTOW, J., 1949, *Ann. Phys., Lpz.*, **5**, 71.

# XCIII. *The Cross Section for the Reaction* $^{10}B(p\alpha)^7Be$ *at Proton Energies below* 200 kev

By G. G. Bach and D. J. Livesey*
Physics Department, University of Birmingham†

[Received March 24, 1955]

## Summary

The cross section for the reaction $^{10}B(p\alpha)^7Be$ has been measured absolutely for proton energies of about 200 kev using magnetic analysis. Values of $0{\cdot}92 \pm 0{\cdot}13$ mb, $0{\cdot}66 \pm 0{\cdot}09$ mb and $0{\cdot}29 \pm 0{\cdot}04$ mb were found for proton energies of 205 kev, 200 kev and 180 kev respectively. Cross sections relative to these values were obtained for proton energies down to 70 kev.

## § 1. Introduction

The absolute yield of the reaction

$$^{10}B + {}^1H \rightarrow {}^7Be + {}^4He + 1{\cdot}147 \text{ MeV} \quad . \quad . \quad . \quad . \quad . \quad (1)$$

has been measured for proton energies between 230 kev and 1600 kev (Burcham and Freeman 1950, Brown, Snyder, Fowler and Lauritsen 1951). The present paper reports an extension of these observations down to a proton energy of 70 kev. The interest of work such as this is not only that evidence may be obtained for resonance levels in the intermediate nucleus $^{11}C$, but also that accurate measurements of the cross section for (pα) reactions in the 100 kev region may be useful in astrophysical theories (Salpeter 1953).

For proton energies above 300 kev the alpha particles emitted at 90° to the incident beam in the $^{10}B(p\alpha)$ reaction have a range less than that of the scattered protons and a magnetic analyser was used in the earlier work to discriminate between the two groups of particles. The same method was adopted in the present experiment for proton energies down to 120 kev ; below this energy the yield was found to be too small for convenience in using the magnetic analyser. Fortunately the alpha particle range for protons of 120 kev energy is sufficiently greater than that of the scattered protons to allow discrimination by absorbers, and a simple target assembly with a detector subtending a large solid angle could be used.

## § 2. Experimental Apparatus

Protons extracted from a radio-frequency ion source (Thonemann, Moffat, Roaf and Sanders 1948) were accelerated in a vertical two-stage vacuum tube. The high-tension supply was a four-stage cascade generator using selenium rectifiers and with an output ripple, after one stage of resistance capacity filtering, of 0·3% under the conditions of the experiment. The accelerating voltage was measured with an accuracy of 1% by a 1300 megohm resistor chain and a microammeter. The protons from the accelerating tube passed through a deflecting magnet on to the $^{10}$B target. A stop limited the useful target size to 6×6 mm and a negatively charged suppressor ring immediately beneath the stop prevented secondary electrons reaching the target from exposed edges. Target currents were always measured with the target at a sufficiently large positive potential to retain secondary electrons. An integrator circuit showed when the target had received a pre-determined charge.

---

* Present address : Windscale Works, Sellafield, Cumberland.

† Communicated by W. E. Burcham.

The $^{10}$B targets used during the experiments were prepared at the A.E.R.E. Harwell by electromagnetic deposition of the isotope on copper. Two thin targets of 90 $\mu$gm cm$^{-2}$ and 120 $\mu$gm cm$^{-2}$ (accurate to 10%) and one thick target (400 $\mu$gm cm$^{-2}$) were used for the cross section determinations. The thickness of this last target was determined by weighing the backing foil before and after deposition.

Fig. 1

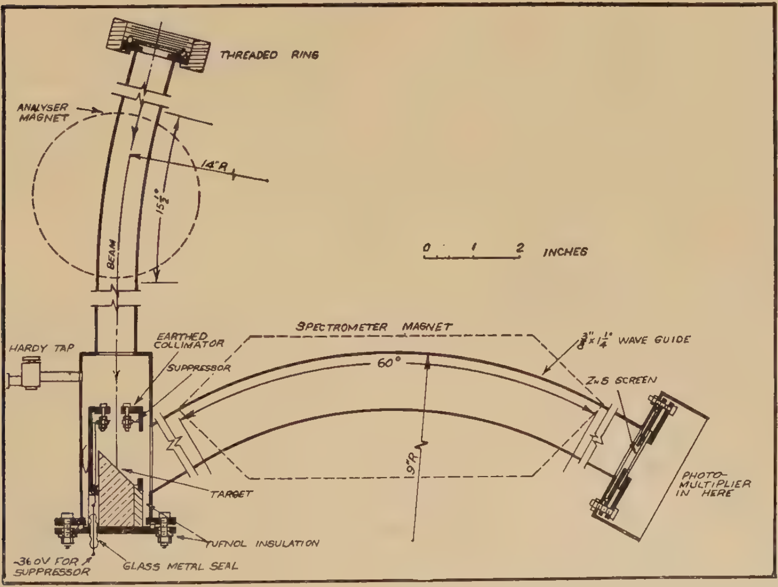

Magnetic analyser, target and detector assembly.

The analyser used for discriminating between alpha particles and protons was a length of 3 cm×1 cm wave guide bent into a 60° arc and placed between the poles of an electromagnet (fig. 1). The maximum field available was 6000 gauss and the mean radius of the analyser vacuum system was 21 cm. Straight sections of waveguide, each 11 cm long, extended beyond the analyser field and joined the analyser at one end to the target assembly and at the other end to a zinc sulphide screen and photomultiplier (EMI type 6260) for particle detection. Preliminary experiments with polonium alpha particles of differing residual ranges indicated that the screens, which were about 1·5 mgm cm$^{-2}$ thick, could be relied upon to count more than 95% of the incident alpha particles.

### § 3. DETERMINATION OF THE ABSOLUTE CROSS SECTION

To determine the cross section for the $^{10}$B(pα) reaction it was necessary to measure :

(i) The total number, $N_\alpha$, of alpha particles emitted into the analyser for a given number, $N_p$, of incident protons.

(ii) The number of disintegrable nuclei per cm$^2$ in the target. This is $nt$ where $n$ is the number of disintegrable nuclei per cm$^3$ and $t$ is the thickness of target from which alpha particles were received into the analyser.

(iii) The solid angle $\Omega_c$ of the analyser in the centre of mass system of coordinates for the $^{10}$B(pα) reaction.

The total cross section is then

$$\sigma = 4\pi \frac{N_\alpha}{N_p} \frac{1}{nt\Omega_c} \quad . \quad . \quad . \quad . \quad . \quad . \quad . \quad . \quad . \qquad (2)$$

assuming an isotropic distribution of alpha particles.

The determination of $N_\alpha$ and the calculation of $t$ depend on whether the energy loss in the target for the alpha particles is greater or less than the energy interval accepted by the analyser. Snyder, Rubin, Fowler and Lauritsen (1950) show that for thin targets,

$$\sigma = \frac{4\pi R}{N_p \Omega_c nt} \int \frac{n_\alpha di}{i} \quad . \quad . \quad . \quad . \quad . \quad . \quad . \quad . \qquad (3)$$

where $t$ is the actual thickness of the target, and for thick targets

$$\sigma = \frac{4\pi N_{\max} R}{N_p \Omega_c} \cdot \frac{\epsilon_1 \dfrac{\partial E_2}{\partial E_1} + \epsilon_2 \dfrac{\cos\theta_1}{\cos\theta_2}}{2E_2 \cos\theta_1} \quad . \quad . \quad . \quad . \quad . \quad . \quad . \qquad (4)$$

In these formulae

(i) $N_\alpha$ is the number of alpha-counts observed for $N_p$ protons when the analyser magnet current setting is $i$ (thin target).

(ii) $R$ is the resolution of the analyser, equal to $2E/\Delta E$ where $\Delta E$ is the range of energies of particles accepted at the energy setting $E$.

(iii) $N_{\max}$ is the maximum number of alpha particles observed for $N_p$ protons over the flat portion of the alpha particle profile from a thick target.

(iv) $E_2$ is the energy of outgoing alpha particles.

(v) $\theta_1$ and $\theta_2$ are the angles made by the incident protons (energy $E_1$) and observed alpha particles with the normal to the target surface.

(vi) $\epsilon_1$ and $\epsilon_2$ are the stopping cross sections of $^{10}$B for protons of 200 kev and alpha particles of 840 kev, taken to be 440 kev mgm$^{-1}$ cm$^2$ and 1820 kev mgm$^{-1}$ cm$^2$ respectively (Allison and Warshaw 1953).

The number of alpha particles observed was in each case multiplied by a factor of 1·64 (Dissanaike 1953) to take account of the particles emerging from the target in the singly charged state. Figure 2 shows a typical alpha particle counting-rate profile obtained from the thick target. For the thin targets the integral in eqn. (3) was evaluated graphically from curves of alpha particle counting rate against analyser magnet current.

Fig. 2

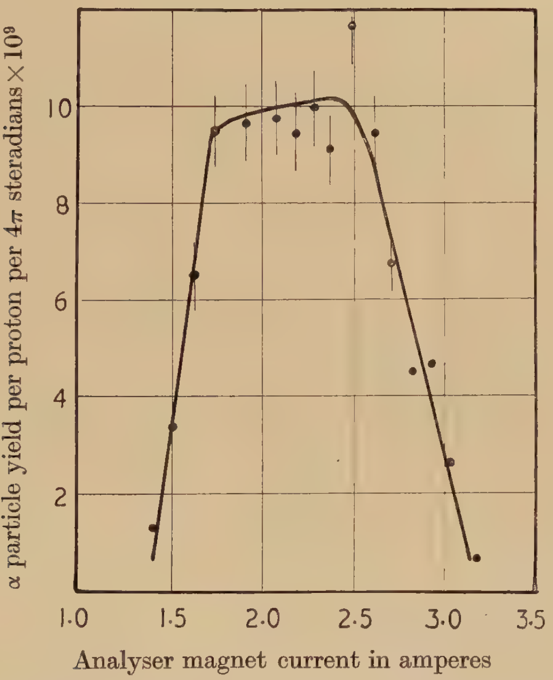

Alpha particle profile obtained from thick $^{10}B$ target (400 $\mu$gm cm$^{-2}$) for $E_p=200$ kev.

In the present experiment $\theta_1=45°$, and $\theta_2=19·6°$. The factor $\Omega_c/R$ was found by observations on protons scattered elastically from thick targets of aluminium, carbon and beryllium. The solid angle $\Omega_c$ in the centre of mass system depends on the target material in the scattering experiments, and was transformed to laboratory coordinates ($\Omega_L$) in each case. The ratio $\Omega_L/R$ is an instrumental factor which should be independent of the reaction being studied.

## § 4. RESULTS

The values of $\Omega_L/R$ found from the scattering experiments are shown in table 1.

Using the mean of these values and transforming $\Omega_L$ back to the centre of mass system for the $^{10}B(p\alpha)$ reaction the cross ections calculated for the $^{10}B(p\alpha)$ reaction for various targets are shown in table 2.

The errors are based on estimated accuracies of determination of the quantities in eqns. (3) and (4). From the values listed we obtain

$$\left.\begin{aligned}\sigma[^{10}\mathrm{B}(\mathrm{p}\alpha)\text{ at }180\text{ kev}]&=0{\cdot}29\pm0{\cdot}04\\ \sigma[^{10}\mathrm{B}(\mathrm{p}\alpha)\text{ at }200\text{ kev}]&=0{\cdot}66\pm0{\cdot}09\\ \sigma[^{10}\mathrm{B}(\mathrm{p}\alpha)\text{ at }205\text{ kev}]&=0{\cdot}92\pm0{\cdot}13\end{aligned}\right\}\text{ millibarns*.}$$

Table 1

| Scatterer | Scattering angle | Proton energy (laboratory system) kev | $\Omega_L/R$ steradians ($\times 10^{-5}$) |
|---|---|---|---|
| Be | 125·2° | 205 | 1·86 |
| C | 124·0° | 205 | 1·88 |
| Al | 121·8° | 205 | 1·82 |

Table 2

| Target thickness ($\mu$gm cm$^{-2}$) | Proton energy (laboratory system) (kev) | Reaction cross section ($\times 10^{-28}$ cm$^2$) |
|---|---|---|
| 90 | 177 | 2·9±0·4 |
| 90 | 199 | 6·6±0·9 |
| 90 | 205 | 7·4±1·1 |
| 90 | 205 | 9·7±1·4 |
| 120 | 205 | 9·0±1·3 |
| 400 | 205 | 10·9±1·4 |

Relative values of the cross section at lower energies were obtained using a thick target and the analyser for proton energies down to 120 kev. For energies below 120 kev a simple target chamber employing range discrimination, and with a much larger solid angle than the analyser was used. The alpha particles were detected by a zinc sulphide screen and photomultiplier. These observations were fitted to the absolute determinations at 180 and 205 kev.

The excitation curve so found is shown in fig. 3, which also includes the low energy points obtained by Burcham and Freeman (1950). A plot of log ($\sigma E$) against $E^{-1/2}$ (fig. 4) showed no anomalies down to $E_p=70$ kev and the slope of this line was within 2% of that calculated from the formula

$$\sigma=\frac{A}{E_p}\exp\left(-\frac{2\pi Ze^2}{\hbar v_p}\right)$$

in which $v_p$ is the velocity in the centre of mass system of the proton incident on $^{10}$B. The variation of the barrier penetrability for the

---

* These values differ slightly from those communicated to Ajzenberg and Lauritsen (*Rev. Mod. Phys.*, 27, 77, 1955).

Fig. 3

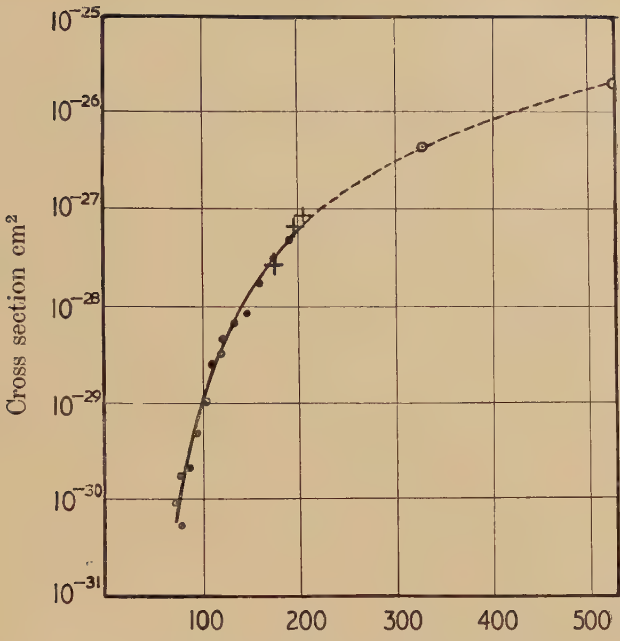

Proton energy 7ev in Laboratory system
Excitation curve for the reaction $^{10}B(p\alpha)^7Be$.
⊙ from Burcham and Freeman (1950); + present work, absolute points;
● present work, relative measurements.

Fig. 4

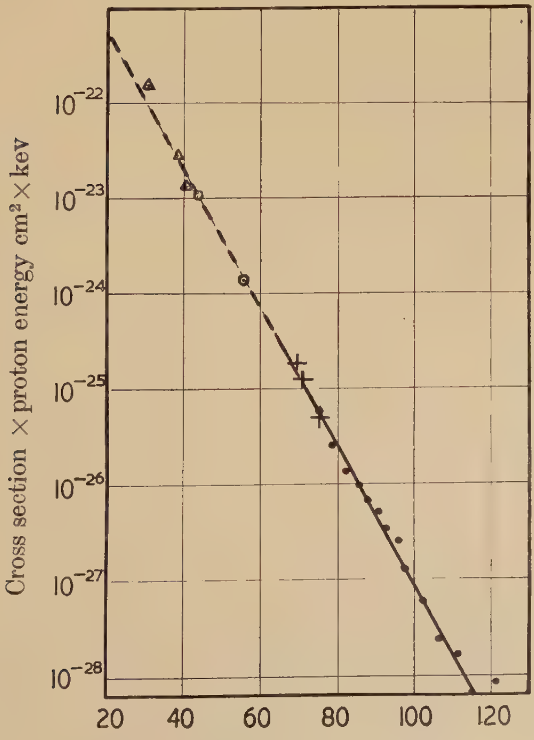

(Proton energy)$^{-\frac{1}{2}}$ kev$^{-\frac{1}{2}} \times 10^5$
Gamow plot for the reaction $^{10}B(p\alpha)^7Be$.
△ from Brown *et al.* (1951); ⊙ from Burcham and Freeman (1950)
+ ● present work.

emergent alpha particles was less than 3% over the proton energy range investigated and has been neglected. No effects due to resonance levels in the $^{11}$C nucleus in the energy range investigated were found.

## ACKNOWLEDGMENTS

We wish to thank Professor W. E. Burcham for helpful discussion and assistance during the course of this work. The $^{10}$B targets were prepared and weighed by Dr. M. L. Smith, A.E.R.E. Harwell and the cascade high-tension generator was loaned by Dr. E. Bretscher of A.E.R.E. One of us (G.G.B.) is grateful for the award of an Athlone Fellowship for the period of this work, while the other (D.J.L.) is indebted to the Department of Scientific and Industrial Research for a maintenance grant.

## REFERENCES

ALLISON, S. K., and WARSHAW, S. D., 1953, *Rev. Mod. Phys.*, **25,** 779.
BROWN, A. B., SNYDER, C. W., FOWLER, W. A., and LAURITSEN, C. C., 1951, *Phys. Rev.*, **82,** 195.
BURCHAM, W. E., and FREEMAN, J. M., 1950, *Phil. Mag.*, **41,** 337.
DISSANAIKE, G. A., 1953, *Phil. Mag.*, **44,** 1051.
SALPETER, E. E., 1953, *Ann. Rev. Nucl. Sci.*, **2,** 51.
SNYDER, C. W., RUBIN, S., FOWLER, W. A., and LAURITSEN, C. C., 1950, *Rev. Sci. Inst.*, **21,** 852.
THONEMANN, P. C., MOFFAT, J., ROAF, D., and SANDERS, J. H., 1948, *Proc. Phys. Soc.*, **61,** 482.

# XCIV. *Scattering of Electrons and Holes by Charged Donors and Acceptors in Semiconductors*

By R. B. DINGLE
Department of Physics, University of Western Australia, Nedlands*

[Received March 16, 1955]

## ABSTRACT

The problem of determining the time of relaxation due to scattering of electrons and holes by charged impurity donors and acceptors in semiconductors is reconsidered in an effort to derive formulae more exact and general than those due to Conwell, Weisskopf, and other authors.

## § 1. INTRODUCTION

THE author and Dr. S. K. Roy (1955) have recently computed the chief integrals which occur in the theory of the electrical, thermal, thermoelectric, optical and magnetic-transport properties of isotropic or polycrystalline elemental semiconductors, on the assumption that the most important scattering processes are those due to (1) thermal agitation with scattering proportional to $E^{1/2}$, where $E$=electron energy, and (2) the presence of charged impurity ions with scattering roughly proportional to $E^{-3/2}$. In connection with these tabulations, it seems desirable to re-examine the theory of the latter scattering process in an effort to establish formulae more accurate than those discussed in the literature (e.g. Conwell and Weisskopf 1946, 1950, Johnson and Lark-Horovitz 1947, Shockley 1950, pp. 258–264), since these largely rely on rather arbitrary cut-off approximations.

Our basic approach is essentially the same as that employed by Mott (1936) in a discussion of the resistance of dilute solid solutions of one metal in another. Substantial alterations are, however, required in Mott's discussion in order to make it applicable to semiconductors, and we shall therefore re-derive the theory, taking due account of

(*a*) the dielectric constant, which must be retained at all stages,

(*b*) the simultaneous presence of holes and electrons, and

(*c*) the degree of degeneracy of the electron and hole systems.

## § 2. THE POTENTIAL ENERGY

### *Screening of Ionized Donors by Electrons*

For the sake of simplicity in exposition, we shall first consider an ordinary n-type impurity semiconductor in which one excess electron is provided by each donor, which therefore becomes singly positively charged. The first approximation to the potential energy $V$ of an incident electron distant $r$ from this positive charge, $V=e^2/\kappa r$ where $\kappa$ is the dielectric constant of the bulk material, would lead to an infinite scattering cross section for incident electrons passing the charged impurity ion, on account of the high probability of small-angle scattering of electrons travelling past at large distances, i.e. of those electrons with large impact parameters. In the well-known treatment by Conwell and Weisskopf (1946, 1950) this difficulty is surmounted by assuming that $V=e^2/\kappa r$ for electrons approaching with impact parameters smaller than $\frac{1}{2}N_{\mathrm{di}}{}^{-1/3}$, where $N_{\mathrm{di}}$ is the number of impurity donor ions per unit volume, while $V=0$ for larger impact parameters. Put another way, large ‘ misses ’ are simply ignored in their treatment. In order to set up a more accurate theory, it is necessary to find a more comprehensive form for $V(r)$, particularly when $r$ is large, taking explicit account of the screening of the positively charged donor ion by the surrounding electron cloud.

---

* Communicated by the Author.

Let $n$ represent the average number of electrons per unit volume in the conduction band (excluding of course electrons actually bound to donors), and $\phi$ the electrostatic potential. Then, since in the presence of the self-consistent field due to $\phi$ the customary space-independent Fermi energy $\zeta_n$ must be replaced by $\zeta_n+e\phi(r)$, $e$ being taken as positive, the number of electrons per unit volume near a positively charged donor ion will be

$$n(r)=\frac{8\pi\sqrt{2}\,m_n{}^{3/2}}{h^3}\int_0^\infty\frac{E^{1/2}\,dE}{\exp\,[\{E-\zeta_n-e\phi(r)\}/kT]+1}, \quad . \quad . \quad (1)$$

where $m_n$ is the effective electronic mass, assuming the energy band to be of standard form (energy proportional to square of wave-vector).

Adopting the notation

$$\mathscr{F}_k(\eta)=\frac{1}{k\,!}\int_0^\infty\frac{x^k\,dx}{\exp\,(x-\eta)+1} \quad . \quad . \quad . \quad (2)$$

for the Fermi–Dirac integrals,* this may be written

$$n(r)=\frac{4\pi m_n{}^{3/2}(2\pi)^{1/2}(kT)^{3/2}}{h^3}\mathscr{F}_{1/2}\left\{\eta_n+\frac{e\phi(r)}{kT}\right\}\text{ where }\eta_n=\zeta_n/kT. \quad . \quad (3)$$

Since we are primarily interested only in the form $\phi(r)$ takes for large $r$, where $\phi$ is necessarily very small, this may be expanded, making use of the general relation

---

* This notation differs from McDougall and Stoner’s (1938) by the presence of the additional factor $1/(k\,!)$, and possesses the following advantages :

(*a*) In the classical limit $\eta\ll 0$, $\mathscr{F}_k(\eta)$ is independent of the order $k$.

(*b*) Interpolation is possible between different *orders* $k$ as well as between different arguments $\eta$.

(*c*) The relation between the function and its derivative is simpler (see (4) above).

The required integrals $\mathscr{F}_{1/2}$ and $\mathscr{F}_{-1/2}$ are tabulated in this form in Dingle and Roy (1955).

$$\mathscr{F}'_k(\eta)=\mathscr{F}_{k-1}(\eta). \qquad . \quad . \quad . \quad . \quad . \quad . \quad (4)$$

Thus, to sufficient accuracy, the space-dependence of the screening charge is

$$\rho(r)=-e\delta n(r)=-\frac{4\pi e^2 m_n{}^{3/2}(2\pi kT)^{1/2}}{h^3}\mathscr{F}_{-1/2}(\eta_n)\phi(r). \quad . \quad . \quad (5)$$

With this form for $\rho(r)$, the solution of Poisson's equation

$$\nabla^2\phi=-4\pi\rho/\kappa, \qquad . \quad . \quad . \quad . \quad . \quad . \quad . \quad . \quad (6)$$

which is spherically symmetric, vanishes for $r\to\infty$, and tends to the known value $\phi\to e/\kappa r$ for $r\to 0$, where the screening cannot be effective, is

$$\phi(r)=\frac{e}{\kappa r}\exp(-r/R), \qquad . \quad . \quad . \quad . \quad . \quad (7)$$

the ' screening distance ' $R$ being given by

$$\begin{aligned} R^{-2}&=\frac{16\pi^2 e^2 m_n{}^{3/2}(2\pi kT)^{1/2}}{\kappa h^3}\mathscr{F}_{-1/2}(\eta_n) \\ &=9{\cdot}923\times 10^{-8}\kappa^{1/2}T^{-1/4}\alpha_n{}^{-3/4}[\mathscr{F}_{-1/2}(\eta_n)]^{-1/2} \text{ c.g.s. units}, \quad . \quad (8) \end{aligned}$$

where $\alpha_n=m_n/m_0$, $m_0$ being the *actual* electronic mass.

It suffices to insert for $\eta_n$ in (8) the ordinary average value ignoring the space-dependence of the electron density. This is determined by the relation

$$n=2h^{-3}(2\pi m_n kT)^{3/2}\mathscr{F}_{1/2}(\eta_n),$$

i.e. $$\mathscr{F}_{1/2}(\eta_n)=2{\cdot}070\times 10^{-16}nT^{-3/2}\alpha_n{}^{-3/2} \text{ c.g.s. units}. \quad . \quad . \quad (9)$$

Extensive tables of the Fermi–Dirac function $\mathscr{F}$ appear in Dingle and Roy (1955). In connection with the present paper we reproduce here a short table of $\mathscr{F}_{1/2}$ and $\mathscr{F}_{-1/2}$.

| $\eta$ | $\mathscr{F}_{1/2}(\eta)$ | $\mathscr{F}_{-1/2}(\eta)$ | $\eta$ | $\mathscr{F}_{1/2}(\eta)$ | $\mathscr{F}_{-1/2}(\eta)$ |
|---|---|---|---|---|---|
| −4·0 | 0·0182 | 0·0181 | 3·5 | 5·458 | 2·026 |
| −3·5 | 0·0299 | 0·0296 | 4·0 | 6·512 | 2·186 |
| −3·0 | 0·0489 | 0·0481 | 4·5 | 7·642 | 2·334 |
| −2·5 | 0·0798 | 0·0776 | 5·0 | 8·844 | 2·473 |
| −2·0 | 0·1293 | 0·1237 | 5·5 | 10·11 | 2·604 |
| −1·5 | 0·2074 | 0·1933 | 6·0 | 11·45 | 2·727 |
| −1·0 | 0·3278 | 0·2940 | 6·5 | 12·84 | 2·845 |
| −0·5 | 0·5075 | 0·4312 | 7·0 | 14·29 | 2·957 |
| 0·0 | 0·7651 | 0·6049 | 7·5 | 15·80 | 3·065 |
| 0·5 | 1·117 | 0·8077 | 8·0 | 17·36 | 3·169 |
| 1·0 | 1·576 | 1·027 | 8·5 | 18·96 | 3·270 |
| 1·5 | 2·145 | 1·249 | 9·0 | 20·62 | 3·367 |
| 2·0 | 2·824 | 1·464 | 9·5 | 22·33 | 3·461 |
| 2·5 | 3·607 | 1·666 | 10·0 | 24·08 | 3·553 |
| 3·0 | 4·488 | 1·853 | | | |

For highly degenerate electron systems, $\eta_n \gg 0$, application of the asymptotic relation

$$\mathscr{F}_k(\eta) \sim \eta^{k+1}/(k+1)! \qquad \ldots\ldots \quad (10)$$

leads to a value for the screening distance

$$\begin{aligned} R_{\text{degenerate}} &= (\pi/3)^{1/6} h\sqrt{\kappa}/4\pi e\sqrt{m_n}\,.\,n^{1/6} \\ &= 3{\cdot}665\times 10^{-5}\kappa^{1/2} n^{-1/6}\alpha_n^{-1/2} \text{ c.g.s. units,} \qquad .\ . \quad (11) \end{aligned}$$

in agreement with Mott (1936, see also Mott and Jones, p. 87, where their $q^{-1}$ equals our $R$).

For non-degenerate electron systems, $\eta_n \ll 0$, the approximation

$$\mathscr{F}_k(\eta) \simeq e^{\eta} \qquad \ldots\ldots\ldots \quad (12)$$

leads to the expression

$$R_{\text{non-degenerate}} = (\kappa kT/4\pi n)^{1/2}/e = 6{\cdot}902\kappa^{1/2}T^{1/2}n^{-1/2} \text{ c.g.s. units.} \qquad .\ . \quad (13)$$

We now consider two typical examples. Suppose a specimen of silicon contains some phosphorus atoms as impurities. Phosphorus has a valency of five and silicon of only four ; in order to permit the phosphorus bonds to fit in with the fundamental structure of the silicon. based on four covalent bonds, one bond of each impurity phosphorus atom is destroyed. The result is that each phosphorus atom acts as a single positive charge and—at least at reasonably high temperatures—provides one electron to wander through the crystal. The degeneracy temperature of the resultant electron system is given by the customary formula (e.g. Mott and Jones 1936, pp. 54, 180)

$$T_{\text{degen.}} = \frac{h^2}{8mk}\left(\frac{3}{\pi}\right)^{2/3} n^{2/3} = 4{\cdot}231\times 10^{-11} n^{2/3}\alpha^{-1} \text{ c.g.s. units,} \qquad . \quad (14)$$

where $n$ is the number of free electrons per unit volume and $\alpha = m/m_0$ as before. The number of silicon atoms per cm³ is $5{\cdot}00\times 10^{22}$.

For our first example, we suppose that one impurity P atom is introduced for every 100 Si atoms, so that $n = 5{\cdot}00\times 10^{20}$ cm$^{-3}$. If we assume that the electrons behave as though perfectly free, so that $\alpha = 1$, then $T_{\text{degen}} = 2665$°K, showing that with this large impurity content the electron system is totally degenerate at room temperature. Since for Si $\kappa = 11{\cdot}9$ (Briggs 1950), we deduce from eqn. (11) that the screening distance $R$ is 4·488 Å. For comparison, the cut-off distance implicitly assumed in the theory of Conwell and Weisskopf (1946, 1950) would be $\frac{1}{2}n^{-1/3} = 6{\cdot}300$ Å. We should, however, remark at this point that the validity of the theory is somewhat dubious for such high impurity concentrations as that considered in this example. For instance, the screening distance $R = 4{\cdot}488$ Å turns out to be not quite twice the average spacing of the Si atoms, $N_{\text{Si}}^{-1/3} = 2{\cdot}714$ Å, so that the insertion of the *bulk* value of the dielectric constant $\kappa$ of Si is questionable. It is also possible that quantum exchange and correlation effects, neglected in the present paper, may influence the results appreciably.

For our second example, we suppose that only one impurity P atom is introduced for every $10^5$ Si atoms, so that $n=5{\cdot}00\times10^{17}\ \mathrm{cm}^{-3}$. Then $T_{\mathrm{degen.}}=26{\cdot}65^{\circ}\mathrm{K}$, showing that the electron system is now quite non-degenerate at room temperature. Equation (13) then gives, at a temperature of 17°C, $R=57{\cdot}34$ Å. For comparison, the Conwell–Weisskopf cut-off distance would be 63·00 Å.

According to our formulae the screening distance is *not* simply proportional to the spacing of the impurity ions $N_{\mathrm{i}}^{-1/3}$ even in the limiting cases of strong and weak degeneracy, so that customary cut-off procedures which assume this are strictly speaking unreliable. Their apparent success is clearly explained by the largely fortuitous rough numerical agreement under normal experimental conditions between the values of the theoretical screening distance $R$ and the assumed cut-off distance $\frac{1}{2}N_{\mathrm{i}}^{-1/3}$.

### *Screening of Acceptors by Holes*

Writing the statistical distribution function for electrons of energy $E_n$, measured upwards from the bottom of the appropriate band, as

$$f_n=\frac{1}{\exp\left[(E_n-\zeta_n)/kT\right]+1}, \qquad (15)$$

that for holes (≡missing electrons) must be

$$f_p=1-f_n=\frac{1}{\exp\left[(\zeta_n-E_n)/kT\right]+1}, \qquad (16)$$

where $E_n$ is the energy the missing electron would have had. Since electrons will normally be missing only from the top of a band, it is convenient to measure the energy $E_p$ of holes downwards from the top of the appropriate band by writing

$$E_p=-A-E_n, \qquad (17)$$

where $A$ is the energy gap between the top of the band supplying the holes and the bottom of the band supplying the electrons. In other words, $-A$ is the energy at the top of the hole band as measured on the energy scale used for the electrons. We may then write, in complete analogy with (15),

$$f_p=\frac{1}{\exp\left[(E_p-\zeta_p)/kT\right]+1}, \qquad (18)$$

where $\zeta_p=-A-\zeta_n$.

Adopting this notation, it is clear that the formulae giving the screening distance when acceptors are surrounded by holes are of just the same form as those for the screening distance when donors are surrounded by electrons. Thus by analogy with (7), (8) and (9),

$$\phi(r)=-\frac{e}{\kappa r}\exp(-r/R), \qquad (19)$$

where

$$R^{-2}=\frac{16\pi^2e^2m_p^{3/2}(2\pi kT)^{1/2}}{\kappa h^3}\mathscr{F}_{-1/2}(\eta_p), \qquad (20)$$

and $\eta_p$ is determined by the relation

$$p=2h^{-3}(2\pi m_p kT)^{3/2}\mathscr{F}_{1/2}(\eta_p), \qquad (21)$$

$m_p$ being the effective hole mass, $p$ the average number of holes per unit volume, and $\eta_p=\zeta_p/kT=-A/kT-\eta_n$. Limiting formulae for complete degeneracy and non-degeneracy may similarly be written down at once by analogy with (11) and (13).

### *Screening of Donors (and Acceptors) by both Electrons and Holes*

It will be seen from (5) that the space-dependence $\rho(r)$ of the screening charge round a positively charged donor ion is proportional to $e^2$, and to this extent is therefore independent of whether these charges are electrons or holes. The physical explanation of the screening of donor ions by holes of *like* charge is that since these holes are repelled from the donor, any incident particle must approach from a region which is already filled with positive charge, and is therefore less affected by the fixed positive charge of the donor, only *changes* in potential energy being effective in scattering processes.

For the screening of donors and acceptors by electrons and holes, we have

$$\phi_{\text{donor}}=\frac{e}{\kappa r}\exp(-r/R)\,;\quad \phi_{\text{acceptor}}=-\frac{e}{\kappa r}\exp(-r/R), \quad . \quad (22)$$

where for either donors or acceptors

$$R^{-2}=\frac{16\pi^2e^2(2\pi kT)^{1/2}}{\kappa h^3}[m_n^{3/2}\mathscr{F}_{-1/2}(\eta_n)+m_p^{3/2}\mathscr{F}_{-1/2}(\eta_p)]. \quad . \quad (23)$$

## § 3. EVALUATION OF THE FERMI-LEVEL

The fundamental quantity $\eta_n=\zeta_n/kT$ (the subsidiary quantity $\eta_p$ being just given in terms of this by the relation $\eta_p=-A/kT-\eta_n$) may be calculated from the condition of overall electrical neutrality

$$n-p=N_{\text{di}}-N_{\text{ai}}, \quad . \quad . \quad . \quad . \quad . \quad . \quad . \quad (24)$$

in which $n$ and $p$ are given in terms of $\eta_n$ (or $\eta_p$) by (9) and (21) respectively, and

$$N_{\text{di}}=\frac{N_d}{2\exp[\eta_n+E_d/kT]+1}, \qquad N_{\text{ai}}=\frac{N_a}{2\exp[\eta_p+E_a/kT]+1}. \quad . \quad (25)$$

Here $N_{\text{d}}$ is the total number of donor atoms introduced, comprising $N_{\text{di}}$ positively charged and $N_{\text{d}}-N_{\text{di}}$ neutralized by bound electrons ; $N_{\text{a}}$ is the total number of acceptor atoms introduced, comprising $N_{\text{ai}}$ negatively charged and $N_{\text{a}}-N_{\text{ai}}$ neutralized by bound holes ; $E_{\text{d}}$ is the energy gap between the bottom of the electron band and the donor levels, namely minus the energy of the donor levels as measured on the *electron* energy scale, i.e. counting upwards from the bottom of the electron band reckoned as of zero energy ; and $-E_{\text{a}}$ is the energy of the acceptor levels as measured on the *hole* energy scale, i.e. counting downwards from the top of the hole band reckoned as of zero energy. Note that $E_{\text{a}}$ (hole scale)$=A-E_{\text{a}}$ (electron scale). The factor 2 multiplying the exponentials in (25) arises from the fact that bound electrons and holes may be held in either of two spin orientations—see, for e.g. Shockley (1950, pp. 248, 475), Landsberg (1952, 1953), Guggenheim (1953).

## § 4. THE TIME OF RELAXATION

In all cases considered in the present paper, the magnitude of the potential energy between an incident electron or hole and a charged ionized donor or acceptor may with sufficient accuracy be written in the form

$$|V(r)|=|e\phi(r)|=\frac{e^2}{\kappa r}\exp(-r/R). \quad . \quad . \quad . \quad (26)$$

The resultant differential elastic cross section $I(\theta)$, defined as the number of particles per unit time scattered through an angle $\theta$ into unit solid angle when on the average one particle is incident with velocity $v$ on unit area per unit time, is given by Born's approximation (e.g. Mott and Massey 1933, p. 119):

$$\sqrt{I(\theta)}=\frac{8\pi^2 m}{h^2 K}\int_0^\infty \sin Kr\,|V(r)|\,r\,dr \quad . \quad . \quad . \quad (27)$$

where $K=4\pi mv(\sin\frac{1}{2}\theta)/h$.

An elementary integration then yields

$$\sqrt{I(\theta)}=\frac{e^2}{\kappa mv^2\{2\sin^2\frac{1}{2}\theta+(h^2/8\pi^2m^2v^2)/R^2\}}. \quad . \quad . \quad (28)$$

As is well-known (e.g. Mott and Jones 1936, p. 262), the reciprocal $\tau^{-1}$ of the time of relaxation is equal to the total probability per unit time that a particle is scattered, except that a factor $(1-\cos\theta)$ must be introduced (as in the theory of gaseous diffusion) to give extra weight to large-angle collisions. Thus if there are $N_i$ charged ions per unit volume,

$$\tau^{-1}=N_i v\,2\pi\int_0^\pi(1-\cos\theta)I(\theta)\sin\theta\,d\theta. \quad . \quad . \quad . \quad (29)$$

Taking $(1-\cos\theta)=x$, this reduces to

$$\tau^{-1}=\frac{2\pi N_i e^4}{\kappa^2 m^2 v^3}\int_0^2\frac{x\,dx}{[x+(h^2/8\pi^2m^2v^2)/R^2]^2} \quad . \quad . \quad . \quad . \quad (30)$$

$$=\frac{2\pi N_i e^4}{\kappa^2 m^2 v^3}\left[\ln(1+\xi)-\frac{\xi}{1+\xi}\right], \quad . \quad . \quad . \quad . \quad . \quad (31)$$

where $\xi=16\pi^2m^2v^2R^2/h^2$, in agreement with Mott (1936) provided we replace his $Z^2$ by $\kappa^{-2}$. Written in terms of the energy $E=\frac{1}{2}mv^2$ of the incident particle,

$$\tau^{-1}=\frac{\pi N_i e^4}{(2m)^{1/2}\kappa^2}g(\xi)E^{-3/2}, \quad . \quad . \quad . \quad . \quad . \quad (32)$$

where $$g(\xi)=\ln(1+\xi)-\xi/(1+\xi) \quad . \quad . \quad . \quad . \quad . \quad . \quad (33)$$

with $$\xi=32\pi^2mR^2E/h^2. \quad . \quad . \quad . \quad . \quad . \quad . \quad . \quad (34)$$

The form of these results, and of $R$, is independent of whether the scattering centre is a donor or acceptor ion. For incident electrons

$m$ must be understood to refer to $m_n$, while for incident holes $m \equiv m_p$. The abbreviation ln refers to the natural logarithm.

It is convenient to define the 'temperature' of an incident particle by the relation $E = kT_{\text{particle}}$, noting that 1 ev$\equiv$11 605°K. Then in c.g.s. units,

$$\xi = 9{\cdot}049 \times 10^{11} \alpha R^2 T_{\text{particle}} \quad . \quad . \quad . \quad . \quad . \quad . \quad (35)$$

where $\alpha = m/m_0$. For incident particles of very low energy, $\xi \ll 1$, $g(\xi) \simeq \frac{1}{2}\xi^2$, and hence $\tau^{-1} \propto \sqrt{E}$ as for scattering by thermal agitation.

## § 5. APPROXIMATION TO THE TIME OF RELAXATION

Owing to the comparative complexity of the function $g(\xi)$ defined by (33), it is necessary to replace it by an approximation before performing the required integration over energies, except of course when the electron system is sufficiently degenerate for the Sommerfeld (1928) asymptotic series to be applicable. Let us first consider the likely magnitude of $\xi$ in practical cases.

In the first example considered in § 3 (one P impurity atom for every 100 Si atoms), the electron system was degenerate, so that $T_{\text{particle}} \doteq T_{\text{degen.}} = 2665$°K. Inserting the value of the screening distance $R = 4{\cdot}488 \times 10^{-8}$ cm previously determined in § 3, it is found that the only important values of $\xi$ lie near $\xi_0 = 4{\cdot}857$.

In the second example (one P for every $10^5$ Si), the electron system was non-degenerate. The incident particles must then be travelling with thermal velocities, so that $T_{\text{particle}} \sim T$. For reasons which will become clear later in this section, we shall take $T_{\text{particle}} = 3{\cdot}672T$ when considering the most important problem, that of the electrical conductivity. Putting $T = 17$°C$=290$°K and $R = 57{\cdot}34 \times 10^{-8}$ cm as deduced in § 3, the important values of $\xi$ lie around $\xi_0 = 316{\cdot}8$.

As already remarked, for degenerate samples the Sommerfeld (1928) asymptotic series is applicable, and the complete function $g(\xi)$ may be used without undue complication. Hence the conclusion to be drawn from these figures is that in all normal circumstances in which an approximation to $g(\xi)$ is really necessary, $\xi$ is considerably greater than unity for incident particles with average energy. Under such conditions, $g(\xi)$ is such a slowly varying function of $\xi$, and therefore of $E$, that it suffices to replace it by a constant of magnitude $g(\xi_0)$.

In order to assess the error introduced by such an approximation, we consider the formula for the electrical conductivity of a non-degenerate electron gas. This involves the integral

$$\int_0^\infty E^{3/2} \tau \exp(-E/kT)\, dE \propto \int_0^\infty x^3 \exp(-x)\, g^{-1}(\xi_0 x/3{\cdot}672)\, dx, \quad . \quad (35)$$

where $x = T_{\text{particle}}/T$. The problem is then to estimate the error caused by taking the slowly varying quantity $g^{-1}(\xi_0 x/3{\cdot}672)$ out from under the integral sign and inserting some suitable value of $x$ in its argument.

Now it is easily found that a quarter of the total value of

$$\int_0^\infty x^3 \exp(-x)\, dx$$

is contributed by values of $x < x_{1/4} = 2{\cdot}537$, a half by $x < x_{1/2} = 3{\cdot}672$ (and hence the introduction of this figure—the median—earlier in the section), and three-quarters by $x < x_{3/4} = 5{\cdot}101$; for these particular $x$-coordinates the factor $g^{-1}(\xi_0 x/3{\cdot}672)$, with $\xi_0 = 316{\cdot}8$ as in our second example, takes the respective values $0{\cdot}2274$, $g^{-1}(\xi_0) = 0{\cdot}2099$, and $0{\cdot}1964$. The error committed by assuming that the factor $g^{-1}$ appearing in the integral may be replaced by $g^{-1}(\xi_0)$, its value at the median (the bisector of the area under the curve of the integrand) will be of the same order of magnitude as the difference between the results of such an assumption, and of those obtained by replacing $g^{-1}$ by $g^{-1}(\xi_0 x_{1/4}/x_{1/2})$ over one-half of the range and by $g^{-1}(\xi_0 x_{3/4}/x_{1/2})$ over the other. Thus the error will be of the order of

$$\frac{0{\cdot}2099 - \frac{1}{2}(0{\cdot}2274 + 0{\cdot}1964)}{0{\cdot}2099} \times 100\% \sim 1\%.$$

We believe that the insertion of the particular value $x = x_{\text{median}}$ in $g^{-1}$, where $x_{\text{median}} = x_{1/2}$ represents the median of the integral remaining after $g^{-1}$ is taken outside the integral sign, will under most circumstances give very much more reliable results than the customary insertion of $x_{\max}$, the coordinate for which the remaining part of the integrand possesses a maximum (e.g. Conwell and Weisskopf 1946, 1950, Shockley 1950, p. 279), since our procedure automatically compensates for the asymmetry of the remaining integrand. Indeed, our method can still be used even if the remaining integrand possesses *no* maximum, as sometimes happens (Dingle and Roy 1955).

## § 6. COMPARISON WITH FORMULAE OBTAINED BY CUT-OFF PROCEDURES

In view of the frequent use of cut-off approximations for interpreting data in the literature, it is particularly interesting to compare our results with those obtained by such means, taking as a basis for comparison the formulae quoted by Shockley (1950). The quantity $\pi N_i e^4 E^{-3/2}/(2m)^{1/2}\kappa^2$ appears as a multiplying factor in both our expression and that given by Shockley* (1950, p. 264). For a semiconductor containing charged donor ions and electrons, we have therefore to compare our equation

$$g(\xi) = \ln(1+\xi) - \xi/(1+\xi)$$

where $\xi$ takes the limiting forms

$$\xi_{\text{degenerate}} = 2\left(\frac{\pi}{3}\right)^{1/3} \frac{\kappa}{e^2 n^{1/3}} E \quad \text{and} \quad \xi_{\text{non-degenerate}} = \frac{8\pi\kappa mkT}{e^2\hbar^2 n} E,$$

---

* Wilson (1953, p. 266) has an additional factor $\frac{1}{2}$ in $\tau^{-1}$.

with Shockley's equation $g(\mathscr{E})=\ln(1+\mathscr{E}^2)$

where*

$$\mathscr{E}=\frac{\kappa}{e^2n^{1/3}}E.$$

It is at once seen that in the limit of complete degeneracy

$$\mathscr{E}/\xi=\tfrac{1}{2}(3/\pi)^{1/3}=0\cdot4924,$$

a pure number. Our formulae then agree with Shockley's at least as far as to which variables are involved. For our first example, with one P atom for every 100 Si atoms, we found in § 5 that $\xi_0=4\cdot857$, giving $\mathscr{E}_0=2\cdot392$, $g(\xi_0)=0\cdot9384$ and $g(\mathscr{E}_0)=1\cdot905$. We conclude, therefore, that for typical degenerate electron systems Shockley's formula gives values of $\tau^{-1}$, and therefore of the resistivity, too high by a factor of about 2. We may also note at this point that owing to differences in their cut-off approximation for the degenerate case, Johnson and Lark-Horovitz (1947) obtain a value of $\tau^{-1}$ smaller than Shockley's by a factor $\pi$: their resistivities would therefore be too *low* by a factor of about 3/2.

In the non-degenerate limit,

$$\mathscr{E}/\xi=h^2n^{2/3}/8\pi mkT=1\cdot389\times10^{-11}\alpha^{-1}n^{2/3}T^{-1} \text{ in c.g.s. units,}$$

and any agreement between the results of our theory and those of arguments based on the customary cut-off approximations must be largely fortuitous. For our second example of one P atom for every $10^5$ Si atoms, $\mathscr{E}/\xi=0\cdot03018$ at room temperature. Thus while $\xi_0=316\cdot8$ as found in § 5, $\mathscr{E}_0=9\cdot560$. These correspond to $g(\xi_0)=4\cdot765$ and $g(\mathscr{E}_0)=4\cdot526$, so that although cut-off procedures for non-degenerate electron systems appear to lead to formulae not even involving the correct powers of the variables, for the typical experimental conditions discussed the numerical results obtained by their use fortunately turn out to be reasonably accurate.

## REFERENCES

BRIGGS, H. B., 1950, *Phys. Rev.*, **77,** 287.

CONWELL, E., and WEISSKOPF, V. F., 1946, *Phys. Rev.*, **69,** 258 ; 1950, *Ibid.*, **77,** 388.

DINGLE, R. B., and ROY, S. K., 1955, to be published.

GUGGENHEIM, E. A., 1953, *Proc. Phys. Soc.* A, **66,** 121.

JOHNSON, V. A., and LARK-HOROVITZ, K., 1947, *Phys. Rev.*, **71,** 374.

LANDSBERG, P. T., 1952, *Proc. Phys. Soc.* A, **65,** 404 ; 1953, *Ibid.*, **66,** 662.

McDOUGALL, J., and STONER, E. C., 1938, *Phil. Trans.* A, **237,** 67.

MOTT, N. F., 1936, *Proc. Camb. Phil. Soc.*, **32,** 281.

MOTT, N. F., and JONES, H., 1936, *Theory of the Properties of Metals and Alloys* (Oxford : University Press).

MOTT, N. F., and MASSEY, H. S. W., 1933, *Theory of Atomic Collisions*, 1st ed. (Oxford : University Press).

SHOCKLEY, W., 1950, *Electrons and Holes in Semiconductors* (New York : van Nostrand).

SOMMERFELD, A., 1928, *Z. Phys.*, **47,** 1.

---

* We have replaced $N_i^{2/3}$ by $n^{2/3}$ since these are equal when there are only charged donors and electrons present.

# XCV. *Cross Sections for the Reaction* $^{12}$C($\gamma$3$\alpha$) *in the Energy Range* 12–18 MeV

By J. H. Carver, H. J. Hay and E. W. Titterton
Australian National University, Canberra*

[Received March 17, 1955]

## Abstract

By combining results obtained from a methane counter with those from nuclear emulsions the cross-sections for the $^{12}$C($\gamma$3$\alpha$) reaction at 17·6, 14·8 and 12·3 MeV are found to be (1·70±0·24), (0·33±0·07) and $(1{\cdot}15\pm0{\cdot}6)\times10^{-28}$ cm$^2$ respectively. Analysis of the data suggests a strong resonance in the excitation function near 12·3 MeV and possible resonances near 15 and 16 MeV.

## § 1. Introduction

Considerable attention has been given to the reaction $^{12}$C($\gamma$3$\alpha$) and the position has been reviewed recently by Titterton (1955). Many observers have determined the cross section for the $^{7}$Li(p$\gamma$) resonance radiation by the photographic plate method, a knowledge of this being important since it is often convenient to determine cross sections for other, rarer, reactions occurring in the emulsion in terms of it. The wide spread of values which have been reported (table 1 and fig. 3) is unsatisfactory and makes a redetermination of the cross section at 17·6 MeV desirable ; at the same time it was hoped that by using other lines in the $^{7}$Li(p$\gamma$) spectrum, particularly the broad one at 14·8 MeV, information could be obtained on the resonance absorption of radiation by states of $^{12}$C, evidence for which had been presented by Goward and Wilkins (1953).

To determine the cross section at 17·6 MeV a methane filled proportional counter was used since this enables data to be collected more quickly and with better energy resolution than is possible by the emulsion method. However, the information obtained is less definite ; only the total disintegration energy is measured and it is impossible to distinguish between events where one particle strikes the counter walls and events due to $\gamma$-rays of energy lower than the main line, although appropriate corrections can be applied. For this reason the proportional counter was used to obtain the absolute cross section at 17·6 MeV while the photographic plate method was employed to investigate the reaction at lower energies and to determine cross section values at 14·8 and 12·3 MeV relative to the 17·6 MeV measurement.

---

* Communicated by the Authors.

## § 2. Description and Performance of Counter

The counter is cylindrical, of length 30 cm and internal diameter 9·1 cm. A tungsten wire of diameter 40 $\mu$ is taken through a Kovar-glass seal inside a 1·5 mm diameter copper capillary tube, hangs along the axis of the counter and is kept taut by a nickel weight; 18 cm of wire is exposed within the counter. The outer pressure chamber is made from stainless steel 1/16 in. thick and lined with a graphite cylinder and end-plates, also of 1/16 in. thickness, which form the cathode surface of the counter. This lining prevents charged particles, produced in the steel walls, from entering the sensitive region. The only important reaction occurring in the graphite at these energies is the reaction under study and consideration of the maximum depth at which a photodisintegration event could occur and still lead to the dissipation of more than 5 mev in the active volume shows that $<0{\cdot}1\%$ of observed pulses are due to reactions occurring in the graphite walls. Attached to the main chamber is a gas purifier of the circulation type containing evaporated sodium metal. This reacts strongly with water vapour and oxygen, the two most objectionable of the common electronegative counter gas contaminants, but does not react with methane. Gas is pumped in and out of the counter through two needle valves, the moving parts of which are enclosed in bronze sylphon bellows to prevent grease from coming into contact with the gas.

The filling procedure was as follows: the air in the counter was replaced by methane and a pellet of sodium dropped into the purifier. The methane was then pumped out until a pressure of $\sim 10^{-4}$ mm Hg was obtained when the sodium was evaporated on to the walls of the purifier tube. Pumping was then continued for half a day, the chamber being outgassed periodically by heating with a flame. Methane was then allowed to pass slowly through a copper coil immersed in solid carbon dioxide and acetone to freeze out water vapour and was admitted to the counter until the pressure reached 2·38 atmospheres.

At this pressure and at the working voltage of 2·4 kv the gas multiplication of the counter was found to be 3 times. The counter pulses observed on an oscilloscope had rise times between 10 and 100 $\mu$sec—a rather greater spread than expected. According to measurements by English and Hanna (1953) of electron mobilities in methane, the spread due to electron straggling would have been expected to be $\sim 3$ $\mu$sec; this difference was not investigated and is not understood. To handle the long pulses satisfactorily rise and clipping time constants of 80 $\mu$sec were used in the amplifier, the output of which was fed to a 120 channel pulse amplitude analyser.

An energy calibration for the counter was obtained using the spectrum of $\alpha$-particles from Th-X and its daughter products decaying with a half-life of 3·65 days. A small amount of polonium was included in the counter to give a continuous check on the calibration. The energy scale was found to be linear to within 1%.

## § 3. THE COUNTER EXPERIMENT

Resonance radiation from the $^7$Li(p$\gamma$) reaction was excited by bombarding a thick lithium metal target with 500 kv protons, the counter being situated with its axis perpendicular to the proton beam, and centre 10·8 cm from the target at 0°. Irradiation was carried out in 8 hour runs, alternating with background runs of similar duration; the $^{12}$C($\gamma 3\alpha$) counting rate was small ($\sim$140 per hour) necessitating a careful measurement of the counter background. Actually the $^{12}$C($\gamma 3\alpha$) peak produced by the 17·6 MeV $\gamma$-rays yields $\alpha$-particles with a total energy of 10·3 MeV, well above the energy of the background due to radioactive contamination, and in 44 hours no background pulses over 9·2 MeV were observed. However, a knowledge of the background, mainly from polonium (100 counts/hour) and radium (20 counts/hour), was important in an analysis of the tail of the 17·6 MeV peak and of peaks due to lower energy $\gamma$-rays.

The radiation was monitored using a thick-walled brass Geiger-counter identical in construction with that described and calibrated by Barnes *et al.* (1952). Readings of pulse counts were recorded at one hour intervals. The relative photodisintegration yield per quantum in the four runs was 1·00 : 1·00 : 1·06 : 0·96.

## § 4. THE CROSS SECTION AT 17·6 MeV

The pulse spectrum resulting from 31 hours irradiation is shown in fig. 1 (*a*) which, after subtraction of the background given in 1 (*b*), leads to the curve of 1 (*c*). The high energy peak contains approximately 2900 counts, has a half-width of 0·8 MeV, and centres at 10·30$\pm$0·06 MeV as expected from the mass data which gives the reaction threshold as 7·28 MeV. Contributions to the spectrum below the main peak come from $\gamma$-ray pile-up pulses, $\alpha$-particles from 17·6 MeV events which are not contained entirely within the counting region, and $^{12}$C($\gamma 3\alpha$) events induced by $\gamma$-rays of energies less than 17·6 MeV. The contribution from $\gamma$-ray pile-up pulses was estimated by extrapolating the low energy tail measured with the kicksorter bias at a reduced value. The ‘ pile-up ’ pulse contribution, although small was significant, amounting to 130 counts per channel at 5 MeV, decreasing to 10 counts per channel at 8 MeV for a 31 hour run.

To allow for losses to the walls a knowledge of the ranges and directions of the $\alpha$-particles is necessary. The correction applied assumes the disintegrations to be two-stage:

$$^{12}\mathrm{C} \rightarrow \alpha + {}^{8}\mathrm{Be}\,; \qquad {}^{8}\mathrm{Be} \rightarrow 2\alpha$$

and to be isotropic, with 93% of the transitions through the 2·9 MeV level of $^8$Be, and the remaining 7% through the ground state. A range–energy relation for $\alpha$-particles in methane was deduced from the curves of Livingstone and Bethe (1937) and correction factors were derived from those for single α-particles to give the fraction of events in which one or two α-particles of a star intercept the boundaries of the counter. The energy distribution of the resulting degraded pulses was calculated and amounts to approximately 42 counts per channel between 6 and 9·5 MeV. The shape of the distribution has little effect on the magnitude of the peak at 17·6 MeV, but makes the yield at lower energies uncertain and it is for

**Fig. 1**

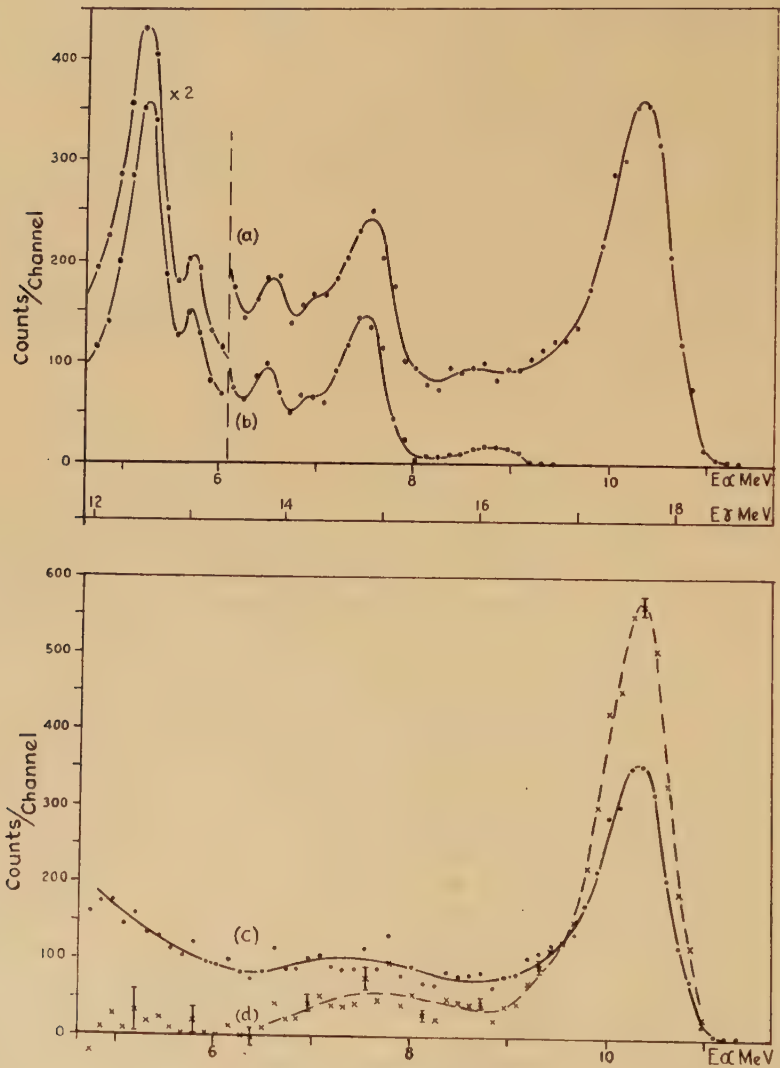

Counter experiment.

(*a*) Pulse spectrum obtained in 31 hours irradiation of $CH_4$ counter. (*b*) Counter background spectrum normalized to 31 hours running time. (*c*) Pulse spectrum resulting from disintegration of $^{12}C$ (difference of (*a*) and (*b*)). (*d*) Corrected distribution.

this reason that the cross section at 17·6 Mev only has been calculated from the counter data.

The final distribution fig. 1 (*d*) was derived from fig. 1 (*c*) by subtracting the 'pile-up' pulse distribution and the pulse distribution arising from wall losses and then adding the loss corrections at the appropriate energy to the 17·6 Mev peak. The peak is asymmetrical probably because the amplifier time constants were shorter than the rise-times of some of the pulses; the value 80 $\mu$sec was chosen for the time constants to give the best compromise between lack of uniformity in pulse height and difficulties due to the $\gamma$-ray 'pile-up' pulses.

A small correction for absorption of radiation in the counter walls was calculated from data given by Heitler (1949). The intensities of the $\gamma$-ray lines were assumed to be in the ratio 17·6 : 14·8 : 12·3 :: 0·62±5% : 0·36±12% : 0·02±50%, the first two being based on data of Stearns and McDaniel (1951) the last figure being based on Inall (1954) and Titterton (1953).

The final value for the cross section at 17·6 Mev is

$$\sigma_{17\cdot6}(^{12}C\gamma 3\alpha)=(1\cdot70\pm0\cdot24)\times10^{-28}\ \mathrm{cm}^2.$$

Table 1. Absolute measurements of the cross section for $^{12}C(\gamma 3\alpha)$

| Author | $\sigma_{\mathrm{mean}}$ | $\sigma_{17\cdot6}$ |
|---|---|---|
| Wäffler and Younis (1949) | $0\cdot8\pm0\cdot3\times10^{-28}$ cm² | |
| Glattli, Seippel and Stoll (1952) | $1\cdot75\pm0\cdot25$ | $2\cdot4\times10^{-28}$ cm² |
| Goward and Wilkins (1953)* | $1\cdot4\pm0\cdot26$ | $1\cdot70\pm0\cdot34$ |
| Greenberg, Taylor and Haslam (1954)† | | 1·7 |
| Present work | $1\cdot19\pm0\cdot20$ | $1\cdot70\pm0\cdot24$ |

* Combination of lithium $\gamma$-rays and bremsstrahlung measurements.

† Bremsstrahlung measurement.

The value for $\sigma_{17\cdot6}$ from Li $\gamma$-rays depends on the relative intensity assumed for the 17·6 Mev line which is not the same in the experiments listed.

## § 5. Photographic Plate Measurements

Incidental to another investigation some 1000 $^{12}C(\gamma 3\alpha)$ 'stars' were measured in Ilford 200 $\mu$ type $E_1$ boron-loaded emulsions which had been exposed to $^7Li(p\gamma)$ resonance radiation. The stars were identified by the usual method of momentum balance and the number-energy histogram is given in fig. 2 (*a*). Three peaks are resolved, the main one at 17·6 Mev contains 742 events, the broad 14·8 Mev group has 86 events while the group centring on 12·5 Mev has 17 events. These numbers may be compared with 2160, 300, 35 observed by Nabholz *et al.* (1952) and 390, 50, 12 observed by Goward and Wilkins (1953).

Loss corrections were made by the geometric method of Goward and Wilkins (1953) and the smooth distribution (full line of fig. 2 (*a*)) obtained. The final result is compared with the methane chamber data in fig. 2 (*b*), the curves being normalized by the area of the 17·6 MEV peaks.

Fig. 2

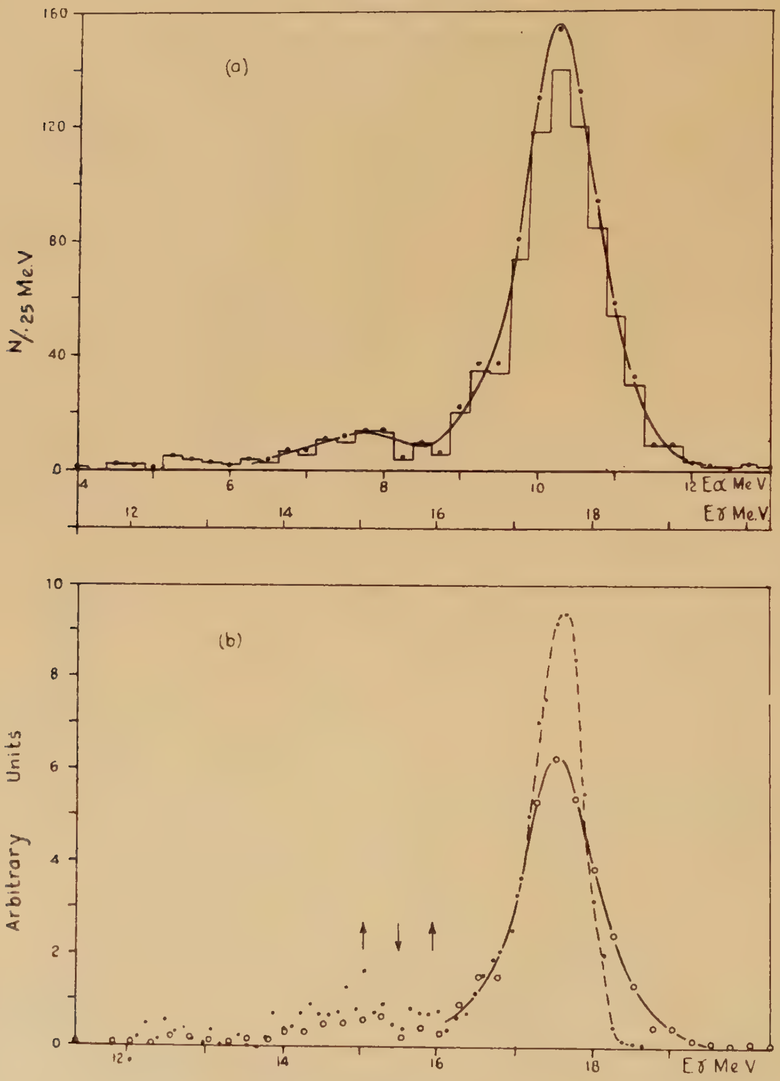

Photographic plate.

(*a*) Histogram of energy released in 845 $^{12}C(\gamma 3\alpha)$ ' stars ' with corrected curve superimposed. (*b*) Comparison of results from methane counter and photographic plate normalized by areas of the high energy peak. • counter, ∘ plate.

## § 6. CROSS SECTIONS AT 14·8 AND 12·3 MEV

Taking the cross section at 17·6 Mev to be $1{\cdot}70 \times 10^{-28}$ cm² and the relative intensities of the 17·6 and 14·8 Mev lines to be as given in § 4 the photographic plate data gives :

$$\sigma_{14{\cdot}8}(^{12}C\gamma 3\alpha) = (0{\cdot}33 \pm 0{\cdot}07) \times 10^{-28}\ \text{cm}^2.$$

The group centring on 12·5 Mev in fig. 2 (*a*) could be due to a reaction of the type $^{12}C(\gamma\gamma')3\alpha$, if a level of $^{12}C$ is available at the appropriate energy. However there is strong evidence from experiments in this laboratory (Titterton 1953, Inall and Boyle 1953, Inall 1954) that there is a weak line at 12·3 Mev corresponding to a transition to a state of $^{8}Be$ at 5·3 Mev. We therefore discard the possibility that the group may be due to the inelastic scattering of $\gamma$-rays and calculate the cross section for the $^{12}C(\gamma 3\alpha)$ reaction at 12·3 Mev taking the intensity of these $\gamma$-rays to be $(2 \pm 1)\%$ of the total radiation. The figure obtained is :

$$\sigma_{12{\cdot}3}(^{12}C\gamma 3\alpha) = (1{\cdot}15 \pm 0{\cdot}6) \times 10^{-28}\ \text{cm}^2.$$

Using the same set of conditions and normalizing all cross sections to our 17·6 Mev figure, cross sections at 14·8 and 12·3 Mev have been calculated from the histograms published by Nabholz *et al.* (1952) and Goward and Wilkins (1953) and are presented in table 2. It will be seen that there is good agreement among the three experiments for the cross section at 14·8 Mev but considerable differences at 12·3 Mev.

Table 2. Cross section for $^{12}C(\gamma 3\alpha)$ at 14·8 and 12·3 Mev, normalized to $\sigma_{17{\cdot}6} = 1{\cdot}70 \times 10^{-28}$. The lower two sets of results were calculated from the published histograms. The relative $\gamma$-ray intensities used are :

$I(17{\cdot}6\ \text{Mev}) = 0{\cdot}62 \pm 5\%$ $I(14{\cdot}8\ \text{Mev}) = 0{\cdot}36 \pm 12\%$ $I(12{\cdot}3\ \text{Mev}) = 0{\cdot}02 \pm 50\%$

| Source | Cross section × relative $\gamma$-ray intensity | | | Cross section in $10^{-28}$ cm² | | | Mean |
|---|---|---|---|---|---|---|---|
| | 17·6 Mev | 14·8 Mev | 12·3 Mev | 17·6 Mev | 14·8 Mev | 12·3 Mev | |
| Present work, $CH_4$ counter | 1·05 | | | 1·70 ± 0·24 | | | |
| Present work | 1·05 ± 2·3 | 0·118 ± 7 | 0·023 ± 16 | | 0·33 ± 0·07 | 1·15 ± 0·6 | 1·19 ± 0·20 |
| Nabholz *et al.* | 1·05 ± 1·4 | 0·144 ± 3·7 | 0·015 ± 11·5 | | 0·40 ± 0·8 | 0·75 | 1·21 ± 0·20 |
| Goward and Wilkins | 1·05 ± 3·2 | 0·130 ± 9 | 0·032 ± 20 | | 0·36 ± 0·07 | 1·6 | 1·21 ± 0·20 |

The high value of $\sigma_{12{\cdot}3}$ implies the presence of a $^{12}C$ level in this region and the resonance absorption of radiation of this energy. Such an interpretation is supported by some of the bremsstrahlung data and by results obtained in a study of the reaction $^{12}C(nn')3\alpha$ by Livesey and

Smith (1953). Excitation functions over the region 12–18 mev have been measured with poor agreement by five groups and are presented in fig. 3 ; the present three points have been plotted for comparison.

Inspection of both the methane chamber and the photoplate data over the width of the 14·8 mev line, fig. 2 (*b*), shows elevation of the points near 15 and 16 mev and a trough at 15·5 mev as indicated by the arrows. Taken separately little weight could be placed on either result, but the two sets of data support each other. Moreover, examination of the photoplate results of Goward and Wilkins (1953) and Nabholz *et al.* (1952) show the same features to be present in each of these experiments. Taken together these results lend support to the presence of peaks in the cross section at 15 mev and 16 mev as observed by Goward and Wilkins (fig. 3) but suggest that the resonances are more marked than their excitation function indicates.

Fig. 3

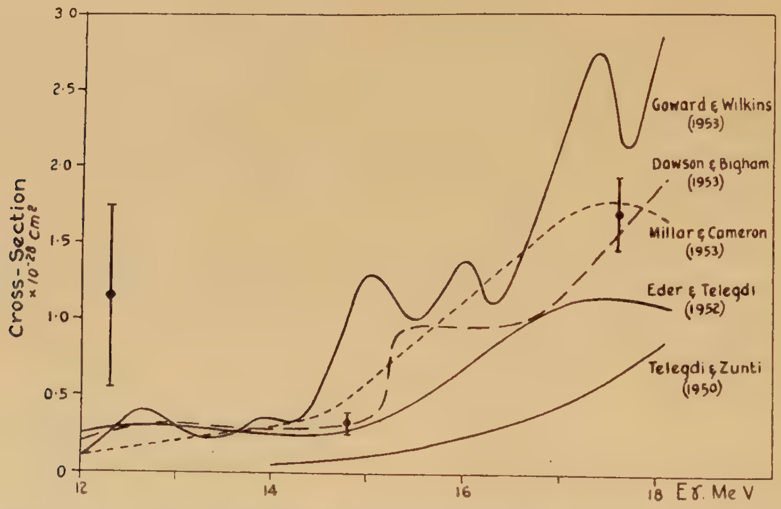

Cross sections for the reaction $^{12}C(\gamma 3\alpha)$ over the region 12–18 mev. ⌶ present results plotted.

The present experiment therefore gives strong evidence for the resonance absorption of γ-radiation by the $^{12}C$ nucleus near to 12·3 mev and suggests the presence of other resonances near 15 and 16 mev.

## References

Barnes, C. A., Carver, J. H., Stafford, C. H., and Wilkinson, D. H., 1952, *Phys. Rev.*, **86**, 359.
Dawson, W. K., and Bigham, C. B., 1953, *Canad. J. Phys.*, **31**, 167.
Eder, M., and Telegdi, V. L., 1952, *Helv. Phys. Acta*, **25**, 55.
English, W. N., and Hanna, G. C., 1953, *Canad. J. Phys.*, **31**, 768.
Glattli, H., Seippel, O., and Stoll, P., 1952, *Helv. Phys. Acta*, **25**, 491.
Goward, F. K., and Wilkins, J. J., 1953, *Proc. Roy. Soc.* A, **217**, 357.

GREENBERG, L. H., TAYLOR, J. G. V., and HASLAM, R. N. H., 1954, *Phys. Rev.*, **95,** 1540.
HEITLER, W., 1949, *The Quantum Theory of Radiation*, 2nd Ed. (Oxford: University Press).
INALL, E. K., and BOYLE, A. J. F., 1953, *Phil. Mag.*, **44,** 1081.
INALL, E. K., 1954, *Phil. Mag.*, **45,** 768.
LIVESEY, D. L., and SMITH, C. L., 1953, *Proc. Phys. Soc.* A, **66,** 689.
LIVINGSTON, M. S., and BETHE, H. A., 1937, *Rev. Mod. Phys.*, **9,** 245.
MILLAR, C. H., and CAMERON, A. G. W., 1953, *Canad. J. Phys.*, **31,** 723.
NABHOLZ, H., STOLL, P., and WAFFLER, H., 1954, *Helv. Phys. Acta*, **25,** 153.
STEARNS, M. B., and MCDANIEL, B. D., 1951, *Phys. Rev.*, **82,** 450.
TELEGDI, V. L., and ZUNTI, W., 1950, *Helv. Phys. Acta*, **23,** 745.
TITTERTON, E. W., 1953, *Aust. J. Science*, **15,** 174; 1955, *Progress in Nuclear Physics IV* (London: Pergamon Press).
WAFFLER, H., and YOUNIS, S., 1949, *Helv. Phys. Acta*, **22,** 614.

# XCVI. *On the Gravitational Effects of Distant Rotating Masses*

By L. Bass and F. A. E. Pirani
Dublin Institute for Advanced Studies, Dublin*

[Received April 28, 1955]

## Summary

Thirring's calculation of the gravitational field near the centre of a rotating spherical shell is corrected and elaborated. First, an additional term, representing elastic stresses, is introduced into the energy-momentum tensor; without this term the conservation laws cannot be fulfilled and the shell could not keep together during rotation. Secondly, the dependence of the gravitational effects on the mass-distribution over the shell is investigated. The quasi-centrifugal forces are to be attributed entirely to the mass-distribution on the shell arising from the mass-increase with velocity.

## § 1. Introduction

In a classical paper, H. Thirring (1918, with minor corrections 1921) calculated the gravitational field near the centre of a rotating thin spherical shell, using Einstein's field equations in the linear approximation (Einstein 1916). Thirring found that the rotating shell produces near its centre forces analogous to the Coriolis and centrifugal forces which arise in rotating reference frames in classical mechanics—his aim was to confirm by an example that Einstein's theory embodies Mach's principle of the relativity of inertia.

However, as Professor C. Lanczos has kindly pointed out to us,† there is an inconsistency between Thirring's assumptions. Thirring assumes that the material of the shell is incoherent, so that its energy-momentum tensor has the form‡

$$T^{\mu\nu}=\rho v^{\mu}v^{\nu} \quad . \quad . \quad . \quad . \quad . \quad . \quad . \quad . \quad (1)$$

where $\rho$ is the density, $v^{\mu}=dx^{\mu}/ds$ the 4-velocity of the matter composing the shell. Thirring proceeds to calculate approximately the gravitational field near the centre of the shell, working to the second order in the angular velocity $\omega$ of the shell, and neglecting the self-gravitation of the shell itself. But to this approximation, the conservation law§

$$T^{\mu\nu}{}_{;\nu}=0 \quad . \quad . \quad . \quad . \quad . \quad . \quad . \quad . \quad . \quad . \quad (2)$$

---

* Communicated by the Authors.

† Private communication.

‡ Greek suffixes range and sum over 1, 2, 3, 4. The units are grams, centimetres and light-seconds, so that $c=1$. The coordinate $x^4=it$ is purely imaginary, the other coordinates real, and the metric has signature $+4$.

§ A semi-colon (;) denotes covariant differentiation.

is not satisfied; if (2) is to be satisfied by (1), the incoherent particles cannot move in circular paths, but must follow geodesics, which is to say that a shell of *incoherent* matter, if set in rotation, will fly apart along the tangents to these paths. To say that the shell should be regarded as composed of distant stars or galaxies is not to resolve the difficulty, because if there is no interaction between them then such stars or galaxies cannot follow the required paths.

This paper is concerned not with the cosmological significance of the problem, but only with the resolution of the inconsistency. This will be effected by supplementing the energy-momentum tensor (1) of incoherent matter by a term representing the 'elastic' interaction between particles of the shell.

In general, such a substitution would require a generally relativistic elasticity theory, but in the present case the symmetry and simplicity of the problem allow us, under natural physical assumptions, to determine uniquely the contribution of such an elastic interaction to the energy-momentum tensor, without developing such a theory.

## § 2. DEFINITION OF THE ENERGY-MOMENTUM TENSOR

We thus adopt for the total energy-momentum tensor of the material of the shell

$$T^{\mu\nu}=\rho v^{\mu}v^{\nu}+E^{\mu\nu}, \qquad \dots\dots\dots \quad (3)$$

where the added term $E^{\mu\nu}$ arises from elastic interactions.

It is clear from the discussion in § 1 that what is needed to hold the shell together is just a tangential stress along the parallels of latitude. One could simply assume this from the outset, and determine the magnitude of this stress from the conservation laws, thus arriving directly at eqns. (14) and (20) below. Alternatively, one may proceed from general assumptions about the properties of $E^{\mu\nu}$ (which would apply also in other circumstances), and show that under these assumptions only the tangential stress term affects the final results, in the approximation considered.

This alternative procedure will now be carried out, but the essential results (beginning with the line below eqn. (19)) can be understood without going through the details of the calculation.

The elastic term $E^{\mu\nu}$ is assumed to have the following properties, which are natural generalizations from classical elasticity theory:

(i) It is symmetric:

$$E^{\mu\nu}=E^{\nu\mu}. \qquad \dots\dots\dots \quad (4)$$

This is perhaps scarcely necessary to mention.

(ii) It has no component normal to the shell:

$$E^{\mu\nu}n_{\nu}=0, \qquad \dots\dots\dots \quad (5)$$

where at any point of the shell $n_{\nu}$ is a 4-normal to the world tube (3-surface) of the shell. This generalization of the corresponding condition in the ordinary theory may be regarded as an application to a thin shell of the continuity conditions of Synge and O'Brien (1952). Its physical meaning is that there is no transfer of elastic energy-momentum across the surface of the shell. Since $v^\mu$ lies in the world tube 3-surface, $v^\mu n_\mu=0$, so that

$$T^{\mu\nu}n_\nu=0,$$

as one would expect.

(iii) It has no component in the direction of motion of the shell:

$$E^{\mu\nu}v_\nu=0. \qquad (6)$$

There will in fact be a contribution to the energy-momentum tensor arising from the elastic energy. By considering an element of the shell in a local reference frame in which it is instantaneously at rest, one can see that this contribution is of the form $ev^\mu v^\nu$, where $e$ is the elastic energy density. This contribution may be incorporated into the kinetic energy-momentum term $\rho v^\mu v^\nu$, and the remainder will naturally satisfy eqn. (6). In general circumstances the term $ev^\mu v^\nu$ could not be neglected—the material density would have to be increased to take account of it—but in the considerations of § 3 it will be neglected, because it is proportional to the square of the stress and therefore of order $\omega^4$, where $\omega$ is the angular velocity of the shell, while the calculations are to be carried out only to order $\omega^2$.

(iv) Its physical components, in a local reference frame in which the relevant point of the shell is instantaneously at rest, are bounded:

$$E^{\mu\nu}h_\mu{}^{(\alpha)}h_\nu{}^{(\beta)}<A, \qquad (7)$$

($A$ a constant for the whole shell), where $h_\mu{}^{(\alpha)}$ denote $v_\mu$ and any three unit vectors orthogonal to $v_\mu$ and to each other.

Under these assumptions, $E^{\mu\nu}$ can be determined uniquely from the symmetry and steady state of the problem. This is a little surprising, since nothing has been assumed about the elastic properties of the shell.

Following Thirring, we consider a thin spherical shell of radius $a$, rotating with constant angular velocity $\omega$ in flat space-time (deviations from flatness due to the presence of the shell are neglected in the neighbourhood of the shell itself). The metric in spherical polar coordinates* is

$$ds^2=(dx^4)^2+(dr)^2+r^2(d\theta)^2+r^2\sin^2\theta(d\phi)^2. \qquad (8)$$

In this coordinate system, the velocity 4-vector of any point of the shell, for a uniform rotation about the axis $\theta=0$, is given by

$$\frac{v^1}{v^4}=\frac{dr}{dx^4}=0, \qquad \frac{v^2}{v^4}=\frac{d\theta}{dx^4}=0, \qquad \frac{v^3}{v^4}=\frac{d\phi}{dx^4}=\frac{\omega}{i}, \qquad (9)$$

so that

$$v^3=-i\omega v^4, \quad (v^4)^2-\omega^2a^2\sin^2\theta(v^3)^2=-1, \qquad (10)$$

---

* Labelled 1, 2, 3, 4 in the order $r$, $\theta$, $\phi$, $x^4$.

and so

$$\left.\begin{array}{c} v^1=v^2=0, \qquad v^3=\omega\chi(\theta), \qquad v^4=i\chi(\theta) \\ \chi(\theta)=(1-\omega^2a^2\sin^2\theta)^{-1/2}. \end{array}\right\} \quad . \quad . \quad . \quad . \qquad (11)$$

In this coordinate system, the unit normal $n_\mu$ at any point of the shell has the covariant components (1, 0, 0, 0). Unit vectors $\lambda_\mu$, $\mu_\mu$ in the $\theta$ and $\phi$ directions have respectively the covariant components $(0, r^{-1}, 0, 0)$, $(0, 0, r^{-1}\operatorname{cosec}\theta, 0)$. Since any point of the shell can be brought instantaneously to rest by Lorentz transformation to a frame with relative velocity $\omega a\sin\theta$, it follows from (7) that the physical components of $E^{\mu\nu}$ must be bounded also in the reference frame defined by (8) (that is, in the Minkowskian frame in which the shell rotates about a fixed axis).

We now write down the conservation eqns. (2), simplified with the aid of conditions (i)–(iv). In these calculations, the density $\rho$ (which is constant in Thirring's work) will be allowed to depend on the latitude

$$\rho=\rho(\theta),$$

because this greater generality willl be required in the physical discussion at the end of § 3. By conditions (i)–(iv), the conservation equations become simply

$$\left.\begin{array}{r} E^{22}+\sin^2\theta(E^{33}+\rho\omega^2\chi^2)=0 \\ \tan\theta\,\partial E^{22}/\partial\theta+E^{22}-\sin^2\theta(E^{33}+\rho\omega^2\chi^2)=0 \\ \tan\theta\,\partial E^{23}/\partial\theta+3E^{23}=0 \\ \tan\theta\,\partial E^{24}/\partial\theta+E^{24}=0 \end{array}\right\}, \quad . \quad . \quad . \quad . \qquad (12)$$

since it is evident from the conditions of the problem that $E^{\mu\nu}$ is independent of $\phi$ and $t$.

Addition of the first two of eqns. (12) leads to

$$\frac{\partial}{\partial\theta}(\sin^2\theta E^{22})=0,$$

whence it follows from condition (iv) and the remark about it just after eqn. (11) above, that

$$E^{22}=0. \quad . \quad . \quad . \quad . \quad . \quad . \quad . \quad . \quad . \qquad (13)$$

From (13) and the first of (12),

$$E^{33}=-\rho\omega^2\chi^2, \quad . \quad . \quad . \quad . \quad . \quad . \quad . \qquad (14)$$

and by (6)

$$E^{34}=-i\rho\omega^3a^2\sin^2\theta\chi^2, \quad . \quad . \quad . \quad . \quad . \quad . \quad . \qquad (15)$$

$$E^{44}=\rho\omega^4a^4\sin^4\theta\chi^2. \quad . \quad . \quad . \quad . \quad . \quad . \quad . \qquad (16)$$

The third and last of (12) are equivalent to

$$\frac{\partial}{\partial\theta}(\sin^3\theta E^{23})=0, \qquad \frac{\partial}{\partial\theta}(\sin\theta E^{24})=0,$$

which, by an argument analogous to that resulting in (13), lead to

$$E^{23}=0, \qquad \ldots \qquad (17)$$

$$E^{24}=0. \qquad \ldots \qquad (18)$$

Equation (5) implies that

$$E^{11}=E^{12}=E^{13}=E^{14}=0. \qquad \ldots \qquad (19)$$

Thus the elastic tensor $E^{\mu\nu}$ is prescribed completely. Rejecting all terms of order higher than the second in $\omega$, one is left with only one non-vanishing component of $E^{\mu\nu}$, namely $E^{33}$, given by (14). The only non-vanishing components of the *total* energy-momentum tensor $T^{\mu\nu}$ are now found from (3) to be

$$T^{34}=i\rho\omega, \quad T^{44}=\rho\chi^2. \qquad \ldots \qquad (20)$$

Transformation to rectangular coordinates

$$x=r \sin\theta \cos\phi, \qquad y=r \sin\theta \sin\phi, \qquad z=r \cos\theta$$

yields

$$T_{\mu\nu}=-\rho\chi^2 \begin{bmatrix} 0, & 0, & 0, & i\omega a \sin\theta \sin\phi \\ 0, & 0, & 0, & -i\omega a \sin\theta \cos\phi \\ 0, & 0, & 0, & 0 \\ i\omega a \sin\theta \sin\phi, & -i\omega a \sin\theta \cos\phi, & 0, & 1 \end{bmatrix}. \qquad \ldots \qquad (21)$$

Comparison with Thirring's expression for $T_{\mu\nu}$ (1918, eqn. (6)) shows that in the present reference frame, all components of the *total* stress vanish upon the introduction of $E^{\mu\nu}$. The elastic stresses are just balanced by the centrifugal forces acting on the shell.

## § 3. THE APPROXIMATE INTEGRATION OF THE FIELD EQUATIONS

In this section the influence of the rotating shell on the metric near its centre will be determined, up to order $\omega^2$ in the angular velocity. We shall only outline the calculations, which follow closely those in Thirring's papers (1918, 1921), where the details may be found. Let the linear approximation to the field be given by

$$\left.\begin{aligned} g_{\mu\nu}&=-\delta_{\mu\nu}+\gamma_{\mu\nu} \\ \gamma_{\mu\nu}&=\gamma_{\mu\nu}'-\tfrac{1}{2}\delta_{\mu\nu}\gamma_{\alpha\alpha}' \end{aligned}\right\} \qquad \ldots \qquad (22)$$

where

and

$$\gamma_{\mu\nu}'=-\frac{k}{16\pi^2}\int\frac{T_{\mu\nu}(x, y, z, t-R)}{R}\,dV_0. \qquad \ldots \qquad (23)$$

Here $k$ is the Newtonian constant of gravitation and $R$ the distance from the (3-dimensional) volume element $dV_0=a^2\,da \sin\theta\, d\theta\, d\phi$ to the point $P$ near the centre of the shell where $\gamma_{\mu\nu}'$ is to be evaluated. The coordinates of $P$ shall be

$$x=r \sin\theta_0, \quad y=0, \quad z=r \cos\theta_0.$$

The expression $R^{-1}$ will be expanded in powers of $ra^{-1}$, powers higher than the second being neglected (cf. Thirring 1918, eqn. (9)). Thus

$$R^{-1}=a^{-1}\{1+ra^{-1}(\sin\theta\cos\phi\sin\theta_0+\cos\theta\cos\theta_0)-\tfrac{1}{2}r^2a^{-2}$$
$$+\tfrac{3}{2}r^2a^{-2}(\sin\theta\cos\phi\sin\theta_0+\cos\theta\cos\theta_0)^2\}. \quad . \quad . \quad . \quad . \quad (24)$$

Besides adding the elastic term to $T^{\mu\nu}$, we shall generalize Thirring's work in the following respect: we shall assume that the density of the material of the shell varies with the latitude according to

$$\rho=\rho_0(1+N\omega^2a^2\sin^2\theta_0), \quad . \quad . \quad . \quad . \quad . \quad . \quad (25)$$

where $\rho_0$ and $N$ are constants. Our purpose is to investigate the effects that would result from compensating the special-relativistic increase in mass of the moving shell. By a straightforward calculation of (23) from (21), (24) and (25), one finds for the components of the metric tensor near the centre of the shell (after a rotation about the $z$-axis to a general point $P$)

$$g_{\mu\nu}=\begin{bmatrix} -1-\frac{1}{2}\gamma_{44}' & 0 & 0 & \frac{4}{3}ikM\omega a^{-1}y \\ 0 & -1-\frac{1}{2}\gamma_{44}' & 0 & -\frac{4}{3}ikM\omega a^{-1}x \\ 0 & 0 & -1-\frac{1}{2}\gamma_{44}' & 0 \\ \frac{4}{3}ikM\omega a^{-1}y & -\frac{4}{3}ikM\omega a^{-1}x & 0 & -1+\frac{1}{2}\gamma_{44}' \end{bmatrix}. \quad . \quad . \quad . \quad . \quad (26)$$

where

$$\gamma_{44}'=4kMa^{-1}\{1+\tfrac{1}{3}\omega^2a^2+\tfrac{1}{15}(1+N)\omega^2(x^2+y^2-2z^2)\},$$

while

$$M=\int\rho\,dV_0=4\pi\rho_0a^2\,da\{1+\tfrac{1}{3}(1+2N)\omega^2a^2\} \quad . \quad . \quad (27)$$

is the total mass of the shell.

The equations of a geodesic near the centre of the shell reduce for small velocities to

$$\left.\begin{aligned} \ddot{x}&=-\tfrac{8}{3}kM\omega a^{-1}\dot{y}+\tfrac{2}{15}(1+N)kM\omega^2a^{-1}x \\ \ddot{y}&=\ \ \tfrac{8}{3}kM\omega a^{-1}\dot{x}+\tfrac{2}{15}(1+N)kM\omega^2a^{-1}y \\ \ddot{z}&=\qquad\qquad\qquad\ -\tfrac{4}{15}(1+N)kM\omega^2a^{-1}z \end{aligned}\right\} . \quad . \quad . \quad . \quad (28)$$

The 'Coriolis' force ($\omega$-terms) is naturally the same as that found by Thirring, since all the additional terms which we have introduced are of order $\omega^2$. The 'centrifugal' force ($\omega^2$-terms) has, compared with Thirring's, an additional factor $\frac{1}{2}(1+N)$. Thus for $N=0$ (the case considered by Thirring), the centrifugal force is just halved by the introduction of the stresses in the shell. The choice $N=-\frac{1}{2}$, which, as may be seen from (27) corresponds to a shell with total mass equal to that of a shell at rest with uniform density $\rho_0$, reduces the centrifugal force to one quarter of Thirring's result.

The most interesting case is

$$N=-1.$$

This corresponds to a mass distribution which just compensates for the special-relativistic increase in density, and represents a uniform mass distribution in the reference frame in which the shell is rotating. This choice leads, by (28), to the annihilation of both the radial and the axial 'centrifugal' forces, leaving the 'Coriolis' force intact.

Thus if Thirring's assumptions are modified merely by the introduction of the elastic stress term (which is essential if the conservation law is to be satisfied) the surviving $\omega^2$-terms in (28) may be attributed entirely to the variation in density between the poles of the shell and its equator (a consequence of the special-relativistic mass increase with motion) and may be abolished by giving the *rotating* sphere a uniform mass distribution. This makes the *signs* of the $\omega^2$-terms immediately plausible, as well as their independence of the sense of rotation.

If this clears up the appearance of an axial component (towards the centre) of the centrifugal force, unexpected and unwanted from the point of view of Mach's principle, it throws further doubt on the interpretation of the $\omega^2$-terms as an 'induced centrifugal force' as demanded by this principle (cf. Einstein 1945). We do not propose any resolution of this problem. If Newton's bucket of water rotates, and the stars are at rest, then the water rises up the sides of the bucket to a paraboloid. According to Mach, this situation is indistinguishable from that at which the bucket is at rest and the stars rotate about it. But in the case of the rotating shell problem the boundary conditions are always Minkowskian—only the shell spins, and not the 'distant' stars.

## ACKNOWLEDGMENTS

We are indebted to Professors Lanczos and Schrödinger for helpful advice and discussions. The second author is indebted to the Royal Society of Canada for a Rutherford Memorial Fellowship during the tenure of which this work was carried out.

## REFERENCES

EINSTEIN, A., 1916, *Ann. Phys.*, **49,** 769 ; 1945, *The Meaning of Relativity*, 2nd edn. (Princeton : University Press), pp. 99 *et seq.*
O'BRIEN, S., and SYNGE, J. L., 1952, *Comm. Dublin Institute for Advanced Studies* A, No. 9.
THIRRING, H., 1918, *Phys. Z.*, **19,** 33 ; 1921, *Ibid.*, **22,** 29.

# XCVII. *A Rotating-Lobe Interferometer and its Application to Radio Astronomy*

By R. Hanbury Brown, H. P. Palmer and A. R. Thompson
Jodrell Bank Experimental Station, Lower Withington, Macclesfield, Cheshire*

[Received November 20, 1954 ; revised April 3, 1955]

### Abstract

An interferometer, operating on the rotating-lobe principle, is described. It is shown how the frequency of the interference patterns observed from discrete radio sources may be controlled and made independent of the baseline length and direction. The application of the instrument to observations with a short north–south baseline and a long (630 $\lambda$) baseline is illustrated by experimental results. It is pointed out that the use of this technique is of particular value for the observation of weak sources with long baselines.

## § 1. Introduction

An important experimental problem in radio astronomy is to measure the apparent angular diameter and the distribution of intensity across the discrete sources. In general this measurement demands a high resolving power which can only be obtained by the use of an interferometer. It is the purpose of the present paper to describe an instrument which has been developed for this type of work and which has been termed a rotating-lobe interferometer. It is shown that the use of this instrument offers certain advantages over previous methods.

## § 2. The Principle of a Rotating-Lobe Interferometer

The principle of a rotating-lobe interferometer can be explained simply in terms of the effective polar diagram of the aerial system. Figure 1 represents two aerials A and B which are separated by a baseline of length $d$ and are connected by identical cables to a multiplier. In one of the two cables there is a continuously variable phase-shifter. If radiation from a distant point source is incident on the aerial system at an angle $\theta_0$ to the normal to the baseline, for any given value of the phase-shift $\phi$, the time-average of the multiplier output will be proportional to

$$P_s\,[g_A(\theta_0)\,g_B(\theta_0)]^{1/2}\cos\left[\frac{2\pi d}{\lambda}\sin\theta_0+\phi\right] \quad . \quad . \quad . \quad . \quad . \quad (1)$$

where $P_s$ represents the flux from the source and $g_A(\theta_0)$, $g_B(\theta_0)$ represent the power gains of the two aerials. The response of the whole system to a point source at any angle may therefore be represented as a polar diagram of lobes of alternate polarity as shown in fig. 2, the angular position of the central lobe of the pattern with respect to the normal being determined by the value of the phase-shift $\phi$.

---

* Communicated by Professor A. C. B. Lovell.

Fig. 1

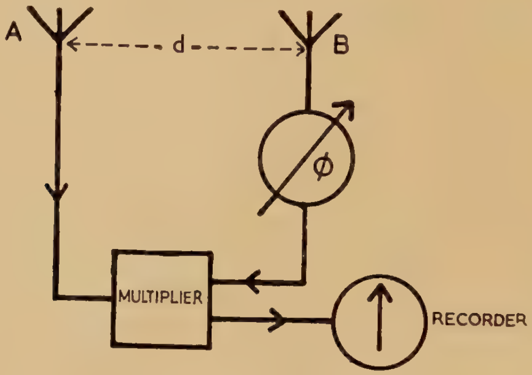

A simple form of interferometer.

Fig. 2

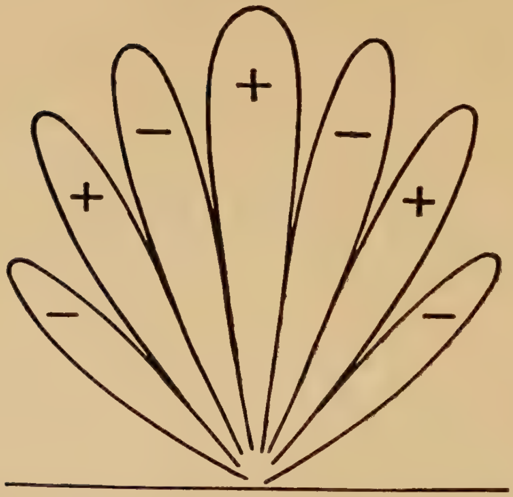

The effective polar diagram of reception of the simple interferometer shown in fig. 1.

As a discrete source transits the normal to the baseline, it will produce an interference pattern on the recorder with an apparent frequency $f_s$ given by

$$f_s \simeq \frac{1}{2\pi}\left[\omega_E \cdot \frac{d}{\lambda} \cdot \cos\delta\cos\alpha\right] \quad . \; . \; . \; . \; . \; . \; . \quad (2)$$

where $\omega_E$ radians sec$^{-1}$ is the rate of angular rotation of the earth, $\lambda$ is the wavelength, $\delta$ is the declination of the source and $\alpha$ is the angle between the direction of the base-line and a line east–west. If the value of $\phi$ is now made to vary slowly with time at a rate $\omega_\phi$ radians sec$^{-1}$, then the lobes of the polar diagram will appear to rotate, while the envelope of their maxima remains stationary. Under these conditions the frequency of the output pattern is modified and becomes

$$f_s' \simeq \frac{1}{2\pi}\left[\omega_E \frac{d}{\lambda} \cos\delta \cos\alpha \pm \omega_\phi\right] \quad . \; . \; . \; . \; . \quad (3)$$

where the choice of sign depends upon the direction of rotation of the phase-shifter. It is therefore possible, by controlling both the speed and direction of the phase-shifter, to vary at will the frequency of the output pattern. Thus, by rotating the lobes in the same direction as the apparent angular motion of the source, the frequency of the pattern may be reduced indefinitely, while by rotating the lobes in the opposite direction, or more rapidly in the same direction, the frequency can be increased to any desired value. As discussed later this facility is of particular value when it is necessary to operate an interferometer with very short or very long baselines, or when the baselines are in a direction close to north–south.

## § 3. Description of a Practical Equipment

### 3.1. *A Simplified Outline*

A rotating-lobe interferometer can be constructed from a number of different circuit arrangements, since there are many ways* in which the relative phase of the signals from the two aerials may be varied. The choice of any particular arrangement must necessarily depend upon the use for which the instrument is intended. The instrument described here has been designed specifically to measure the distribution of intensity across both weak and intense sources, using baselines which may be of widely different lengths and oriented in any direction.

A simplified block diagram of the instrument is shown in fig. 3. A and B represent the two aerials which are connected by cables to separate receiving channels. The output from aerial A is amplified at the signal-frequency $f_0$ and fed to a mixer, where it is heterodyned by a local oscillator of frequency $f_1$. The output from aerial B is treated in the same way, except that the frequency of the local oscillator is $f_2$ and therefore differs from that used in the other channel. The outputs of the two mixers are amplified at intermediate-frequencies $(f_0-f_1)$, $(f_0-f_2)$, and are combined in a detector to form a beat-frequency $(f_1-f_2)$. This beat-frequency is amplified and rectified in a phase-sensitive rectifier. The reference voltage of the phase-sensitive rectifier is generated by combining the two local oscillators in a mixer; the beat-frequency between the oscillators is then fed through a continuously variable phase-shifter to operate the rectifier. The output of the phase-sensitive rectifier is passed through a time-constant and is displayed in the usual way on a pen recorder.

---

* An interferometer using a rotating phase-shifter in one aerial, but no phase-sensitive rectifier, has been described by Little and Payne-Scott (1951). Also Bolton and Slee (1954) have used an interferometer in which the relative phase of the local oscillator at two mixers was varied slowly to produce a moving lobe-pattern.

Following the method used above it is convenient to discuss the operation of this system in terms of its effective polar diagram of reception. The use of two local oscillators of different frequency may be regarded as a method of introducing a continuous variation of $2\pi\ (f_1-f_2)$ radians sec$^{-1}$ into the relative phase of the signals from the two aerials. Thus the lobes of the polar diagram appear to rotate at $\lambda/d\ (f_1-f_2)$ radians sec$^{-1}$, and a discrete source in transit will produce an alternating component in the output of the detector given by

Fig. 3

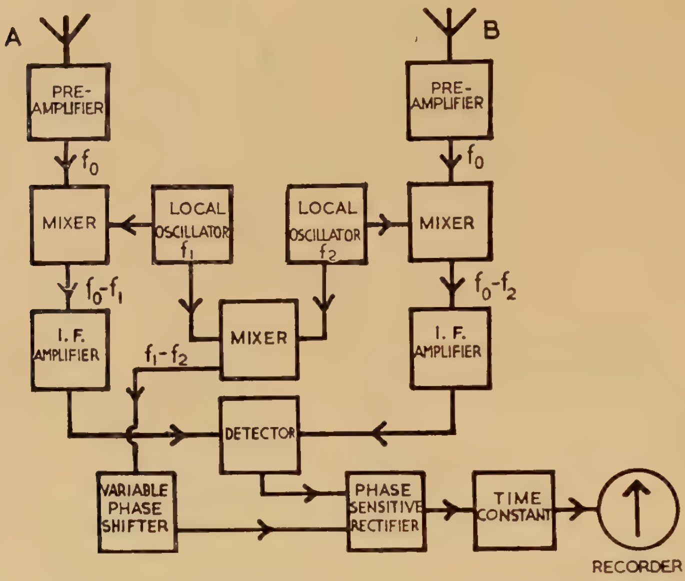

A simplified block diagram of the interferometer.

$$P_s\,[g_A(\theta_0)\,g_B(\theta_0)\,G_A\,G_B]^{1/2}\cos\left[\omega_E\frac{d}{\lambda}\,.\cos\delta\cos\alpha\pm2\pi\,(f_1-f_2)\right]t \quad . \quad (4)$$

where $G_A$, $G_B$ are the power gains of the two channels.

The output of the phase-sensitive rectifier is proportional to the amplitude of the input wave and to the cosine of the phase-angle between this wave and the reference voltage. It therefore consists of an alternating component of low-frequency given by

$$P_s\,[g_A(\theta_0)\,g_B(\theta_0)\,G_A\,G_B]^{1/2}\cos\left[\omega_E\frac{d}{\lambda}\,.\cos\delta\cos\alpha\pm\omega_\phi\right]t \quad . \quad . \quad (5)$$

where $\omega_\varphi$ is the rate of change of the phase of the reference voltage and the choice of sign depends upon the direction of the phase-shifter.

A comparison of eqns. (4) and (5) shows that the use of a phase-sensitive rectifier brings the rotating lobes apparently to rest, and that the frequency of the interference pattern is determined in the usual way by the rotation of the earth if the phase-shifter is stationary. If, however, the phase-shifter is varied, then the angular frequency of the pattern is changed by the same amount. Thus it follows from eqns (3) and (5) that the phase-shifter shown in fig. 3 may be used to control the frequency of the interference pattern in precisely the same way as a phase-shifter is one aerial cable (fig. 1).

### 3.2. *Some Details of the Apparatus*

A schematic diagram of the complete apparatus is shown in fig. 4; although it differs in detail from the simple scheme in fig. 3, the principle

Fig. 4

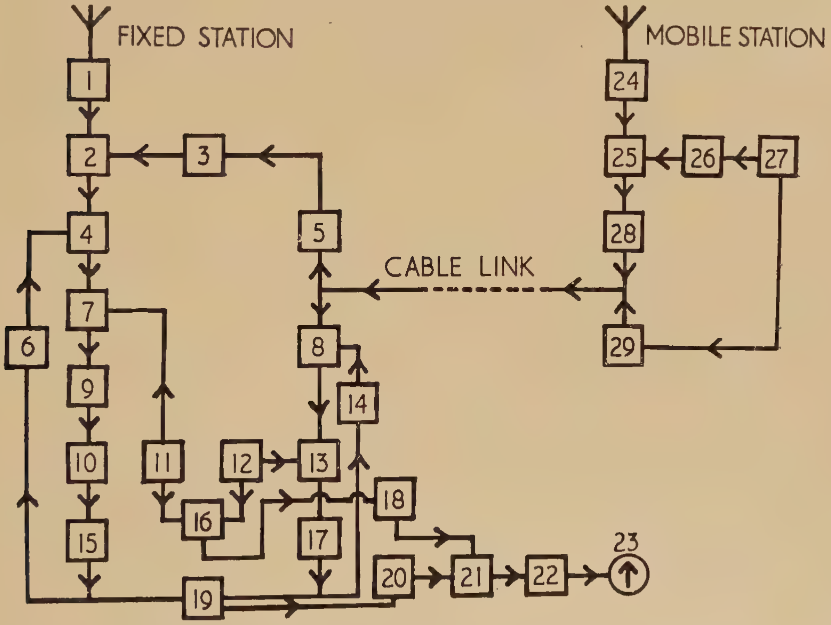

A complete block diagram of the interferometer.

(1) Preamplifier (158·2 Mc/s); (2) First mixer; (3) Frequency multiplier (×12); (4) Intermediate frequency amplifier (10 Mc/s); (5) Amplifier (14·02 Mc/s); (6) Automatic gain control; (7) Second mixer; (8) Intermediate frequency amplifier (10 Mc/s); (9) Intermediate frequency amplifier (3·76 Mc/s); (10) Delay cable; (11) Crystal oscillator (6·240 Mc/s); (12) Crystal oscillator (6·241 Mc/s); (13) Second mixer; (14) Automatic gain control; (15) Intermediate frequency amplifier (3·76 Mc/s); (16) Mixer; (17) Intermediate frequency amplifier (3·76 Mc/s); (18) Magslip phase-shifter driven by velodyne; (19) Multiplier; (20) Selective amplifier (1000 c/s); (21) Phase-sensitive rectifier; (22) Time-constant; (23) Recorder; (24) Preamplifier (158·2 Mc/s); (25) First mixer; (26) Frequency multiplier (×12); (27) Crystal oscillator (14·02 Mc/s); (28) Intermediate frequency amplifier (10 Mc/s); (29) Amplifier (14·02 Mc/s).

of operation is unchanged. The equipment is divided into a fixed and a mobile station. The signal received at the mobile station is heterodyned to a convenient intermediate frequency (10 Mc/s) and is transmitted over a coaxial cable together with the fundamental frequency of the local oscillator. At the fixed station this signal is amplified at 10 Mc/s and fed to a second mixer ; the local-oscillator fundamental is multiplied and used to heterodyne the signal received by the aerial at the fixed station. This latter signal is also amplified at 10 Mc/s and fed to a second mixer. The frequency difference between the two channels is introduced at the second mixers by the use of two second local oscillators which differ in frequency by about 1000 c/s. The signals are then amplified at the second intermediate frequency and are combined in a multiplier. The signal from the fixed aerial is delayed in the second intermediate frequency amplifier to compensate for the delay in the signal from the mobile aerial. The output of the multiplier contains a beat-frequency of 1000 c/s which is amplified in a selective amplifier and applied to a phase-sensitive rectifier. The beat-frequency between the two second local-oscillators is formed in a separate mixer and is fed to the phase-sensitive rectifier through a rotating magslip phase-shifter driven at an adjustable speed by a velodyne motor.

## § 4. The Equipment in Operation

The instrument described above was designed to measure the apparent angular diameter of the discrete sources observed in a previous survey with the large fixed paraboloid (218 ft.) at Jodrell Bank. For the present purpose the large paraboloid was used as the fixed aerial of the interferometer and the mobile aerial usually consisted of a small array of about 35 m$^2$ aperture ; however, for observations of the most powerful sources the mobile aerial was occasionally a single dipole. The measurements were carried out by observing the sources with baselines of different length and direction as they transited the meridian, and their apparent angular diameter was found from the well-known relation between the distribution of intensity across a source and the relative amplitude of the interference pattern at different aerial spacings.

The results of the first series of measurements have already been reported (Hanbury Brown, Palmer and Thompson 1954). It was found that several of the intense sources have angular diameters of the order of one or two degrees, hence these sources were completely resolved with baselines of less than about 60 $\lambda$. On the other hand a number of the sources, particularly those at high galactic latitudes, showed little trace of being resolved with a baseline of 500 $\lambda$.

These preliminary measurements illustrate clearly the need for an interferometer which will operate over a wide variety of baseline lengths ; furthermore since the sources may not be radially symmetrical, as in the case of the intense source in Cygnus, it is essential that the instrument should operate with a baseline in any direction. Equation (2) shows that, if the frequency of the pattern is determined only by the rotation of the earth, then it is proportional to the length of the baseline and to the cosine of the angle between the baseline and a line east–west. Thus for very short baselines, or for baselines close to north–south, the frequency of the pattern is low. If the baseline is comparable in length with the aperture of either of the aerials, it becomes difficult in practice to measure the amplitude of the interference pattern during the transit of the source through the aerial beam. Conversely, if the baseline is long, the frequency of the pattern becomes inconveniently high and it is necessary to reduce the time-constant of the receiver output. Since the signal-to-noise is proportional to the square-root of the time-constant, it follows that, for long baselines, the overall sensitivity of the equipment will be reduced.

Fig. 5

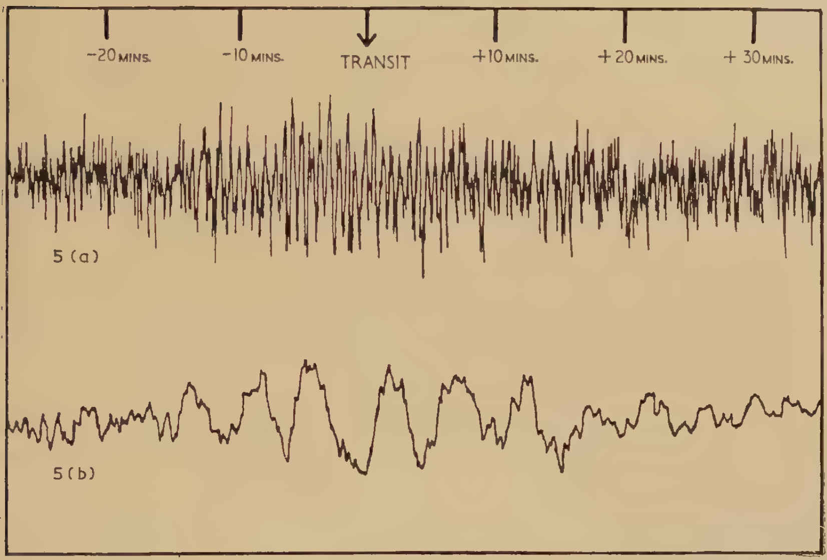

The use of a rotating lobe interferometer to decrease the frequency of an interference pattern.

(*a*) Record of a weak source observed with a baseline of 630 $\lambda$ in a direction east and west, taken with the phase-shifter stationary. The output time constant is 4 seconds.

(*b*) Record of the same source taken under identical conditions but with the phase-shifter rotating and decreasing the frequency of the pattern, and the output time constant increased to 30 seconds.

N.B. For both these records the 218 ft. paraboloid was used as one aerial of the interferometer. At a frequency of 158·2 Mc/s the beam is narrow and the interference pattern is therefore restricted to about 10 minutes on either side of transit.

Practical experience shows that the difficulties outlined above can be substantially reduced by the use of the equipment described in the present paper. Observations* have been made with baselines in several directions and with a variety of lengths between 21 λ and 630 λ. It was found that, with the exception of very short baselines as mentioned later, it was always possible to bring the frequency of the interference pattern to a convenient standard value by adjusting the speed and direction of the phase-shifter. As an example fig. 5 shows a record of a weak source observed with a baseline of 480 λ and with the phase-shifter stopped ; while fig. 5 (*b*) shows a record of the same source, taken under identical conditions, but with the phase-shifter adjusted to slow down the interference pattern to a convenient value, and a greater output time constant. It is clear that a considerable increase in the effective signal-to-noise ratio has been gained by the use of this technique.

Fig. 6

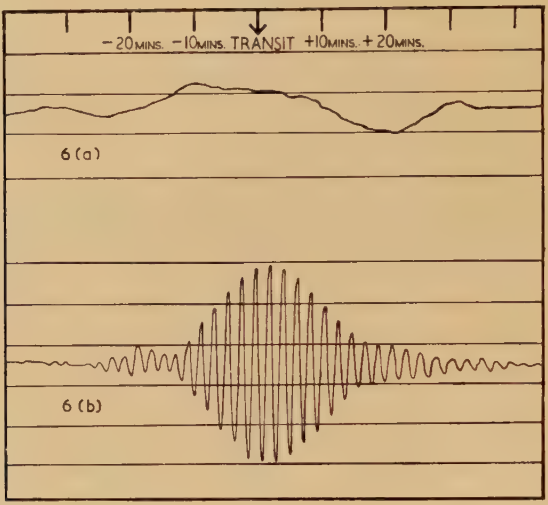

The use of a rotating lobe interferometer to increase the frequency of an interference pattern.

(*a*) A record of an intense source taken with a baseline 50 λ in a direction north–south and with the phase-shifter at rest in an arbitrary position.

(*b*) A record taken under identical conditions but with the phase-shifter rotating and increasing the frequency of the interference pattern.

As an example of the reverse operation, namely the speeding up of a pattern, fig. 6 (*a*) shows a record of the transit of the intense source in Cassiopeia made with a baseline of 50 λ oriented north–south and with the phase-shifter at rest in an arbitrary position. The amplitude of this pattern varies with the position of the phase-shifter and in the example shown it happens to be small. Figure 6 (*b*) shows a record of the same source made under identical conditions, but with the phase-shifter rotating at a speed chosen to give a pattern of convenient frequency.

---

* For observations with baselines exceeding 500 λ the cable was replaced by a radio link.

Although the equipment operated satisfactorily under nearly all conditions, some difficulty was experienced when the phase-shifter was used to increase the frequency of patterns from weak sources observed with very short baselines. Thus, when the aerials were separated by a distance of less than about 40 $\lambda$, approximately the diameter of the large paraboloid, a small and almost constant output was observed from the multiplier even in the absence of a source. If the phase-shifter was stationary, this output represented a small displacement of the zero of the records and was unimportant ; however, with the phase-shifter rotating, the output was converted to a sine-wave and tended to confuse the records of weak sources. It is to be expected that, when the baseline is comparable with the dimensions of the aerials, there should be an output due partly to receiver noise cross-coupled between the aerials and partly to the background radiation from the sky. This problem has not yet been investigated completely ; however it appears that in the present equipment the limitation is set by the considerable mutual impedance which exists, at close aerial spacings, between the mobile aerial and the elevated primary feed of the fixed paraboloid. The extent to which the performance at short baselines can be improved by reduction of this mutual impedance remains to be investigated.

## § 5. Discussion

In the simplest form of interferometer the output powers of two spaced aerials are added together, either before or after amplification, and the total power is recorded. Thus, in addition to the interference pattern produced by a discrete source, the output contains components proportional to the receiver noise and to the background radiation. The presence of these large components imposes serious limitations on the observation of weak sources and a considerable gain in effective sensitivity results from their removal. In principle this can be accomplished by the use of the simple system shown in fig. 1 in which the outputs of the two aerials are multiplied rather than added. But in practice this method is not attractive since the design of a satisfactory multiplier is difficult when the signal is very small compared with the noise.

An effective way of overcoming this difficulty has been developed by Ryle (1952) and is termed ‘ phase-switching ’. In this system the phase of one of the spaced aerials is reversed periodically by a mechanical switch and therefore, when the outputs of the two aerials are combined, signals which are mutually coherent in the two aerials produce switch-frequency components in the amplitude of the combined output. These components are selected from the output of the receiver and are rectified in a phase-sensitive rectifier operated in synchronism with the phase-reversing switch. It has been shown (Ryle 1952) that this system removes the mean value of the receiver noise and background radiation from the output of the phase-sensitive rectifier. It can also be shown that the effective polar diagram of the aerial system is a series of alternate positive and negative lobes similar to that shown in fig. 2.

The interferometer described in the present paper also eliminates the mean value of the unwanted components from the output. In fact the principles of operation of the present system and the phase-switching system are similar, and the latter may be regarded as a special form of rotating-lobe interferometer in which the lobes are rotated in discrete jumps rather than continuously. A comparison of the two systems suggests that, in general, the phase-switching technique is preferable for the precise measurement of the celestial coordinates of discrete sources. For this type of measurement it is essential to know the relative phase of the signals in the two aerials and, if the baseline is not too long, this can be best achieved by connecting the aerials to a common receiver through identical cables. Under these conditions phase-switching has the considerable practical advantage that it is much simpler to introduce a phase-reversing switch into one of the cables than a continuously variable phase-shifter. On the other hand, if the baseline is so long that separate amplifiers must be used for each aerial, or if a precise knowledge of the relative phase of the signals is unimportant, then the technique described in the present paper has certain advantages. For example the use of two local oscillators of different frequency is reasonably simple and avoids the use of a mechanical phase-reversing switch ; furthermore the frequency difference between these oscillators, which corresponds to the phase-switching frequency, is not limited by mechanical considerations.

The most interesting property of the present instrument, and one which offers the greatest potential advantage over previous methods, is the simplicity with which the frequency of the interference patterns can be controlled. This property is likely to prove useful for interferometers working on long wavelengths with restricted baselines, for the measurement of the intensity distribution across sources using baselines close to north–south, and for observations of weak sources, or the detailed structure of intense sources, with long baselines. The last of these applications, namely the use of long baselines, is of particular interest. Thus it follows from the analysis given above that, by the proper use of lobe-rotation technique, the resolving power of an interferometer can be increased without loss of sensitivity until the limit is set by other factors such as the instability of propagation.

## ACKNOWLEDGMENTS

The authors wish to thank Professor A. C. B. Lovell for his interest in this investigation. One of us (A. R. T.) is indebted to the Department of Scientific and Industrial Research for a maintenance grant.

## REFERENCES

BOLTON, J. G., and SLEE, O. B., 1954, Reported in *Special Report No.* 3, p. 44 (U.R.S.I. Brussels).

HANBURY BROWN, R., PALMER, H. P., and THOMPSON, A. R., 1954, *Nature, Lond.*, **173,** 945.

LITTLE, A. G., and PAYNE-SCOTT, R., 1951, *Aust. J. Sci. Res.* A, **4,** 489.

RYLE, M., 1952, *Proc. Roy. Soc.* A, **211,** 351.

# XCVIII. *The Surface Energies of the Alkali Metals*

By J. W. Taylor
Atomic Energy Research Establishment, Harwell*

[Received March 25, 1955]

## Abstract

The surface energies of the alkali metals sodium, potassium and lithium and their temperature coefficients have been measured experimentally. The values for lithium and sodium are in good agreement with similar theoretically calculated surface energies obtained by Stratton (1953). The disparity between the experimental and theoretical surface energy values for potassium and that between the experimental and theoretical temperature coefficients of the three metals is discussed.

## § 1. Introduction

A number of theoretical approaches have been made to the calculation of the surface energies of metals, but the final verification of such treatments was not possible due to the lack of accurately measured experimental values. In particular, experimentally determined surface energies for the metals lithium, sodium and potassium are germane since the physical basis of the majority of these calculations is most nearly fulfilled by these metals.

Prior to this study, experimental data on the surface energies of the three metals was incomplete. No measurements had been made on lithium and such values as existed for potassium (Quarterman and Primak 1950) were neither accurate nor comprehensive. The only accurate data for sodium was that reported by Poindexter and Kernaghan (1929) which leads to a surface energy value of 206 ergs/cm$^2$ at 98°c and a temperature coefficient of $-0{\cdot}05$ ergs/cm$^2$/°c. A second determination on sodium has recently been reported by Addison, Kerridge and Lewis (1954); their results are referred to subsequently.

The surface energies of the metals sodium, potassium and lithium have now been determined experimentally and these values allow a more exact comparison with calculated values, thus leading to a verification of the analytical methods employed.

## § 2. Experimental

The maximum bubble pressure method was employed in the experimental study for the following reasons. A fresh metal surface is formed in successive determinations thus minimizing surface-contamination

---

* Communicated by the Author.

errors, always a danger with the alkali metals. The measurements may be effected remotely with no direct observation on the liquid metal being necessary. The physical parameters involved are well defined, while an analysis by Porter (1930) has established the mechanics of bubble formation and detachment. Finally there is a direct theoretical relationship between the parameters measured and the surface energy of the liquid; this obviates any need for an empirical calibration procedure.

The maximum pressure required to form and detach a bubble from an orifice immersed in a liquid may be analysed as follows :

$$P_{\max}=g.h.(\rho-\rho_0)+\frac{2\sigma}{r}, \quad \ldots \ldots \ldots \quad (1)$$

where $P_{\max}$=maximum pressure, $h$=depth of immersion of the orifice tip, $\rho$=liquid density, $\rho_0$=gas-phase density, $\sigma$=surface energy of the liquid, and $r$=effective orifice radius.

In applying eqn. (1) it is necessary to ascertain whether $r$ is the external, internal, or some intermediate radius of the orifice at the point of detachment of the bubble. Furthermore, a correction must be applied for the distortion of the bubble from a spherical form due to the gravitational effect of the varying head of liquid within it. Porter's analysis (1930) was employed in the selection of the effective orifice radius while Sugden's method of correction (1922) was applied for bubble distortion ; both factors have been discussed at length by the author (Taylor 1954).

The metals employed were prepared by vacuum distillation under conditions designed to remove both heavy metal and metalloid impurities ; analyses of the metals are contained in table 1.

Table 1. Analyses of Alkali Metals

| Metal | Purity (%) | Impurity content (p. p. m.) |
|---|---|---|
| Na | 99·995 | B, 40 ; K, 20 ; O, 5–10 |
| K | 99·895 | Na, 10 |
| Li | >99·95 | Na, <100 ; Cl, <400 |

Steps were taken to ensure that this purity was maintained during the transfer of the metals from the purification still to the measuring apparatus.

This apparatus is shown diagrammatically in fig. 1. The orifice tube (C) is movable, via a Wilson seal, through the cover plate of vessel (A), the positioning of the orifice tube being facilitated by means of the circuit (H). The latter is ‘ made ’ when the orifice tip first touches the liquid metal surface and the levelling arms (G) and ($G_1$) may then be zeroed. Subsequently the orifice tip may be located at any required depth by means of a screw-gauge applied over the levelling arms ; the accuracy of this setting is ±0·0005 cm. Orifice tubes were made of mild steel for measurements in lithium and of stainless steel for sodium and potassium. The orifice tip was given a metallographic polish, on a surface perpendicular to the tube axis; the tube diameters were measured optically to an accuracy of ±0·01%. The manometer (E) could be read under ideal conditions to an accuracy of ±0·02 cm but in practice a slight pulsing of the manometer levels caused this error to be slightly higher; low density, low vapour pressure vacuum oil was employed as manometer fluid. Bubble formation and detachment is effected through the tombac bellows (F), a fine screw-thread attached to the latter ensuring a slow and controlled rate of bubble formation. Cleanliness of the apparatus was ensured by prior electropolishing of all metal parts coming in direct contact with the liquid metals, while a high-vacuum system ensured freedom from gaseous contamination; high-purity argon was employed as the blanket gas during the measurements.

Fig. 1

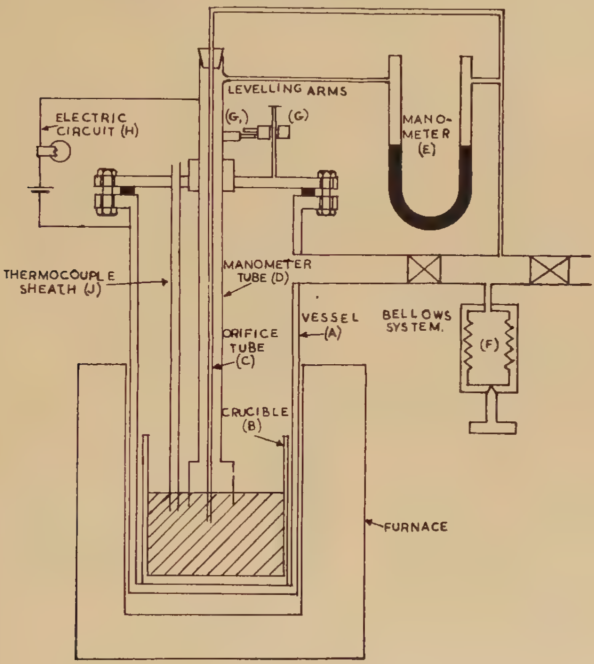

Apparatus (diagrammatic).

The transfer of the high-purity metals into the apparatus was effected via a steel bulb which was filled directly from the purification still, and attached subsequently to the measuring apparatus. No contamination of the liquid occurred during this transfer process.

Surface energy measurements were normally made on a charge of 150–200 cubic centimetres of liquid at three separate depths at any one temperature. The average of six separate determinations was taken as the maximum pressure at any given depth and temperature.

## § 3. Results

The surface energy–temperature relationships determined experimentally are presented in figs. 2, 3 and 4 for sodium, potassium and lithium respectively; the experimental data were corrected for bubble distortion in accordance with Sugden's method (1922). The surface energy values at the respective melting temperatures are: 191 ergs/cm² for sodium (melting temperature 98°c), 101 ergs/cm² for potassium (melting temperature 64°c) and 398 ergs/cm² for lithium (melting temperature 179°c), while the corresponding temperature coefficients of surface energy are: —0·1 ergs/cm²/°c, —0·11 ergs/cm²/°c and —0·14 ergs/cm²/°c.

Fig. 2

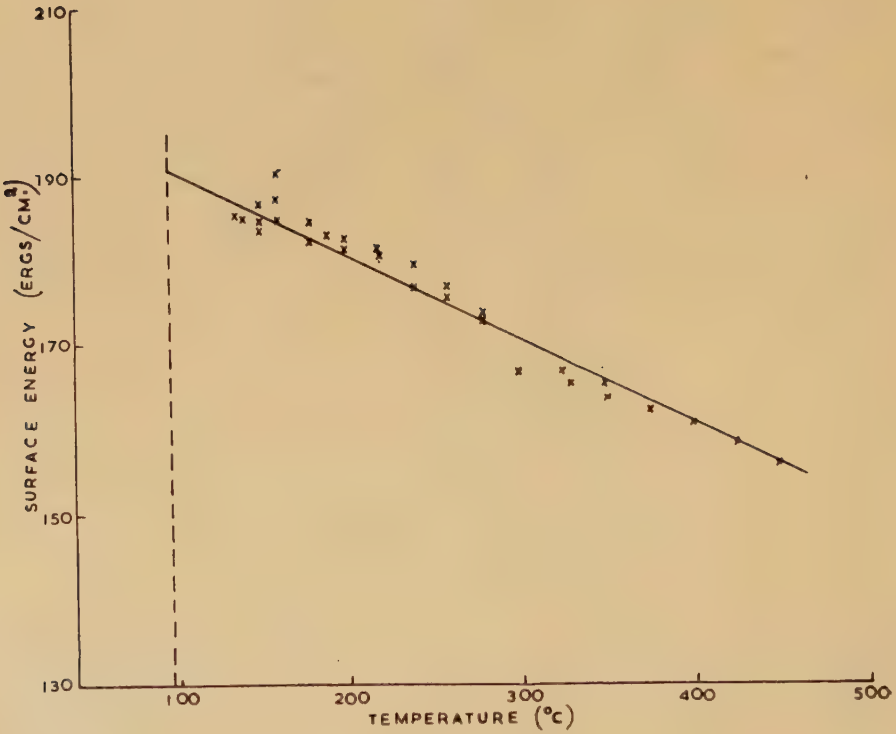

Surface energy–temperature relationship for sodium.

Fig. 3

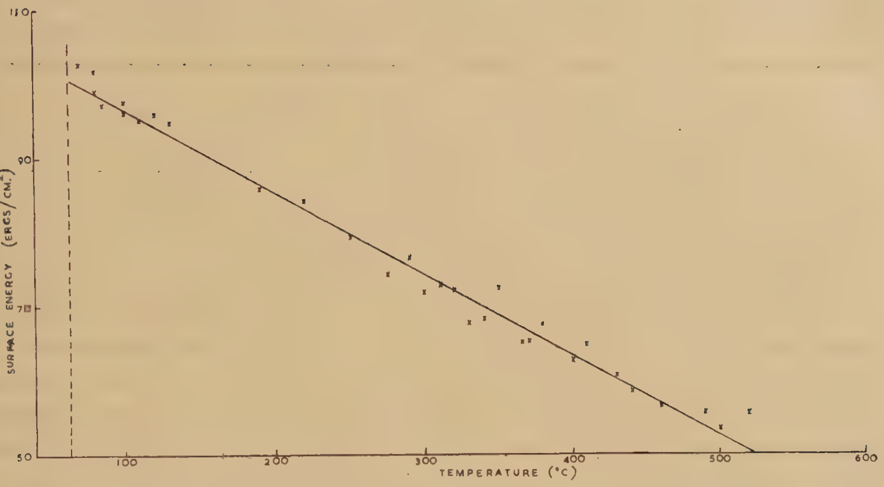

Surface energy–temperature relationship for potassium.

Fig. 4

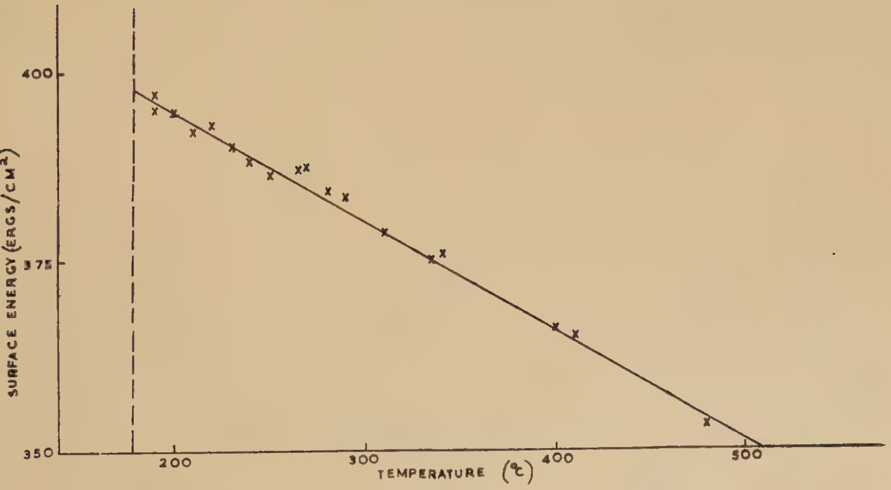

Surface energy–temperature relationship for lithium.

The accuracy of these experimental surface energy values is controlled by the errors involved in the several physical parameters employed in the final calculations. These sources of error are listed in table 2.

Table 2. Percentage Error in Physical Parameters

| Metal | Na | K | Li |
|---|---|---|---|
| Physical parameter | Percentage error | | |
| Density of manometer fluid | ±0·1 | ±0·1 | ±0·1 |
| Orifice diameter | ±0·01 | ±0·01 | ±0·01 |
| Orifice depth setting | ±0·1 | ±0·1 | ±0·1 |
| Density of liquid metal | ±0·1 | ±0·1 | ±0·2 |
| Maximum pressure measurement | ±2·0 | ±2·5 | ±0·3 |

In the case of sodium and potassium the maximum error is in the individual maximum-pressure readings on account of the low surface energy component of the maximum pressure for these liquids; this error is relatively smaller for lithium due to its higher surface energy. The fact that pressure readings were made at three separate depths at any one temperature probably reduces the magnitude of this error slightly and it is considered that the values are accurate to ±2% in the case of sodium and potassium and ±1% for lithium. This is the order of magnitude of the scatter of the experimental points shown in figs. 2, 3 and 4. In addition, density–temperature relationships, derived from the measurements at different depths, show a similar accuracy in relation to previously determined values (fig. 5).

Fig. 5

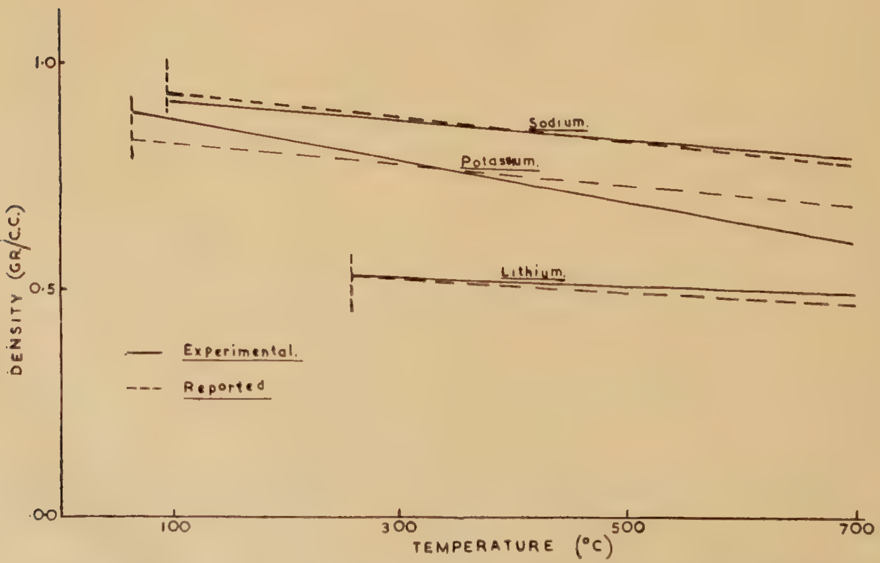

Density–temperature relationships for sodium, potassium and lithium.

Finally the present experimental data for sodium is in good agreement with a recent independent determination (Addison, Kerridge and Lewis 1954) which gives a surface energy of 195 ergs/cm² at 98°C and a temperature coefficient of $-0{\cdot}1$ ergs/cm²/°C.

## § 4. THEORETICAL CALCULATIONS OF SURFACE ENERGY

A number of theoretical calculations of the surface energies of metals have been made and these have been discussed in detail by Ewald and Juretschke (1953). Hence only a brief reference will be made to the several treatments with which the present experimental data are compared.

Two of the earliest calculations were those by Gogate and Kothari (1935) and by Samoilovich (1945). Employing a free-electron model the former considered the electron motion in the surface of a metal which, for this purpose, was regarded as a two-dimensional plane film. From a consideration of the kinetic energy of electrons confined within such a surface film, a relationship was established between the total energy, the kinetic energy, and the surface energy of the system in relation to its surface area. The treatment by Samoilovich (1945) was based on the density gradient which exists at a metal surface. An anisotropic strain tensor is thus produced at the surface so that, when the surface area is increased, energy is expended in doing so. The overall force-density within the metal was calculated using the Thomas–Fermi–Weizsäcker approximation (1935) and this density was then equated to that in the surface.

Fundamentally the two foregoing analyses cannot be regarded as accurate due to the assumptions made regarding the boundary conditions at the surface of a metal. Furthermore the accuracy of the Weizsäcker approximation appears to be in some doubt (Ewald and Juretschke 1953) and leads to excessively high surface energy values.

Subsequent treatments have given more detailed consideration to the exact boundary conditions existing at a metal surface. In particular, the existence of a definite potential step at the surface is recognized with its consequent effect on electron distribution. Thus Brager and Schuchowitzky (1946) calculated, by a wave-mechanical treatment, the energy increase associated with the formation of a new surface, assuming an infinite potential step at the surface. However, this step at the surface of a metal has a finite value and for this reason the previous treatment is oversimplified. Huang and Wyllie (1949) have extended the analysis to the case where the potential step has a finite value. In addition they have included a term in the expression for surface energy which takes account of the electrostatic charge at the metal surface consequent on the irregular charge distribution in this region.

Further refinements of the surface energy calculations have been proposed by Huntington (1951) and also by Stratton (1953), both of whom consider the phenomenon of charge conservation at the metal surface. Thus Huang and Wyllie (1949) defined both the position and the height of the potential step and consequently it was uncertain whether the negative charge external to the surface would be completely balanced by the positive charge within. Of the two modified treatments, that by Stratton (1953) is the more complete. The analysis employed a free-electron gas model and established the surface energy component of the total free energy of the metal by considering the energy of the electron gas confined within a finite potential well. The electronic charge density remote from the surface was balanced by the positive ionic charge density inside the potential well. The final surface energy expression included a contribution from the electrostatic surface double-layer and a term correcting the surface energy at absolute zero for effects at higher temperatures.

## § 5. Comparison of Theoretical and Experimental Values

The several calculated surface energies of the metals sodium, potassium and lithium are compared with the experimental values in table 3; where the theoretical treatments permit, the values are compared at the respective melting temperatures. Temperature coefficients of the surface energies are also compared where possible.

Table 3. Calculated and Experimental Surface Energy Values

| Author(s) | Surface energy at the melting temperature (ergs/cm$^2$) | | | Temperature coefficient of surface energy (ergs/cm$^2$/°c) | | |
|---|---|---|---|---|---|---|
| | Na | K | Li | Na | K | Li |
| Gogate and Kothari (1935) | 278 | 121 | 639 | −0·22 | −0·24 | −0·18 |
| Samoilovich (1945) | 400* | 224* | 655* | —* | —* | —* |
| Brager and Schuchowitzky (1946) | 780* | 330* | 1730* | —* | —* | —* |
| Huang and Wyllie (1949) | 440 | 180 | 890 | −0·12 | −0·08 | −0·19 |
| Stratton (1953) | 190 | 70 | 400 | −0·06 | −0·04 | −0·07 |
| Experimental | 191 | 101 | 398 | −0·10 | −0·11 | −0·14 |

* Values at 0°K; no temperature effect considered.

The surface energy values as calculated by Gogate and Kothari (1935), Samoilovich (1945), Brager and Schuchowitzky (1946), and Huang and

Wylie (1949), are from one and a half to three times the experimental values in the case of the three metals.

Stratton's treatment (1953) appears to give excellent agreement between the calculated and the experimental values for sodium and lithium. However it must be recalled that the two sets of results are not strictly comparable since the theoretical values are for the solid at the melting temperature, no term being included for the change in surface energy on melting. An order of magnitude to this change on melting may be obtained from the relative interfacial tensions between the solid and liquid phases at the melting temperatures; these interfacial tensions may be calculated from supercooling data (Turnbull 1950). On this basis the interfacial tensions were 30 ergs/cm$^2$ for lithium and 20 ergs/cm$^2$ for sodium. Assuming that the difference between the surface energy of the solid and the liquid phase at the melting temperature is of the same order of magnitude as the interfacial tension, the corrected theoretical surface energy values would be 370 ergs/cm$^2$ for lithium and 170 ergs/cm$^2$ for sodium, values still in good agreement with the corresponding experimental data.

Stratton's calculated surface energy for potassium is considerably lower than the experimental value, and any correction to the calculated data for the change in surface energy on melting would only serve to accentuate the existing discrepancy. A factor accounting for this disparity may be the failure of the free-electron–gas model when applied to potassium. In Stratton's analysis (1953) the periodic potential of the ionic core is replaced by an equivalent uniform potential field and this approximation is only true when the potential spread round the positive ion core is small. A similar effect appears to be reflected in Stratton's values for the other monovalent metals copper, silver and gold where the calculated surface energy values are all considerably lower than the experimental values.

In comparing the theoretical and experimental temperature coefficients of surface energy it appears that the best agreement was obtained in the case of Huang and Wyllie's (1949) analysis. This agreement would seem to be somewhat fortuitous since their treatment of the effect of temperature on surface energy was oversimplified, that of Stratton (1953) being physically more exact. Stratton's values are somewhat lower than those obtained experimentally but this difference may not be entirely due to errors in the two sets of values. Once again, the theoretical values are strictly applicable to the solid state only and in extending these to the liquid no account is taken of changes in lattice properties on melting. The changes in lattice properties which do occur on melting, e.g. increased lattice vibrations, are of such a nature that a higher temperature coefficient of surface energy would be expected in the liquid than in the solid phase. Thus the comparison of theoretical and experimental temperature coefficients of surface energies cannot be made rigorously.

## § 6. CONCLUSIONS

The surface energies of the alkali metals sodium, potassium and lithium have been determined experimentally as: 191 ergs/cm$^2$, 101 ergs/cm$^2$ and 398 ergs/cm$^2$ at the respective melting temperatures. The temperature coefficients of the surface energy were found to be :$-0{\cdot}10$ ergs/cm$^2$/°C for sodium, $-0{\cdot}11$ ergs/cm$^2$/°C for potassium and $-0{\cdot}14$ ergs/cm$^2$/°C for lithium.

The most rigorous theoretical calculation (Stratton 1953) of the surface energies of metals leads to values for lithium and sodium which are in good agreement with the experimental data for these metals. The agreement between the experimental and calculated data is poor in the case of potassium but it is suggested that this may be a consequence of the failure of the free-electron–gas model when applied to potassium.

## ACKNOWLEDGMENTS

I should like to acknowledge the interest taken in this work by Dr. H. M. Finniston and I would thank Mr. G. W. Horsley for providing the purified metals.

This paper is published by the kind permission of the Director of the Establishment.

## REFERENCES

ADDISON, C. C., KERRIDGE, D. H., and LEWIS, J., 1954, *J. Chem. Soc.*, 2861.
BRAGER, A., and SCHUCHOWITZKY, A. A., 1946, *Acta Phys.*, **21**, 13.
EWALD, P. P., and JURETSCHKE, H., 1953, *Structure and Properties of Solid Surfaces* (Cambridge: University Press).
GOGATE, D. V., and KOTHARI, D. S., 1935, *Phil. Mag.*, **20**, 1136.
HUANG, K., and WYLLIE, G., 1949, *Proc. Phys. Soc.* A, **62**, 180.
HUNTINGTON, H. B., 1951, *Phys. Rev.*, **81**, 1035.
POINDEXTER, F. E., and KERNAGHAN, E., 1929, *Phys. Rev.*, **61**, 235.
PORTER, A. W., 1930, *Phil. Mag.*, **9**, 1065.
QUARTERMAN, L. A., and PRIMAK, W. L., 1950, *J. Amer. Chem. Soc.*, **72**, 3035.
SAMOILOVICH, A., 1945, *Acta Phys.*, **20**, 97.
STRATTON, R., 1953, *Phil. Mag.*, **44**, 519, 1236.
SUGDEN, S., 1922, *J. Chem. Soc.*, **121**, 858.
TAYLOR, J. W., 1954, *J. Inst. Metals*, **83**, 143.
TURNBULL, D., 1950, *J. Chem. Phys.*, **18**, 769.
WEIZSÄCKER, C. F., 1935, *Z. Phys.*, **96**, 431.

# XCIX. *Proton–Proton Elastic Scattering at* 950 MeV

By P. J. DUKE, W. O. LOCK and P. V. MARCH
Department of Physics, University of Birmingham,

W. M. GIBSON and R. McKEAGUE
Department of Physics, Queen's University, Belfast

and

I. S. HUGHES and H. MUIRHEAD
Department of Natural Philosophy, University of Glasgow*

[Received April 6, 1955]

## SUMMARY

Ilford G5 emulsions exposed to a 950 MeV proton beam from the Birmingham synchrotron, have been searched for proton–proton elastic collisions. Forty-six such events have been found in 950 metres of proton track, equivalent to a cross section for elastic scattering of 15·5±2·5 mb. The angular distribution of the scattered protons in the centre-of-mass system shows a strong forward peak in agreement with results obtained at Brookhaven by cloud chamber and counter workers.

## § 1. INTRODUCTION

UNTIL recently studies of proton–proton scattering were limited to energies below 660 MeV. Proton synchrotrons have now extended the available range up to 1 BeV at Birmingham in Great Britain and to several BeV at Berkeley and Brookhaven in the United States. In this paper we report the preliminary results of an experiment to study the elastic scattering of 950 MeV protons by the hydrogen nuclei normally present in nuclear research emulsions. This technique, initiated by Goldhaber (1952, 1953), is being used by Kao and Clark (1954) to study proton–proton scattering at 420 MeV, and it has been widely used in the study of pion–proton scattering. Proton–proton scattering experiments at 900 MeV and 1000 MeV have been briefly reported by the Brookhaven cloud chamber and counter groups respectively (Morris, Garrison, Fowler, Fowler, Shutt, Thorndike and Whittemore 1955, Smith, McReynolds and Snow 1955).

## § 2. METHOD

Ilford G5 normal nuclear research emulsions 2 in. × 2 in. × 400 $\mu$ in size, were exposed to a single pulse of the scattered-out proton beam of the Birmingham synchrotron (Moon, Riddiford and Symonds 1955). The

---

* Communicated by P. B. Moon, F.R.S.

energy of this beam is $950^{+30}_{-50}$ Mev. The beam intensity used was about $2\times 10^4$ protons per square cm. The emulsions were searched by following each track along its length and all events found, including scatterings, were recorded. The low beam intensity reduced the chance of an observer accidentally changing from one track to another during the scanning. An elastic interaction of an incident proton with a hydrogen nucleus in the emulsion will produce an event having two secondary tracks, i.e. an event of type 2p. To identify these interactions the projected angles, dips and grain densities of the primary and secondary tracks of every 2p event were measured, except when :

(1) either track was identified by inspection as an $\alpha$-particle or heavier nucleus, or

(2) an additional track of length less than $5\,\mu$, due to a recoil nucleus, was observed.

In order to calculate the true angles in space (say, $\alpha_1$ and $\alpha_2$), of the secondary particles relative to the direction of motion of the primary particle it is necessary to know the shrinkage factor of the emulsion at the time at which the measurements are made. The method by which this was achieved has been described elsewhere (Duke, Lock, March and Munir 1955).

When a moving proton collides elastically with a proton at rest the conservation laws yield the following equation for the relation between $\alpha_1$, $\alpha_2$ and the total energy of the system $E$, measured in units of the proton rest-mass :

$$\tan\alpha_1\tan\alpha_2=2/E. \qquad (1)$$

For the energy $950^{+30}_{-50}$ Mev, $\tan\alpha_1\tan\alpha_2$ will be $0{\cdot}66^{+0.02}_{-0.01}$. Such an event must also be coplanar. This may be expressed by the condition that $\phi=0$ where $\phi$ is the angle which the primary particle makes with the plane containing the two secondary particles.

Now
$$\sin\phi=\frac{\cos\delta_0\cos\delta_1\cos\delta_2}{\sin\Theta}\times[\tan\delta_2\sin\theta_1-\tan\delta_1\sin\theta_2+\tan\delta_0\sin(\theta_2-\theta_1)] \qquad (2)$$

where $\delta_0$, $\delta_1$ and $\delta_2$ are the dip angles of the primary and of the secondary particles, $\theta_1$ and $\theta_2$ are the projected angles of the secondaries to the direction of motion of the primary and $\Theta$ is the true angle in space between the secondary tracks. For an elastic collision between free protons $\Theta=\alpha_1+\alpha_2$, which at this energy must lie between 78° and 90°. Events in which $\phi\leqslant 5°$ and $\Theta$ is between 70° and 95° were carefully remeasured ; the errors in $\phi$ and $\Theta$ were usually less than 1°. The wide limits used ensured that no elastic interaction was lost.

For each of these events we have inserted the larger of the two measured values of $\alpha$ into eqn. (1), and obtained the value expected for the other. The deviation $\Delta_\alpha$ of the measured value of the smaller $\alpha$ from that expected should be zero for an elastic collision. On a plot of $\phi$ against $\Delta_\alpha$, true elastic collisions will be represented by points within experimental error of the origin.

## § 3. Results

The path length followed in plates of known shrinkage factor is at present 710 metres and the total number of 2p events found is 390. Figure 1 is a plot of $\phi$ against $\Delta_\alpha$ for those 62 events with $\phi \leqslant 5°$ and $|\Delta_\alpha| \leqslant 5°$. There is a definite grouping of the experimental points around the origin. Consideration of the error involved in the individual determinations of $\phi$ and $\Delta_\alpha$ leads us to expect that an elastic p–p collision will be represented by a point within a semi-circle of radius 1·5°. Elastic collisions of the incident protons with protons bound in a nucleus probably account for the majority of the experimental points lying outside this boundary. Their distribution indicates that 2 of the 35 events within the semi-circle are also caused by such collisions. Thus we obtain for the mean free path, $\lambda$, for elastic free proton–proton collisions the value $710/33 = 21{\cdot}6 \pm 4{\cdot}0$ metres. Assuming the free hydrogen content of the emulsion to be $(3{\cdot}13 \pm 0{\cdot}06) \times 10^{22}$ atoms per cm$^3$ (Waller 1955) the cross section for elastic scattering is $14{\cdot}8 \pm 2{\cdot}5$ mb. Systematic errors due to the selection procedure used are expected to be less than the quoted statistical uncertainty.

Fig. 1

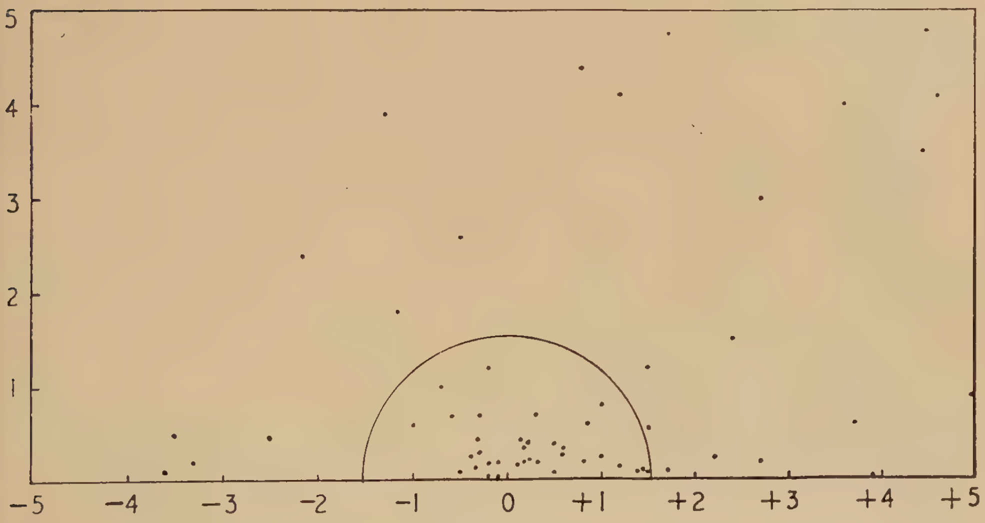

$\Delta_\alpha$ in degrees

A plot of the degree of coplanarity, $\phi$, against the deviation from angular correlation $\Delta_\alpha$, for 62 events of type 2p, with $\phi \leqslant 5°$ and $|\Delta_\alpha| \leqslant 5°$.

In the preliminary stages of the experiment some scanning was carried out on emulsions whose shrinkage factor was not accurately known. Thus the values of $\Delta_\alpha$ for the events found are liable to contain a rather large uncertainty, but the values of $\phi$ are almost independent of the shrinkage factor. Following the same procedure as that outlined above, 13 elastic free p–p events were found in 237 metres of track, corresponding to a cross section of 17 ± 5 mb. For all 46 events in 947 metres $\lambda = 20{\cdot}6 \pm 3{\cdot}5$ metres and $\sigma = 15{\cdot}5 \pm 2{\cdot}5$ mb.

We may calculate the angles, $\alpha^*$, of the secondary particles with respect to the primary in the centre-of-mass ($C$) system by means of the relationship $\tan\alpha = (1-\beta_c{}^2)^{1/2} \tan \alpha^*/2$ where $\beta_c$ is the velocity of the $C$-system. For an incident proton energy of 950 Mev $\beta_c$ is 0·58 and we have $\tan \alpha^*/2 = 1{\cdot}23 \tan \alpha$. The angular distribution thus obtained for the 35 events within the $1\frac{1}{2}^{c}$ semi-circle together with the 13 events on the plates of unknown shrinkage factor is given in the table in units of 10° in order that it may be compared directly with the Brookhaven data, and in four equal units of solid angle.

| Angle in $C$-system in degrees | Number of events | Morris *et al.* normalized† | Four equal units of solid angle | Number of events | $d\sigma/d\omega$ in mb per steradian |
|---|---|---|---|---|---|
| 0 ($2\frac{1}{2}$)–10 | 2 | 1 | 0 –$41\frac{1}{2}$° | 25 | $5{\cdot}3 \pm 1{\cdot}0$ |
| 10–20 | 8 | 9 | $41\frac{1}{2}$–60° | 15 | $3{\cdot}1 \pm 1{\cdot}0$ |
| 20–30 | 7 | 11 | 60 –$75\frac{1}{2}$° | 6 | $1{\cdot}3 \pm 0{\cdot}5$ |
| 30–40 | 6 | 7 | $75\frac{1}{2}$–90° | 2 | $0{\cdot}4 \pm 0{\cdot}3$ |
| 40–50 | 12 | 5 | | | |
| 50–60 | 5 | 4 | | | |
| 60–70 | 1 | 5 | | | |
| 70–80 | 6 | 3 | | | |
| 80–90 | 1 | 3 | | | |

† The total number of events given by Morris *et al.* is 70.

## § 4. DISCUSSION

The cross section for elastic p–p scattering which we have found is 15·5 ± 2·5 mb. A value of 21 mb may be obtained from the cloud chamber work of Morris *et al.* using their value of 38 ± 6 mb for the total cross section. If this latter quantity is taken to be 49 ± 2 mb, as given by Shapiro, Leavitt and Chen (1954), then the data of Morris *et al.* yields an elastic cross section of 26 mb. Smith *et al.* find a value of 19 ± 3 mb, which is based on an extrapolation of their data from 30° to 0°. It appears possible that the elastic scattering cross section decreases slightly between 400 and 1000 Mev, for its value at 437 Mev is 23·8 ± 1·2 mb (Sutton, Fields, Fox, Kane, Mott and Stallwood 1955).

In the present experiment the minimum scattering angle which we can detect is approximately 1°, which corresponds to an angle in the $C$-system of $2\frac{1}{2}$°. The range of the recoil proton in such a case is about 5 $\mu$. Thus the angular distribution given in the table is for angles between $2\frac{1}{2}$ and 90° in the $C$-system, and the experimentally determined cross section is for the same range of angles. The minimum angle in the laboratory system is probably about the same in the cloud chamber experiment quoted above, and is much greater (30°) in the case of the counter experiment of Smith *et al.*

We have made no correction for scanning efficiency because we believe that our scanning procedure has no appreciable loss factor. The results of Morris *et al.* are also not corrected for loss.

The angular distribution which we have obtained is in good agreement, within the statistics, with that obtained by Morris *et al.* at an incident proton energy of 900 MeV, and by Smith *et al.* at 1000 MeV. It shows a strong forward peak in marked contrast to the isotropic distribution at 400 MeV (Hartzler and Siegel 1954). The deviations from isotropy begin

Fig. 2

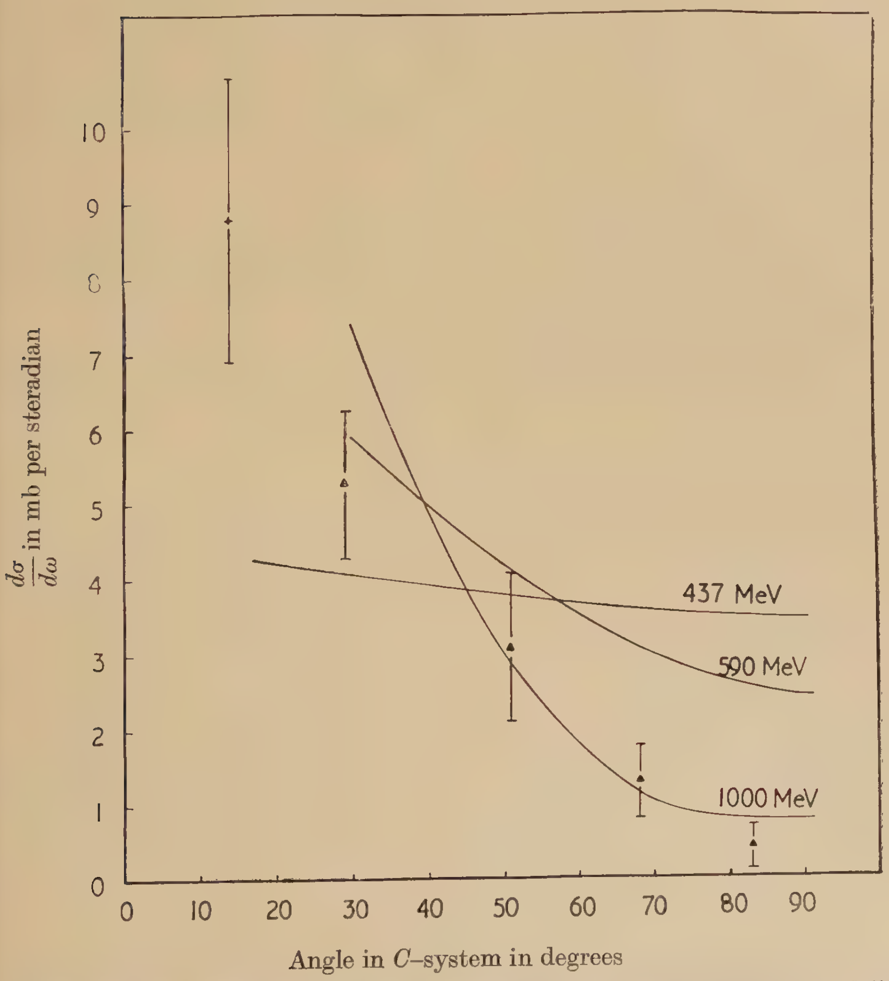

The angular distribution in the $C$-system for p–p elastic scattering at different energies. The full lines represent the results of Sutton *et al.* at 437 MeV and Smith *et al.* at 590 and 1000 MeV. The points marked ▲ represent our results at 950 MeV; the point + is obtained from a combination of our results and those of Morris *et al.* for the angular interval 0–20°.

to show at small angles at 428 MeV (Hartzler and Siegel 1954) and at 437 MeV (Sutton *et al.* 1955). The work of Bogachev and Vzorov (1954) and of Selektor, Nikitin, Bogomolov and Zombkovsky (1954) in the U.S.S.R. (460–660 MeV) and of Smith *et al.* (1955) in the U.S.A. (440–1000 MeV) shows that as the bombarding energy rises the differential cross section. increases markedly at small angles and decreases at large angles This is illustrated in fig. 2 in which we have plotted the data of Sutton *et al.* at 437 MeV and Smith *et al.* at 590 MeV and 1000 MeV, together with our experimental points. It is of particular interest to determine the behaviour of the differential cross section at the small angles. Because of the poor statistics in the range 0–20° (mean angle 14°) we have combined our results with those of Morris *et al.*, normalized to our value at the cross section. We thus obtain the point shown which indicates that the differential cross section is still rising at small angles, although perhaps not as sharply as would be indicated by a direct extrapolation of the counter results of Smith *et al.*

A study of the small angle (1°–5°) single scatterings observed in the course of the scanning indicates that the incident proton beam is not appreciably polarized. In any case our procedure has included the observation of events in all azimuthal planes, and the results should therefore be independent of the polarization of the beam.

Work is in progress on the analysis of the remaining 2p events in terms of (*a*) inelastic free p–p collisions and (*b*) elastic and inelastic collisions with bound nucleons.

## ACKNOWLEDGMENTS

We wish to express our thanks to Miss O. Archibald, Mrs. S. E. Baker, Miss P. Gavigan, Miss M. J. Lewis, Mrs. E. R. Lock, Mrs. N. Palmer, Mrs. B. R. Stephens and Mrs. M. Whittaker for carrying out the arduous scanning involved, to Mr. C. Waller of Ilford Limited for supplying data on the properties of G5 emulsion and to Dr. G. Feldman, Mr. B. A. Munir and Dr. J. Vilain at Birmingham and Mr. J. G. McEwen at Belfast for many useful discussions.

The authors at Belfast (W. M. G. and R. McK.) and Glasgow (I. S. H. and H. M.) would like to express their thanks to Professor Moon for enabling them to take part in this work which was carried out as part of a programme of research supported by the Department of Scientific and Industrial Research. Two of us (P. J. D. and P. V. M.) are indebted to this body for Maintenance Grants.

## REFERENCES

BOGACHEV, N. P., and VZOROV, I. K., 1954, *Doklady. Acad. Nauk. S.S.S.R.*, **99,** 931,

DUKE, P. J., LOCK, W. O., MARCH, P. V., and MUNIR, B. A., 1955, *J. Sci. Inst.* (in press).

GOLDHABER, G., 1952, *Phys. Rev.*, **87,** 220 ; 1953, *Ibid.*, **89,** 1187.

HARTZLER, A. J., and SIEGEL, R. T., 1954, *Phys. Rev.*, **95,** 185.

KAO, S. K., and CLARK, A. F., 1954, *Phys. Rev.*, **95,** 662 (A).

MOON, P. B., RIDDIFORD, L., and SYMONDS, J. L., 1955, *Proc. Roy. Soc.* A, **230,** 204.

MORRIS, T. W., GARRISON, J. D., FOWLER, E. C., FOWLER, W. B., SHUTT, R. P. THORNDIKE, A. M., and WHITTEMORE, W. L., 1955, *Bull. Am. Phys. Soc.*, **30,** 28 (A) and private communication.

SELEKTOR, Y. M., NIKITIN, S. Y., BOGOMOLOV, E. G., and ZOMBKOVSKY, S. M., 1954, *Doklady. Acad. Nauk. S.S.S.R.*, **99,** 967.

SHAPIRO, A. M., LEAVITT, C. P., and CHEN, F. F., 1954, *Phys. Rev.*, **95,** 663 (A).

SMITH, L. W., MCREYNOLDS, A. W., and SNOW, G., 1955, *Phys. Rev.*, **97,** 1186.

SUTTON, R. B., FIELDS, T. H., FOX, J. G., KANE, J. A., MOTT, W. E., and STALLWOOD, R. A., 1955, *Phys. Rev.*, **97,** 783.

WALLER, C., 1955, private communication.

## C. *Photometric Measurement of Ionization in Cloud Chambers*

By I. BUTTERWORTH
The University, Manchester*

[Received February 21, 1955 and in revised form May 18, 1955]

### ABSTRACT

It has been found possible to measure the ionization of a cloud chamber track by photometry of the chamber photograph. The method is applicable to tracks, the photographic images of which consist of unresolved drop images. Its application does not interfere with accurate measurement of the magnetic rigidity of the particle causing the track. The use of the method has been investigated by studying tracks in a typical chamber and is illustrated by mass measurements on 3 K-mesons. The relative merits of this photometric method and the drop counting method of measuring ionization are discussed.

### § 1. INTRODUCTION

THE mass of a particle producing a track in a cloud chamber may be found by combining measurements of magnetic rigidity (which gives the momentum of the particle) and of ionization. The direct method of measuring ionization is to count the drops in a track. If this is to be done without sacrificing accuracy of momentum measurement, the tracks must be formed in a light gas and photographed at a comparatively large magnification (Cowan 1954, Blackett 1954). This has certain disadvantages which are discussed in § 7.

The present experiment was therefore undertaken to see if it is possible to measure the ionization density of tracks using photographs in which the images of the individual drops in a track are not resolved.

Three properties of the image of such a track might conceivably be used to measure ionization : the width, the structure and the mean blackness.

Track width has been used (Burhop 1954) to measure ionization in high pressure chambers. It could not be used for the discontinuous tracks formed in a standard chamber.

Using the structure of the track image, i.e. the variations in blackness along its length, one might hope to find a quantity depending on ionization but not on chamber and photographic conditions. Such a quantity could be used to measure the ionization density of a track without reference to that of other tracks. Preliminary studies in this direction were not promising and were therefore discontinued.

The mean blackness of a track image depends on the track illumination, expansion conditions and film development as well as on ionization. In

---

* Communicated by H. J. J. Braddick.

general these change from expansion to expansion, and may be different for tracks appearing at the same expansion but in different parts of the chamber. Thus track image blackness cannot give an absolute measure of ionization. It has been found possible, however, to use it to compare the ionization densities of tracks formed and photographed under roughly the same conditions.

The blackness of two track images may be compared in several ways, and a number of blackness-comparing parameters have been studied to see if they might be used to compare ionizations. It has been found most convenient to measure the blackness of a track image by a quantity which will be called the ‘ obscuration ’, $T$, of the image. This is defined by

$$T=(t_b-t)/t_b \quad . \quad . \quad . \quad . \quad . \quad . \quad . \quad . \quad . \quad . \quad (1)$$

where $t$ is the optical transmission of the track image and $t_b$ is that of the portions of film on either side of the image.

## § 2. Apparatus and Experimental Details

To test the feasibility of the method, tracks formed in the Pic-du-Midi chamber described by Armenteros *et al.* (1951) have been studied. This is a cylindrical chamber, 28 cm in diameter, 10 cm deep, and is operated in a magnetic field of ca. 7500 gauss. The gas filling, which was at a pre-expansion pressure of 90 cm Hg, consisted of 85% Argon and 15% Oxygen. Tracks were photographed on Ilford 5G.91 film at a magnification of 0·1.

To measure the obscuration of a track image a microphotometer, using the Fürth scanning principle (Fürth 1943, Fürth and Oliphant 1948), was constructed. A rectangular shaped light-spot was focused onto the film by a lens system attached to the prong of a tuning fork. The film was arranged so that the 60 c/s vibration of the fork caused the light-spot to scan a section of film normal to and including the track image. The scan amplitude was about ten times the width of a track image. Light transmitted by the film fell on a photomultiplier. Since this had a linear response,

$$T=(i_b-i)/i_b \quad . \quad . \quad . \quad . \quad . \quad . \quad . \quad . \quad . \quad . \quad (2)$$

where $i$ is the multiplier current produced by light transmitted by the track image and $i_b$ is that produced by light transmitted by neighbouring portions of film. If $R_b$ and $R$ are resistances carrying the multiplier currents, such that first $i_b$ and then $i$ develop equal voltages, then $T=R-R_b/R$. It was thus possible to make measurements of obscurations in terms of resistances only, i.e. independent of multiplier sensitivity, amplifier gain, incident light intensity etc.

The length of the light-spot being 250 $\mu$, each measurement gave the obscuration of a 250 $\mu$ long section of track image. A whole track image was measured in contiguous sections. A straight track image 2 cm long could be measured in 20 min. The light-spot was 72 $\mu$ wide. (The track image width was such that 90% of the drop images were contained within a width of 75 $\mu$.)

## § 3. OBSCURATION AS A MEASURE OF IONIZATION

If $T_1/T_2$, the relative obscuration of two track images, is to be used for comparing ionizations, we must establish that this ratio is independent of the conditions under which the tracks are formed and photographed, provided that these are the same for the two tracks.

For example, if the intensity of the light illuminating the two tracks is the same, $T_1/T_2$ must not depend on this intensity. A fortunate peculiarity of the stereoscopic cameras used to photograph the Pic-du-Midi chamber allowed this point to be investigated. This is the fact that photographs taken by one of the cameras are slightly denser than those taken by the other. Thus each track is photographed twice at different exposures. This is similar to having the same track photographed twice under differing illuminations.

In this way the effect of exposure on the image of a track of medium density has been compared with the effect on the image of a track of minimum ionization density. There is no evidence that the ratio $T_1/T_2$ for two such tracks depends on exposure. The measurements show, with 90% certainty, that if a change of exposure alters $T_1$ and $T_2$ by $q\%$, any alteration of $T_1/T_2$ is less than $0{\cdot}18\ q\%$.

There is, however, a more powerful test of the usefulness of $T_1/T_2$ as a means of comparing ionizations.

## § 4. STUDY OF PARTICLES OF KNOWN IONIZATION

Suppose $I_1$ and $I_2$ are the ionization densities of two tracks formed and photographed under the same conditions. If $T_1/T_2$ is to be useful for comparing ionizations we must have $T_1/T_2=f(I_1\ ;\ I_2)$, where $f(I_1\ ;\ I_2)$ is independent of chamber and photographic conditions. Of course obscuration can only directly measure the droplet density $n$ of a track and not its ionization density. Now $n=\epsilon I$, where $\epsilon$ is the condensation efficiency, a quantity which will in general vary from expansion to expansion. Thus $T_1/T_2$ can only be independent of chamber conditions if it is given by $T_1/T_2=f(I_1/I_2)=f(n_1/n_2)$. If this is to be true for all values of $I_1$ and $I_2$ the function must be a power law, $T_1/T_2=(I_1/I_2)^n$.

The best way of deciding whether $T_1/T_2$ is independent of chamber conditions is the following. $T_1/T_2$ is measured for many pairs of tracks and a graph of $T_1/T_2$ *vs* $I_1/I_2$ is drawn. Chamber and photographic conditions are the same for both tracks of a given pair, but they vary widely from pair to pair. If $T_1/T_2$ depends only on $I_1/I_2$, then, despite the variation of conditions from pair to pair, all the points on the $T_1/T_2$ *vs* $I_1/I_2$ graph will lie on a single curve. In this case $T_1/T_2$ is a useful quantity for measuring relative ionization. If $T_1/T_2$ depends on chamber conditions the points are spread over the graph.

To provide data for such a graph (fig. 1), penetrating cosmic ray shower photographs have been selected, each containing an identifiable proton or deuteron track (identified by visual ionization estimation and momentum measurement), together with at least one track at approximately minimum ionization. Ionizations were found by measuring the momenta and assuming the nature of the particles giving the tracks. Where possible a proton or deuteron has been compared with more than one minimum ionizing particle so as to reduce errors. $T_2$ and $I_2$ are then weighted mean values for the minimum ionization tracks.

No track contributing to the graph has an ionization greater than $6\times$ minimum.

Fig. 1

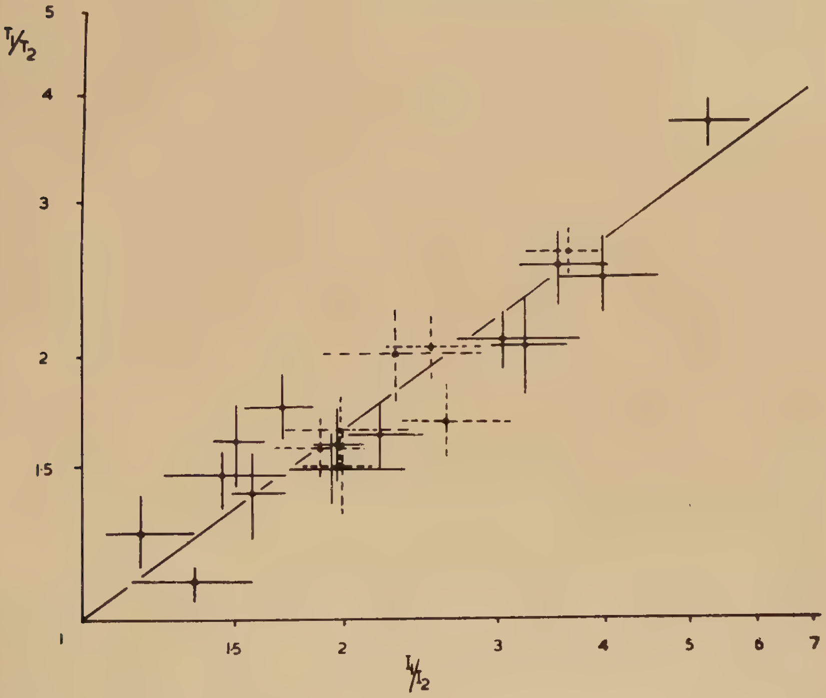

The minimum ionizing particles have been carefully selected so that there is no ambiguity as to their nature. Protons have been excluded by using only negative particles. Supposed electrons have been used only if their momentum was less than $8\times10^7$ ev/$c$, at which momentum they are distinguishable from mesons by visual ionization estimation. Supposed mesons have been used only if their momentum exceeded $5\times10^8$ ev/$c$. The number of electrons found in penetrating showers with momenta above $5\times10^8$ ev/$c$ is very small ($<1\%$ of the total number of particles). All mesons have been assumed to be $\pi$-mesons. For any that are really K-mesons the derived ionization is wrong. However, assuming that less than 20% of the mesons are K-mesons, it can be shown in every case that the chance that the derived ionization is wrong because the particle is really a K-meson is less than the chance that it is equally wrong because of measurement errors.

Only tracks on the same photograph have been compared. The spatial separation of tracks selected for comparison has been limited so that the effect on $T_1/T_2$ of variations of conditions throughout the chamber is small compared with the effect of intrinsic blackness fluctuations (these are discussed below).

When measuring the mean obscuration for a track, as when measuring ionization by drop-counting, it is statistically desirable to reject the contribution from the largest clusters. In drop-counting it is most important to decide on a limiting acceptable cluster size and to adhere to it rigidly. However, because of the saturation effects discussed below, the contribution of a large cluster to the mean obscuration is less important than its contribution to a drop count, and a rigid rejection criterion is not so important. Clusters have therefore been rejected simply on the strength of their visual appearance. The rejection criterion was chosen so that on the average one cluster was rejected for every 5 cm of track.

The points on this graph of $T_1/T_2$ *vs* $I_1/I_2$ are those shown in fig. 1 with continuous error-bars. The errors in $I_1/I_2$ derive from errors in measuring momenta. Errors shown vertically result from intrinsic ionization fluctuations which cause the mean blackness for any given track to deviate in general from the mean blackness for tracks of that velocity. The size of this error is found from the distribution about the mean obscuration of measurements for individual sections of a track. Compared with this error, errors arising in the microphotometer are negligible. All errors are given as standard deviations.

The different points on the graph refer to tracks photographed under widely varying conditions. The image obscuration for a track of given ionization varies by an amount equivalent to an ionization ratio of $>2{\cdot}5$ for tracks on the same photograph. Despite this wide variation in conditions, there is no evidence for a scattered distribution of points over the graph. They fit, within the errors, a single curve. Moreover, they are consistent with the power law relation between $T_1/T_2$ and $I_1/I_2$ which is required if $T_1/T_2$ is to be independent of chamber conditions. Thus the facts that the points fit a power law and that no dependence of $T_1/T_2$ on chamber conditions is apparent are in agreement.

To test further if $T_1/T_2$ is independent of chamber and photographic conditions, it is useful to group together points which refer to tracks taken under similar conditions and see if there are systematic differences between the groups. Of course, with so few points on the graph the statistical weight of a conclusion based on grouping of points is never very high. Classifications have been made according to the image-blackness for a track of given ionization, according to the degree of film development and according to the degree of focusing of the track images. In no case is there evidence for systematic difference between groups.

We have that $T_1/T_2=(I_1/I_2)^n$. Making a least squares fit to the graph points $n=0{\cdot}73\pm0{\cdot}035$.

In addition to protons and deuterons occurring in penetrating showers, 7 positive secondary particles from $\Lambda^0$-decays have been compared with approximately minimum ionizing particles. The latter were selected as described above. None of the $\Lambda^0$-secondaries have ionizations greater than $6\times$ minimum.

Results for the $\Lambda^0$-secondaries can be treated in two alternative ways.

Firstly, knowing the ionizations of the ‘ minimum ’ particles, we can deduce the ionizations of the $\Lambda^0$-secondaries, using the $T_1/T_2$ *vs* $I_1/I_2$ graph that has already been drawn. Combination with momentum measurements then allows the masses of the particles to be found. The measured masses, with standard deviation errors, are shown in fig. 2 (*a*).

Fig. 2

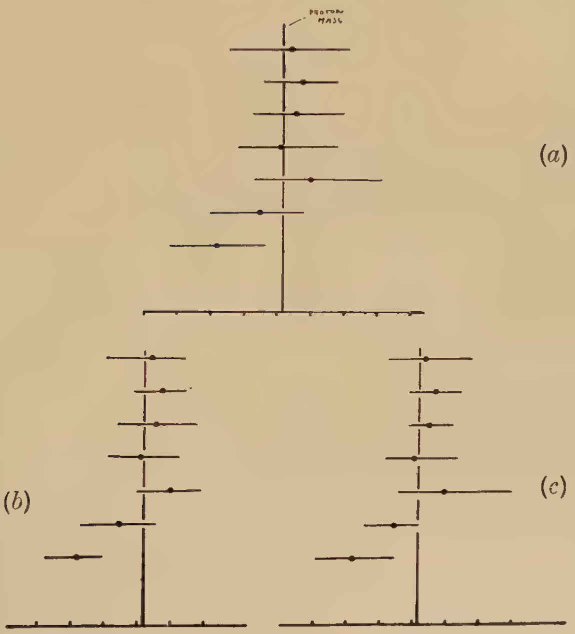

They are all consistent with the mass of a proton. In figs. 2 (*b*) and 2 (*c*), the contributions to the total mass error from the errors in measuring ionization and momentum are shown separately. They are seen to be comparable and equal to *ca.* 200 $m_e$.

Alternatively, the $\Lambda^0$-secondaries may be treated as known protons and a further set of points on the $T_1/T_2$ *vs* $I_1/I_2$ graph obtained. If this is done the points shown by dotted lines in fig. 1 result. These new points are consistent with the old. A least squares fit to all the points gives $n=0{\cdot}72\pm0{\cdot}028$ in $T_1/T_2=(I_1/I_2)^n$.

We may summarize the above results as follows.

It appears that the relative image-obscuration of two tracks, $T_1/T_2$, may be used to measure the relative ionization density of the tracks. No evidence has been found for dependence of $T_1/T_2$ on factors other than relative ionization density.

We may therefore conclude that photometry is a valid and usable method for comparing the ionization density of tracks. Limitations to this conclusion are discussed below.

It is very difficult to describe fully conditions obtaining in an unresolved track image and to calculate theoretically how its obscuration should vary with ionization. It has only been possible to calculate the behaviour of simple track models. Such calculations show that the observed obscuration–ionization relationship is reasonable.

## § 5. RANGE AND ACCURACY OF PHOTOMETRIC IONIZATION MEASUREMENTS

### 5.1. *Range*

At ionizations of less than 6 × minimum, $T_1/T_2$ for two tracks is independent of chamber and photographic conditions over a wide range of conditions. However, for the following reason, this cannot be true if $T_1$ refers to a track of high ionization density.

There are a number of 'saturation' effects which tend to reduce the image-obscuration of a dense track: vapour depletion, photographic saturation, and the fact that obscuration, given by (1), approaches a limit of 1 for very dense tracks. If then a dense track is compared with one of low ionization density, $T_1/T_2$ will be reduced by these effects. The reduction will be greater if chamber and photographic conditions lead to dense tracks than if they lead to weak. Thus for two such tracks $T_1/T_2$ depends on chamber conditions.

Even tracks of low ionization density contain clusters where saturation effects occur. The denser a track, the more dense clusters it contains. Thus $T_1/T_2$ must depend to some degree on chamber conditions for all comparisons. The dependence for the present tracks is found to be unimportant if $T_1$ refers to an ionization of less than 6 × minimum. It is found to become significant at ionizations 6 × minimum.

Thus, for the present photographs, photometric ionization measurement is essentially limited to ionizations of less than 6 × minimum.

### 5.2. *Accuracy*

(*a*) *Random Errors.* As indicated in § 4, intrinsic fluctuations in ionization are the main source of error. Because of saturation effects for large clusters, the effect of fluctuations on a photometric measurement of ionization depends somewhat on chamber conditions. Under average conditions it is found that the error in a measurement of ionization is given by

$$\delta I/I = 1{\cdot}6/n^{1/2} \quad . \quad . \quad . \quad . \quad . \quad . \quad . \quad . \quad (3)$$

where $n$ is the number of primary ionizing collisions made by the particle in forming the considered length of track. Of course only relative ionization is measured, and both the track of interest and those with which it is compared contribute to such an error. Thus, to measure the ionization of a track to the highest degree of accuracy, it will, in general, be necessary to use more than one comparison track.

(*b*) *Systematic Errors.* In addition to random errors there is the possibility of systematic errors arising because conditions are not the same for compared tracks.

Fig. 3

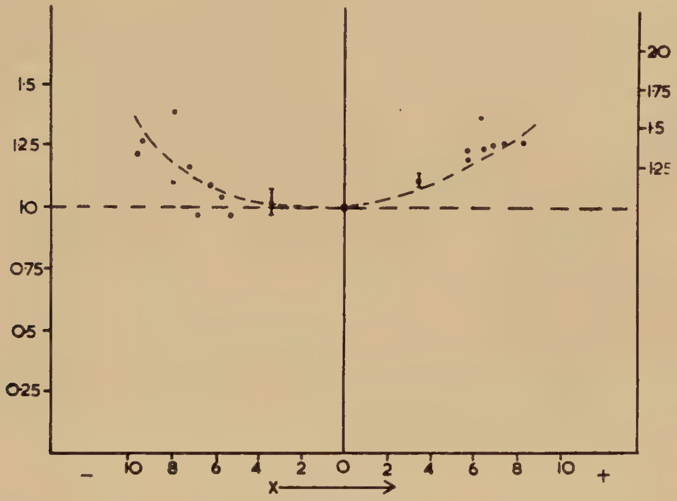

Thus, fig. 3 shows (left-hand ordinate scale) that the obscuration for a track of given ionization depends markedly on its lateral location in the chamber. The right-hand scale shows the error introduced into a photometric comparison of the ionizations of laterally separated tracks.

The points on fig. 3 were obtained by comparing separated tracks of equal ionization. Points shown with errors represent means of several such comparisons. Those shown without errors represent single comparisons.

The lateral effect is due primarily to changes in the angle through which the light reaching the camera is scattered at the drops. The intensity of scattered light depends markedly on scattering angle (Webb 1935, Lander and Nielsen 1953) which differs by 20° for tracks at the side and at the centre of the chamber. Effects of variations in light beam intensity are small compared with this effect. Figure 3 can be used to correct measurements of $T_1/T_2$ for laterally separatedt racks provided the corrections are not large.

Spatial separations in other directions do not produce such marked effects. Thus, within the illuminated volume of the chamber. obscuration varies with the distance of the track behind the window of the chamber by less than 10%. Nor is there a marked dependence of obscuration on the height of the track in the chamber. This shows that the vertical temperature gradient, maintained so as to give convective stability, does not markedly affect condensation efficiency. This has been confirmed by Uttley (private communication) who has made drop counts in this chamber. The size of the temperature gradient is not known. For a larger chamber, a larger temperature difference between top and bottom would be needed to give the same convective stability, and vertical variations of obscuration, or droplet density in a drop counting experiment, would be more important.

It is clearly convenient to be able to compare tracks on different photographs.

Without standardized development, comparison of photographs on different lengths of film is impossible. For photographs on a single length of film it is a question of how steady chamber conditions can be kept. The charging time of the lamp condensers must be smaller than the least permitted interval between photographs, or the flash intensity depends on the actual interval. It is also essential to check the constancy of operating conditions, in particular the lamp voltage and chamber temperature, preferably recording these at each expansion. This was not done when the tracks studied in the present experiment were obtained, and so comparison of tracks in different photographs has in general not been attempted. However, measurements show that chamber conditions are frequently sufficiently constant to allow comparison of tracks formed at different expansions for periods of several hours.

## § 6. PHOTOMETRIC MEASUREMENT OF MASSES

To illustrate the use of the photometric method, results are given below of mass measurements on three K-mesons. The ionization of the particles

Mass Measurement on K-mesons

| Particle | Photometric Measurement of Mass (in $m_e$) with errors | | | Mass from visual estimation |
|---|---|---|---|---|
| | (*a*) | (*b*) | (*c*) | (*d*) |
| Charged *V*-particle | 860 | +175<br>−200 | +330<br>−860 | 1580±160 |
| Non-decaying particle from interaction | 1000 | +165<br>−165 | +290<br>−320 | 850±250 |
| Charged *V*-particle | 1220 at two standard deviations level | | | 1660±160 |

(*a*) Best value for mass.
(*b*) Error, putting $\delta p$ and $\delta I$ equal to one standard deviation ($p$=momentum).
(*c*) Error, putting $\delta p$ and $\delta I$ equal to two standard deviations.
(*d*) $\delta p$ put equal to one standard deviation; $I$ has to be estimated subjectively, probably roughly equivalent to one standard deviation.
The errors are combined quadratically.

was found photometrically in the same way as for the $\Lambda^0$-secondaries. Momentum measurement then allowed masses to be determined.

The table shows the results of the measurements. For comparison, mass values based on visual ionization estimates are also given.

All three particles are positively charged. For neither of the decaying particles is it possible to make measurements on the decay product.

For a given chamber, the accuracy with which the mass of any particle can be found in this way may be calculated using (3), (4), and knowledge of the momentum errors in the chamber.

## § 7. COMPARISON OF THE PHOTOMETRIC AND DROP COUNTING METHODS OF MEASURING IONIZATION

Both the photometric and drop counting methods of measuring ionization are much superior to the unreliable method of visual estimation.

In both methods it is only possible to measure up to a limiting ionization; in drop counting because drops become unresolved, in photometry because of saturation effects. Thus upper limit is raised if the photographic magnification is increased or the density of the chamber gas is reduced. The advantages of photometry over drop counting result from the fact that because resolved drop images are not required, either a smaller magnification or denser gas may be used. Comparison with drop counts made in the Pic-du-Midi chamber by Uttley (to be published) shows that for the same limiting ionization the number of drop images per cm$^2$ of track image can be 9 times as large in photometry as in drop counting. This means that either a denser gas giving 9 times as many ion pairs per cm or a magnification smaller by a factor 3 may be used. The advantages of doing one or other of these will be discussed in turn.

### 7.1. *Advantage of Using a Denser Gas*

In both photometry and drop counting $\delta I/I = 1{\cdot}6/n^{1/2}$ gives the error in an ionization measurement. Use of a denser gas reduces this error for a track of given length. The accuracy of momentum measurement on a track is probably not very dependent on gas density.

### 7.2. *Advantage of Using a Low Magnification*

Use of a low magnification makes photography more economical. Thus the area of film used in a single camera varies as $m^2$ ($m$=magnification). Moreover, the camera aperture giving optimum depth of focus and resolution gives a depth of focus varying as $m^{-2}$. Thus if several differently focused cameras are used to photograph a deep chamber, the total area of film used varies as $m^4$.

It is furthermore found, using the photometric method, that the relation between $T_1/T_2$ and $I_1/I_2$ is little affected by slight defocusing of the track images. In the present experiment the method has been successfully applied to tracks varying in distance from the camera by 2 to 3 times the depth of focus.

Other advantages of the photometric method are that it requires no modification of the chamber and can be applied to existing film records.

### 7.3. *Disadvantages of Photometry*

The first important disadvantage of the photometric method is its slowness. This results from two causes : (1) the variation of conditions throughout the chamber must be investigated ; (2) not only the interesting track must be measured but also the comparison tracks, and this involves obscuration measurement, stereoscopic reprojection and momentum measurement. Thus it takes several hours to measure the ionization of a track photometrically.

This disadvantage becomes less important as conditions are made more uniform throughout the chamber and steadier with time.

A second disadvantage is that the requirements for the successful intercomparison of tracks formed at different expansions are somewhat more stringent in photometry than in drop counting.

The comparison of the photometric and drop counting methods of measuring ionization may then be briefly summarized as follows. For the same degree of accuracy in ionization measurement, the photometric method is the less expensive. It is however the slower method.

## ACKNOWLEDGMENTS

I am indebted to Professor P. M. S. Blackett for the encouragement and facilities he has afforded this work, and to Dr. H. J. J. Braddick, under whose guidance the experiment was carried out, for his constant interest and advice.

I am very grateful to Dr. C. C. Butler for allowing me to use cloud chamber films belonging to the Pic-du-Midi group of the Imperial College of Science and Technology. He and all the members of this group have been most helpful and co-operative.

Discussions with Professor J. G. Wilson, the late Dr. J. Podolanski, the late Dr. G. M. D. B. Jones, Mr. J. A. Newth, and Mr. C. A. Uttley have been much appreciated.

I am grateful to the Department of Scientific and Industrial Research for a maintenance grant.

## REFERENCES

ARMENTEROS, R., BARKER, K. H., BUTLER, C. C., and CACHON, A., 1951, *Phil. Mag.*, **42,** 113.

BLACKETT, P. M. S., 1954, *Il Nuovo Cimento*, **11,** Supple. No. 2, 264.

BURHOP, E. H. S., 1954, *Il Nuovo Cimento*, **11,** Supple. No. 2, 341.

COWAN, E. W., 1954, *Phys. Rev.*, **94,** 161.

FÜRTH, R., 1943, *Proc. Phys. Soc.*, **55,** 34.

FÜRTH, R., and OLIPHANT, W. D., 1948, *J. Sci. Inst.*, **25,** 289.

LANDER, R. L., and NIELSEN, C. E., 1953, *Rev. Sci. Inst.*, **24,** 20.

WEBB, C. G., 1935, *Phil. Mag.*, **19,** 927.

WILSON, J. G., 1951, *The Principles of Cloud Chamber Technique* (Cambridge : University Press).

# CI. *The Structure and Magnetic Properties of the Alloy* $Mn_3AlC$

By R. G. Butters and H. P. Myers
The Department of Mining and Metallurgy, The University of British Columbia,
Vancouver 8, Canada *

[Received May 4, 1955]

## Abstract

An alloy of composition close to $Mn_3AlC$ was prepared by induction melting. In the as-cast state the alloy was feebly magnetic at room temperature and the magnetic property was retained after homogenization at 1000°c. This alloy was composed of a single phase possessing an ordered face centred cubic structure with lattice parameter 3·869 Å. The ordered structure is similar to that found in the alloy $Mn_3ZnC$, the properties of which have been described elsewhere. The alloy $Mn_3AlC$, is strongly magnetic at low temperatures having a saturation moment at 0°K of 99·6 ergs/g/oersted equivalent to a Bohr magneton number 1·20 per Mn atom, the Curie temperature being 15°c. The paramagnetic susceptibility measured over the temperature range 65–800°c, was found to vary with temperature in a manner different from a normal ferromagnetic material, the $1/\chi$–$T$ graph possessing pronounced curvature concave to the temperature axis.

## § 1. Introduction

Over a certain range of composition it is possible to obtain single phase ternary alloys of manganese, carbon, and aluminium possessing a face centred cubic structure showing pronounced ordering. The alloy of composition $Mn_3AlC$ exhibits the maximum ordering and has a detailed structure isomorphous with the alloy $Mn_3ZnC$ (Butters and Myers 1955). This latter alloy possesses interesting magnetic properties, being ferrimagnetic at low temperatures ; it is therefore of considerable interest to know the detailed magnetic properties of similar ternary alloys and this paper describes the properties of those alloys containing manganese aluminium and carbon.

## § 2. Preparation of the Alloys

The materials used in this work were manganese of 99·9% purity donated by the Electromanganese Corporation of America, aluminium of 99·99% purity donated by the Aluminum Company of Canada and graphite of spectroscopic grade.

---

*Communicated by W. Sucksmith, F.R.S.

The alloys were melted and chill cast under an argon atmosphere. Interest was centred on the composition $Mn_{60}Al_{20}C_{20}$ but other alloys in which the carbon content was maintained at 20 atomic % and the proportions of manganese and aluminium varied, were prepared. In the as-cast state the micro-structure indicated pronounced coring; this was removed by annealing at 1000°C for ten days, the homogenization taking place rather slowly. All specimens were sealed in evacuated quartz tubes for the homogenization treatment.

The alloys are extremely unstable in air, particularly so under humid conditions, and it was essential that specimens be kept in a desiccator. The compositions referred to in later sections are the nominal compositions of the alloys; the actual compositions were determined by chemical analysis and found to be in good agreement with the nominal values, the results of the analyses are given in § 5 where the influence of the manganese in excess of 60 atomic % is discussed.

### § 3. STRUCTURE AND LATTICE PARAMETER

Alloy specimens were prepared and examined under the microscope and by x-ray diffraction technique. The alloys were very hard and powders were easily prepared for Debye–Scherrer diffraction photographs. It was not necessary to anneal the powders to obtain sharp diffraction lines and all x-ray studies were made on unannealed powders. Fe $K\alpha$ and Cr $K\alpha$ radiations were used. Debye–Scherrer photographs showed the alloy $Mn_3AlC$ to possess an ordered face centred cubic structure with lattice parameter 3·869 Å. The intensities of the diffraction lines were measured using a Geiger counter spectrometer and were found consistent with an ordered structure similar to that already determined for the alloy $Mn_3ZnC$ (Butters and Myers, *loc. cit.*). In this arrangement the manganese atoms are located at the face centre positions, the aluminium at the cube corners and the carbon atoms at the body centre positions.

The calculated intensities of diffraction lines arising from this structure and those actually observed for the alloy $Mn_3AlC$ are given in table 1. The temperature factor was omitted in these intensity calculations but the atomic scattering factors were corrected for any depression due to behaviour in the region of absorption edges (James 1948).

The measured intensities given in table 1 may be compared with those found for the alloy $Mn_3ZnC$. The superlattice lines are taken to be those with $\Sigma h^2=1, 2, 5, 6, 9, 10, 13$ and 14, and the geometrical factor occurring in the expression for the line intensity takes the values

$$(f-f_{Mn}-f_C)^2 \text{ when } \Sigma h^2 \text{ odd}$$

and

$$(f-f_{Mn}+f_C)^2 \text{ when } \Sigma h^2 \text{ even}$$

where $f$ is the atomic scattering factor for zinc or aluminium and $f_{Mn}, f_C$ the same quantity for manganese and carbon respectively.

Zinc possesses an atomic scattering factor equal, approximately, to the sum of the scattering factors of manganese and carbon, and in this system the intensities of the superlattice lines are controlled by the small contribution of the carbon atom which leads to lines with $\Sigma h^2$ even having greater intensity than those with $\Sigma h^2$ odd. On the other hand the atomic scattering factor of aluminium is much less than the sum of the atomic scattering factors of manganese and carbon and superlattice lines with $\Sigma h^2$ even have less intensity than those with $\Sigma h^2$ odd.

This reversal of the intensities of superlattice lines in the two alloys $Mn_3ZnC$ and $Mn_3AlC$ is to be expected on the basis of the assumed structure for these alloys and is actually observed in the Debye–Scherrer powder photographs but some of the diffraction lines arising from the aluminium alloy were too weak to be measured accurately with the Geiger counter spectrometer and a complete quantitative comparison is not possible.

Table 1

| Line index $\Sigma h^2$ | Intensity | |
|---|---|---|
| | Measured | Calculated |
| 1 | 5·5 | 8·9 |
| 2 | 0·5 | 1·6 |
| 3 | 44 | 38·8 |
| 4 | 21·4 | 21·5 |
| 5 | 1·8 | 2·4 |
| 6 | not measurable | 0·6 |
| 8 | 26·5 | 22·6 |
| 9 | not measurable | 2·7 |
| 10 | not measurable | 0·9 |
| 11 | 100 | 100 |

The measured and calculated intensities are based on a value 100 for the line $\Sigma h^2 = 11$.

Specimen composition $Mn_{60\cdot7}Al_{19\cdot6}C_{19\cdot7}$; Lattice parameter 3·868 Å.

Chromium Kα radiation was used for this intensity work.

The occurrence of the intensity reversal between the lines with $\Sigma h^2$ odd and $\Sigma h^2$ even is further evidence for the correctness of the assumed structure, being additional to the agreement between observed and calculated intensities found for the stronger diffraction lines of the two alloys.

For a fixed carbon content of 20 atomic % the single face centred cubic structure occurs over the composition range Mn 60–69 atomic % Al 20–11 atomic%. The exact limits of this phase have not yet been determined, the primary interest being the magnetic properties of alloys with composition close to $Mn_3AlC$. Preliminary investigations have shown however that for a fixed carbon content of 20% a two-phase alloy results when the manganese content is increased to 70% or reduced to 58% and it seems that although the Mn : Al atom ratio may be increased to values considerably greater than 3, very little reduction, if any, can be made to this ratio and maintain a single-phase alloy. If, however, the Mn : Al atom ratio is kept constant at the value 3 a certain variation in carbon content is allowed. Single-phase alloys have been prepared with 15% carbon but carbon in excess of 20% is dispersed as graphite.

Fig. 1

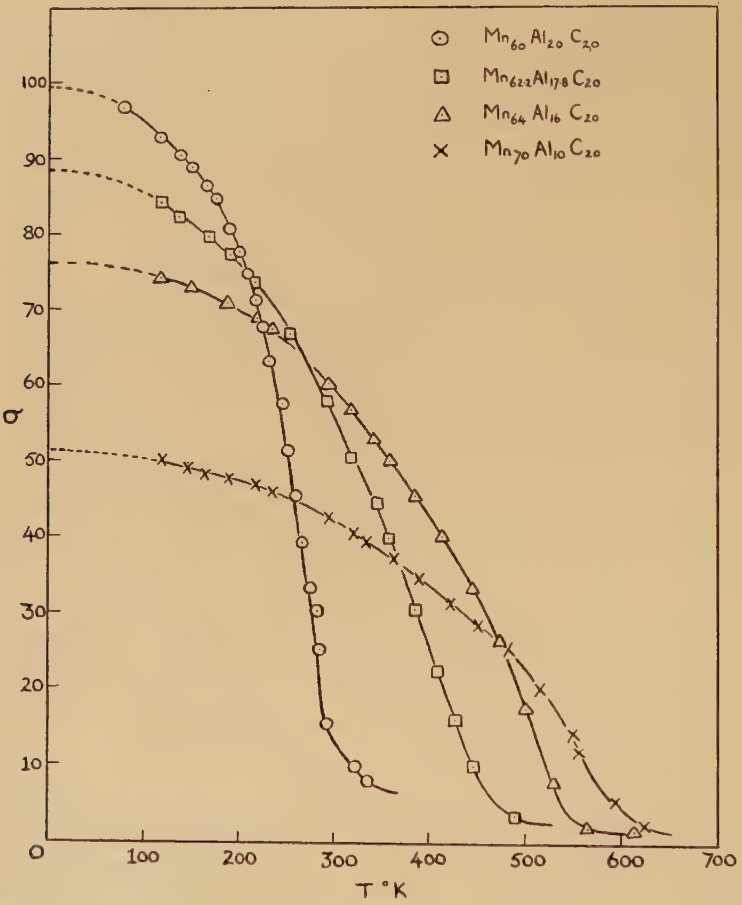

The variation of the saturation magnetization with temperature for alloys of different composition.

The alloys used for the magnetic work all contained a fixed carbon content of 20 atomic % and the composition was varied by increasing the manganese content. Very little change in lattice parameter was found for considerable variation in composition which implies that in these alloys manganese and aluminium have almost the same atomic diameter of 2·73 Å, the manganese being slightly greater in size than the aluminium atoms.

## § 4. MAGNETIC PROPERTIES

The saturation magnetization in an external field of 16 200 oersteds, and its variation with temperature were measured for alloy specimens using a Sucksmith ring balance. The paramagnetic behaviour above the Curie temperature was determined for the alloy $Mn_3AlC$ using a similar but more sensitive ring balance. All magnetic measurements were made on coarsely powdered specimens which were found to saturate easily in the fields used. High temperature measurements were carried out *in vacuo* or a reduced atmosphere of argon. The use of coarse powders required a special specimen carrier for the paramagnetic measurements; this was made as an annular boat machined from graphite. Such a boat held about 120 mg material which was sufficient for the measurements. The carrier was diamagnetic and a correction was therefore determined for the temperature range used in these experiments (65–800°c).

Fig. 2

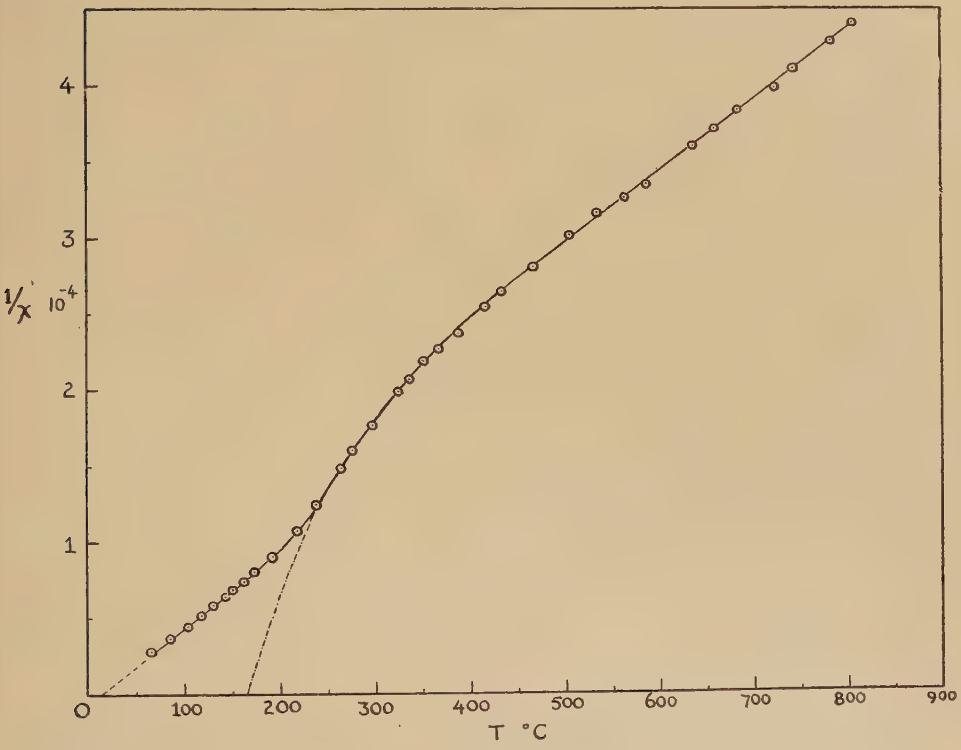

The paramagnetic behaviour of $Mn_3AlC$, $\chi$ is referred to a gram of alloy.

The variation of the saturation magnetization with temperature is shown in fig. 1, the values at 0°K being extrapolated value from $\sigma$–$T^2$ graphs and the Curie temperatures determined by plotting $\sigma^2$ against $T$.

It is immediately seen that increasing the manganese content decreases the saturation magnetization and causes an increase in the Curie temperature.

The variation of the paramagnetic susceptibility above the Curie temperature for the alloy $Mn_3AlC$ is shown in fig. 2, the shape of the graph is unlike that usually observed for ferromagnetic substances and possesses a curvature concave to the temperature axis similar to that found in the paramagnetic behaviour of the ferrite class of magnetic substances. The curvature of the $1/\chi, T$ graph prevents a determination of the Curie constant for the alloy.

## § 5. Discussion

The alloy $Mn_3AlC$ possesses an ordered structure which is independent of heat treatment, the structure of the homogenized alloy being the same whether slowly cooled or quenched from 1000°c. It hardly seems correct therefore to class this observed ordering as typical of normal superlattice formation. Furthermore, the presence of partial ordering even in alloys differing widely from the optimum composition $Mn_3AlC$ suggests that another mechanism must be found for the observed regular structures.

For alloys containing a fixed carbon content of 20 atomic % the manganese aluminium atom ratio may be increased to values considerably greater than 3, the optimum value, but a second phase is produced when this ratio is decreased. This implies that the aluminium atoms cannot occupy face centre positions in this structure. A possible interpretation is that the carbon atom prefers manganese nearest neighbours and a consideration of atomic diameters leads to the conclusion that the carbon must be considered bonded to the manganese atoms. (The behaviour of the Mn, Zn, C alloys with the same structure is similar in this respect.) The regularity of the structure may be understood if it is assumed that vacant d orbitals of the manganese are used in the bonds with the carbon atoms ; increasing the manganese content would not affect this mechanism but the low manganese limitof the phase can be appreciated, for if aluminium occupies a face centre position there is no simple way whereby the aluminium can provide d orbitals to form bonds with carbon.

If then the tendency to form an ordered structure is governed by bond formation the preservation of the order after different heat treatments can be understood. On the other hand, the equivalence of the six manganese atoms in the unit cell of $Mn_3AlC$ demands that the carbon on the average be bonded equally to each. We do not wish to discuss a detailed model for this process since we believe that additional data obtained from neutron diffraction experiments will enable a more precise appreciation to be made.

The saturation magnetization varies with temperature in a normal manner and there are no indications of any anomalous behaviour as found in $Mn_3ZnC$. The Bohr magneton value of 1·21 is similar in magnitude to the value found in the zinc alloy and very different from the value 4 found for manganese in the Heusler alloys. The paramagnetism of

$Mn_3AlC$ above the Curie temperature is definitely unusual for a metal and indiates ferrimagnetic rather than ferromagnetic properties. For an arbitrary value of Curie constant the equation derived by Néel (1948) for the paramagnetic susceptibility of a ferrite may be fitted accurately to the experimental points. If, however, ferrimagnetism is a proper interpretation of the paramagnetic behaviour then there is an unusually large difference between the ferromagnetic Curie temperature and the $\theta_p$ of Néel's treatment ($\theta_p$ will be *ca.* 160°c) this difference being about 150° compared with the usual 40 to 50° for this difference.

Other than the low Bohr magneton value for the manganese atoms and the form of the $1/\chi$–$T$ curve there is no direct evidence for a ferrimagnetic interpretation but the manganese–manganese distances in the alloy $Mn_3AlC$ should favour negative interactions. In $Mn_3AlC$ and $Mn_3ZnC$ these distances are 2·73 Å and 2·76 Å respectively, and at low temperatures $Mn_3ZnC$ is known to be ferrimagnetic. Furthermore, Guillaud (1953) using data obtained from $Mn_4N$, MnSb, MnAs, and other compounds suggests that negative interactions will be found when manganese atoms are separated by less than 2·81 Å. An interpretation of the results in terms of ferrimagnetism would therefore seem appropriate.

Table 2

| ominal alloy composition | $Mn_{60}Al_{20}C_{20}$ | $Mn_{62\cdot2}Al_{17\cdot8}C_{20}$ | $Mn_{64}Al_{16}C_{20}$ | $Mn_{70}Al_{10}C_{20}$* |
|---|---|---|---|---|
| easured alloy composition | $Mn_{60\cdot7}Al_{19\cdot6}C_{19\cdot7}$ | $Mn_{61\cdot95}Al_{17\cdot97}C_{20\cdot08}$ | $Mn_{64\cdot05}Al_{15\cdot61}C_{20\cdot34}$ | — |
| $a$ Å | $3{\cdot}868_9$ | $3{\cdot}874_7$ | $3{\cdot}874_7$ | $3{\cdot}874_5$ |
| $\theta$ °c | 15 | 156 | 250 | 307 |
| $\sigma$ | 99·6 | 88·5 | 76 | 51·5 |
| $_B$ per Mn atom | $1{\cdot}20_5$ | $1{\cdot}05_6$ | 0·89 | — |

* This alloy contained a small amount of a second phase, the manganese contributing to the gnetic moment would therefore be less than 70 atomic % but can not be estimated accurately.

Increasing the manganese content beyond 60 atomic % causes an increase in the Curie temperature and a decrease in the saturation moment of the alloy. Assuming that only the manganese atoms contribute to the magnetization the Bohr magneton number ($p_B$) per manganese atom was calculated for each alloy. For this purpose the alloys were analysed chemically for each constituent element. The totals in all cases were within the limits 100±0·5% by weight and the atomic percentages were determined by scaling to 100%. The nominal and determined compositions with the calculated $p_B$ values are given in table 2. The variation of $p_B$ number with the manganese content in excess of 60 atomic % is shown in fig. 3. Since the alloy containing 70 atomic % Mn had a small amount of a second phase present the values are not sufficiently accurate to be compared with the other alloys. The remaining alloys give results which show a linear decrease in moment with manganese in excess of 60 atomic % and the gradient of the graph indicates that the magnetization is reduced by $5 \pm 0{\cdot}5\ \mu_B$ per manganese atom in excess of 60 atomic %. Manganese atoms in excess of 60 atomic % must replace Al atoms at cube corners and the magnetic results indicate that they probably exist in $3d_5 4s_2$ states and give rise to a moment antiparallel to that of the manganese atoms at face centre positions.

Fig. 3

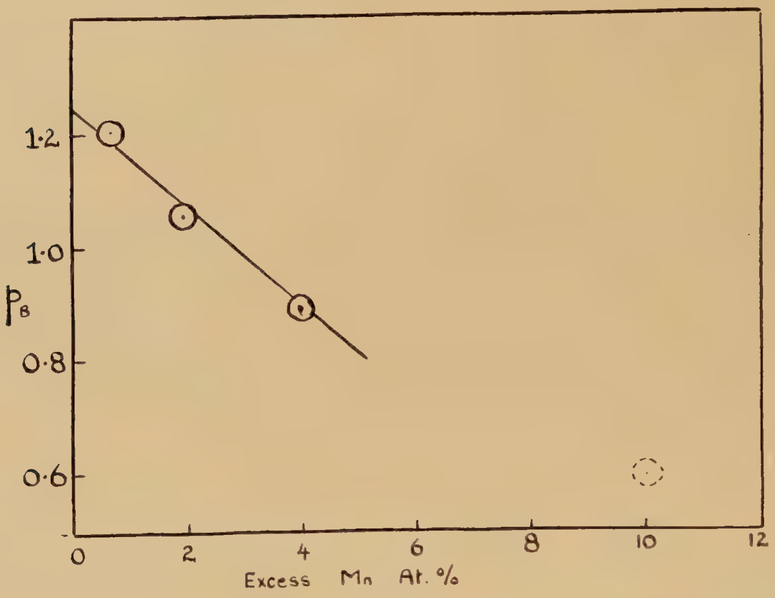

The variation in Bohr magneton value with manganese content in excess of 60 atomic %.

## ACKNOWLEDGMENTS

The authors wish to acknowledge the contribution of Mr. G. Smith in helping with the chemical analysis of alloy specimens. This work was carried out with the aid of funds provided by the Defence Research Board of Canada through Grant 281, Project Number D44-95-35-02 ; the support of the National Research Council is also gratefully acknowledged.

## REFERENCES

BUTTERS, R. G., and MYERS, H. P., 1955, *Phil. Mag.*, **46**, **132**.
GUILLAUD, C. P., 1953, *Rev. Mod. Phys.*, **25**, **119**.
JAMES, R. W., 1948, *The Optical Principles of the Diffraction of X-rays* (London : G. Bell and Sons).
NÉEL, L., 1948, *Ann. Phys.*, **3**, **137**.

# CII. *The High Temperature Susceptibility of a Lattice of Permanent Dipoles*

By B. K. P. Scaife
Dublin Institute for Advanced Studies *

[Received in revised form May 11, 1955]

## Summary

Pople's recent criticism of the results obtained, for the high temperature susceptibility of a permanent dipole lattice, by Van Vleck and by Rosenberg and Lax is shown to be unjustified. Two alternative derivations are given of the relations obtained by Van Vleck *et al.* It is shown that Kirkwood's correlation parameter, $g$, depends upon dipole–dipole interactions.

## § 1. Introduction

The problem of the electric polarization of a system of permanent dipoles arranged on a lattice has received considerable attention. Van Vleck (1937, 1940) has given an exact classical treatment of the problem and has obtained an expansion for the high temperature susceptibility in powers of $(1/T)$ as far as the terms in $(1/T)^3$. Rosenberg and Lax (1953) have reorganized Van Vleck's treatment and have extended his expansion to include the term in $(1/T)^4$. Recently Pople (1953) has stated that the results obtained by Van Vleck and by Rosenberg and Lax are in error. In the treatment given here it is shown that Pople's criticism is unjustified, and that the results obtained by the previously mentioned authors are correct.

## § 2. Formulation of the Problem

The starting point of this discussion is the general relation for the dielectric constant, $\epsilon$, of a uniformly polarized body, of volume $v$,

$$(\epsilon-1)=(4\pi P/E)=(4\pi\langle \mathbf{M}\,.\,\mathbf{e}\rangle/vE)\dagger \quad . \quad . \quad . \quad . \quad . \quad . \quad (2.1)$$

where $P$ is the dipole moment per unit volume, $\mathbf{E}$ $(=\mathbf{e}E)$ is the uniform potential gradient existing in the volume $v$, and $\mathbf{M}$ is the total instantaneous dipole moment of the volume.

For simplicity it will be assumed in the following that the volume, $v$, is spherical in shape. This spherical specimen of dielectric may be *in vacuo* or surrounded by an infinite volume of its own medium. It will be shown that identical expressions for $(\epsilon-1)$ are obtained in both cases.

---

* Communicated by the Author.

† $\langle\ \rangle$ denotes an average. $\langle\ \rangle^\circ$ indicates that the average must be evaluated when the external field is zero.

Provided the spherical volume is sufficiently large to be considered as a macroscopic specimen, we may obtain the following relations from (2.1), thus:

(*a*) *sphere in vacuo,*

$$3[(\epsilon-1)/(\epsilon+2)]=[4\pi\langle \mathbf{M}\,.\,\mathbf{e}\rangle_{\text{vac}}/v\mathscr{E}] \quad . \quad . \quad . \quad . \quad . \qquad (2.2)$$

where $\mathscr{E}$ denotes the external field in which the sphere is situated, and

(*b*) *sphere embedded in its own medium,*

$$(\epsilon-1)=[4\pi\langle \mathbf{M}\,.\,\mathbf{e}\rangle/vE]. \quad . \quad . \quad . \quad . \quad . \quad . \quad . \quad . \qquad (2.3)$$

Fröhlich (1949), following the work of Kirkwood (1939), has shown that (2.2) and (2.3) may be written, ignoring saturation, in the following form,

$$(a) \qquad 3[(\epsilon-1)/(\epsilon+2)]=[4\pi\langle \mathbf{M}^2\rangle^{\circ}_{\text{vac}}/3vkT] \quad . \quad . \quad . \quad . \qquad (2.4)$$

$$(b) \qquad [(\epsilon-1)(2\epsilon+1)/3\epsilon]=[4\pi\langle \mathbf{M}^2\rangle^{\circ}/3vkT], \quad . \quad . \quad . \quad . \quad . \qquad (2.5)$$

where $k$ is Boltzmann's constant and $T$ the absolute temperature. $\langle \mathbf{M}^2\rangle^{\circ}_{\text{vac}}$ is the mean square fluctuation of the dipole moment of a dielectric sphere *in vacuo* and $\langle \mathbf{M}^2\rangle^{\circ}$ is the mean square fluctuation of the dipole moment of a dielectric sphere embedded in an infinite volume of its own medium*. It is particularly to be noted that (2.5) has been obtained by considering the surroundings of the sphere on a strictly macroscopic basis.

The problem is therefore, to evaluate $\langle \mathbf{M}^2\rangle^{\circ}_{\text{vac}}$ and $\langle \mathbf{M}^2\rangle^{\circ}$, and to show that the values so obtained, when inserted in (2.4) and (2.5) yield the same result for $(\epsilon-1)$. Attention will be confined to lattices of tetrahedral symmetry.

## § 3. EVALUATION OF $\langle \mathbf{M}^2\rangle^{\circ}_{\text{vac}}$

The evaluation of $\langle \mathbf{M}^2\rangle^{\circ}_{\text{vac}}$ will be first discussed as it is somewhat more straightforward than that of $\langle \mathbf{M}^2\rangle^{\circ}$. The procedure and notation adopted here are the same as in Pople's (1953) work. We may write

$$\langle \mathbf{M}^2\rangle^{\circ}_{\text{vac}}=\langle \sum_{i,j}^{N} \boldsymbol{\mu}_i\cdot\boldsymbol{\mu}_j\rangle^{\circ}_{\text{vac}} \quad . \quad . \quad . \quad . \quad . \quad . \quad . \qquad (3.1)$$

where $N$ is the number of dipoles, all of equal magnitude, and $\boldsymbol{\mu}$ is the dipole moment of a molecule.

We assume that all dipoles in the sphere are equivalent. Consequently,

$$\langle \mathbf{M}^2\rangle^{\circ}_{\text{vac}}=N\langle \sum_{j}^{N}.\boldsymbol{\mu}_i\cdot\boldsymbol{\mu}_j\rangle^{\circ}_{\text{vac}}. \quad . \quad . \quad . \quad . \quad . \quad . \qquad (3.2)$$

To obtain an expression for $\langle \mathbf{M}^2\rangle^{\circ}_{\text{vac}}$ we must evaluate the following integral

$$\langle \mathbf{M}^2\rangle^{\circ}_{\text{vac}}=\left[N\int \sum_{j}^{N}.\boldsymbol{\mu}_i\cdot\boldsymbol{\mu}_j \exp(-U/kT)\,d\Omega\right]\left[\int \exp(-U/kT)\,d\Omega\right]^{-1}, \qquad (3.3)$$

where $U$ is the total interaction energy of the system, for a given configuration, and $d\Omega$ is an element of configuration space. In the case which we are considering, $U$ takes the simple form

---

* Mean square *fluctuation* since $\langle \mathbf{M}\rangle^{\circ}_{\text{vac}}=\langle \mathbf{M}\rangle^{\circ}=0$.

$$U=\sum_{i>j}^{N} w_{ij}, \qquad (3.4)$$

where, in Pople's notation,

$$w_{ij}=\epsilon_{\alpha\beta}^{(ij)}\mu_{i\alpha}\mu_{j\beta}. \qquad (3.5)$$

$\epsilon_{\alpha\beta}^{(ij)}$ is the dipole interaction tensor,

$$\epsilon_{\alpha\beta}^{(ij)}=R_{ij}^{-5}[R_{ij}^{2}\delta_{\alpha\beta}-3R_{ij\alpha}R_{ij\beta}]. \qquad (3.6)$$

$\mathbf{R}_{ij}$ is the radius vector joining lattice site $i$ to lattice site $j$. Greek suffixes denote Cartesian components of a tensor and may take the values 1, 2 or 3; repeated suffixes are to be summed.

After expansion of the exponentials in the integrals in (3.3) and using the facts that

$$\int \boldsymbol{\mu}_i \cdot \boldsymbol{\mu}_j \, d\Omega=0 \quad \text{for} \quad i\neq j,$$

and

$$\int . \boldsymbol{\mu}_i \cdot \boldsymbol{\mu}_j . w_{kl} \, d\Omega=0 \quad \text{for all } i,\ j,\ k, \text{ and } l,$$

we obtain

$$\langle \mathbf{M}^2 \rangle_{\text{vac}}^{\circ}=N\mu^2+N\left[\int \sum_{j(\neq i)}^{N} \sum_{k}^{N} . \boldsymbol{\mu}_i \cdot \boldsymbol{\mu}_j w_{ik} w_{jk} \, d\Omega\right]\left[k^2T^2\int d\Omega\right]^{-1}$$

$$+\text{terms involving } (1/T)^3 \text{ and higher powers.} \qquad (3.7)$$

Note that only finite sums are involved in (3.7), in contrast to Pople's calculation, and therefore the order of summation is immaterial. Integration of (3.7) over $\Omega$ yields

$$\langle \mathbf{M}^2 \rangle_{\text{vac}}^{\circ}=N\mu^2+(1/27)[N\mu^2/k^2T^2]\sum_{j(\neq i)}^{N}\sum_{k}^{N}\epsilon_{\alpha\beta}^{(ik)}\epsilon_{\alpha\beta}^{(jk)}, \qquad (3.8)$$

where

$$\epsilon_{\alpha\beta}^{(ik)}\epsilon_{\alpha\beta}^{(jk)}=3R_{ik}^{-5}R_{jk}^{-5}[3(\mathbf{R}_{ik} . \mathbf{R}_{jk})^2-R_{ik}^{2}R_{jk}^{2}]. \qquad (3.9)$$

Equation (3.8) may be written

$$\langle \mathbf{M}^2 \rangle_{\text{vac}}^{\circ}=N\mu^2+(1/27)[N\mu^6/k^2T^2]\left[\sum_{j}^{N}\sum_{k}^{N}\epsilon_{\alpha\beta}^{(ik)}\epsilon_{\alpha\beta}^{(jk)}-\sum_{k}^{N}\epsilon_{\alpha\beta}^{(ik)}\epsilon_{\alpha\beta}^{(jk)}\right]. \qquad (3.10)$$

But because the lattice is assumed to have tetrahedral symmetry and because the specimen is spherical in shape,

$$\epsilon_{\alpha\beta}^{(ik)}\sum_{j}^{N}\epsilon_{\alpha\beta}^{(jk)}=0 \qquad (3.11)$$

and so (3.10) becomes

$$\langle \mathbf{M}^2 \rangle_{\text{vac}}^{\circ}=N\mu^2-(2/9)[N\mu^6/k^2T^2]\sum_{k(\neq i)}^{N} R_{ik}^{-6}. \qquad (3.12)$$

If the substitution $\psi=[4\pi N\mu^2/3vkT]$ is made, (2.4) becomes, in conjunction with (3.12),

$$3[(\epsilon-1)/(\epsilon+2)]=\psi-B\psi^3 \qquad (3.13)$$

where

$$B=2(v/4\pi N)^2 \sum_{k(\neq i)}^{N} R_{ik}^{-6} \quad . \quad . \quad . \quad . \quad . \quad . \quad (3.14)$$

is a number depending on the type of lattice. For the simple, body-centred, and face-centred cubic lattices $B$ has the values 0·10642, 0·09196 and 0·09154, respectively, for large $N$ (Pople 1953). Equation (3.13) is in agreement with the result obtained by Van Vleck (1937)* and Rosenberg and Lax (1953). Equation (3.13) may also be written in the form

$$(\epsilon-1)=\psi\left[1+\frac{\psi}{3}+\frac{\psi^2}{9}-B\psi^2+\dots\right]. \quad . \quad . \quad . \quad (3.15)$$

## § 4. EVALUATION OF $\langle \mathbf{M}^2 \rangle^\circ$

The evaluation of $\langle \mathbf{M}^2 \rangle^\circ$ differs from that of $\langle \mathbf{M}^2 \rangle^\circ_{\text{vac}}$ because one has to include in the potential energy term of the Boltzmann integral the interaction energy of the sphere with its surroundings. This energy of interaction, $W$, will be computed by considering the surroundings of the sphere on a macroscopic basis. It will be assumed, as Fröhlich (1949) has done, that $W$ and $\mathbf{M}$ are related in the following manner,

$$W=-(\tfrac{1}{2})\mathbf{M}^2[4\pi/3v][2(\epsilon-1)/(2\epsilon+1)]=-\rho\mathbf{M}^2. \quad . \quad . \quad (4.1)$$

Equation (4.1) may be derived on the assumption that $\mathbf{M}$ may be treated as a point dipole situated at the centre of the spherical region. This last assumption does not give rise to any error in the terms of the expansion for $(\epsilon-1)$ evaluated here. Further, the use of averaged quantities in the expression for $W$ may be justified. Proofs of these statements will, it is hoped, be given elsewhere.

Thus, for the problem in hand, $U$ is given by

$$U=W+\sum_{i>j}^{N} w_{ij}. \quad . \quad . \quad . \quad . \quad . \quad . \quad . \quad (4.2)$$

Pople (1953) attempted to evaluate $\langle \mathbf{M}^2 \rangle^\circ$, but used an incorrect expression for $U$. The value of $U$ given by (4.2) contains, besides the sum $\sum_{i>j}^{N} w_{ij}$, which in this calculation is *finite*, the factor $W$, which was omitted in Pople's work.

From (4.2) we have

$$\langle \mathbf{M}^2 \rangle^\circ = N\left[\int \sum_{j}^{N} \cdot \boldsymbol{\mu}_i \cdot \boldsymbol{\mu}_j \exp\left\{-(W+\sum_{i>j}^{N} w_{ij})/kT\right\} d\Omega\right] \times \left[\int \exp\left\{-(W+\sum_{i>j}^{N} w_{ij})/kT\right\} d\Omega\right]^{-1}. \quad . \quad . \quad (4.3)$$

A slight digression must be made here to consider the temperature dependence of $\rho$ (see eqn. (4.1)), because we are only interested in those terms of the expansion of $\langle \mathbf{M}^2 \rangle^\circ$ which do not involve powers of $(1/T)$

---

* The expansion given by Van Vleck (1940) for $(\epsilon-1)$ appears to contain a misprint. Equation (3.15) may be derived directly from the result given in his earlier paper (1937).

greater than the second. Clearly, the leading term in (4.3) will be $N\mu^2$, and so (2.5) must be of the form

$$[(\epsilon-1)(2\epsilon+1)/3\epsilon]=\psi[1+\lambda(1/T)+\sigma(1/T)^2+\ldots]; \quad . \quad . \quad (4.4)$$

by suitable manipulation of (4.4) it may be shown that

$$\rho=\psi[1+\text{terms involving powers of }(1/T)]. \quad . \quad . \quad (4.5)$$

A calculation, similar to that given in § 3, yields the result

$$\langle \mathbf{M}^2\rangle^\circ=N\mu^2+(2/9)[N^2\mu^4/kT][4\pi/3v]\psi-B\psi^3. \quad . \quad . \quad (4.6)$$

And so we obtain

$$[(\epsilon-1)(2\epsilon+1)/3\epsilon]=[\psi+(2/9)\psi^3-B\psi^3+\ldots]. \quad . \quad . \quad (4.7)$$

Equation (4.7) may also be written,

$$(\epsilon-1)=\psi\left[1+\frac{\psi}{3}+\frac{\psi^2}{9}-B\psi^2+\ldots\right]. \quad . \quad . \quad . \quad (4.8)$$

This result is the same as (3.15) which, as previously stated, is in agreement with Van Vleck (1937) and Rosenberg and Lax (1953). The expression derived, by Pople for $\langle \mathbf{M}^2\rangle^\circ$ is in fact equal to $\langle \mathbf{M}^2\rangle^\circ_{\text{vac}}$. Replacing $\langle \mathbf{M}^2\rangle^\circ$ by $\langle \mathbf{M}^2\rangle^\circ_{\text{vac}}$ in (2.5) gives Pople's expression for $(\epsilon-1)$.

## § 5. DISCUSSION

In correspondence Pople has raised certain objections to the method of calculation employed in this paper. He states that the relation

$$\langle \boldsymbol{\mu}_i\cdot\boldsymbol{\mu}_j\rangle^\circ_{\text{vac}}=\left[\int\cdot\boldsymbol{\mu}_i\cdot\boldsymbol{\mu}_j\exp(-U/kT)\,d\Omega\right]\left[\exp(-U/kT)\,d\Omega\right]^{-1} \quad . \quad . \quad . \quad (3.3a)$$

is strictly valid only when $N$, the number of dipoles, is very large and that (3.3) will be valid only if both lattice site $i$ and lattice site $j$ are surrounded by a very large number of dipoles. He considers that one should write

$$\langle \boldsymbol{\mu}_i\cdot\boldsymbol{\mu}_j\rangle^\circ_{\text{vac}}=\left[\int\cdot\boldsymbol{\mu}_i\cdot\boldsymbol{\mu}_j\exp(-U/kT)\,d\Omega\right]\left[\int\exp(-U/kT)\,d\Omega\right]^{-1}+X \quad . \quad . \quad . \quad (5.1)$$

where $X\to 0$ as $N\to\infty$, and that it must be proved that $NX$ is negligible in the present calculation, where $N$, although large, is finite.

It would seem that the following discussion overcomes these objections. For a system of $n$ particles whose total energy, $E$, is constant, and where the number of particles with energy $\epsilon_i$ is $n_i$, the probability $P$ of finding the system in a particular state is given by

$$P=(n\,!)(n_1\,!\;n_2\,!\;n_3\,!\;\ldots\;n_i\,!\;\ldots)^{-1}\,.\,\text{const.} \quad . \quad . \quad (5.2)$$

for Maxwell–Boltzmann statistics. In the usual way (Tolman 1938) one finds that the most probable value of $n_i$ is given by

$$n_i=\exp(-\alpha-\beta\epsilon_i), \quad . \quad . \quad . \quad . \quad . \quad . \quad (5.3)$$

where $\alpha$ and $\beta$ are constants, on the assumption that

$$\log n_i ! = n_i \log n_i - n_i. \qquad (5.4)$$

Equation (5.4) will only be a valid approximation when $n_i$ is very large. However, one may use a better approximation than (5.4) for $\log n_i !$, namely

$$\log n_i ! = n_i \log n_i - n_i + (\tfrac{1}{2}) \log 2\pi n_i. \qquad (5.5)$$

To this approximation one finds that the most probable value of $n_i$ becomes

$$n_i = \exp(-\alpha - \beta\epsilon_i) \exp[-(\zeta-\alpha)-(\eta-\beta)\epsilon_i - \xi/n_i], \qquad (5.6)$$

where $\zeta$, $\eta$ and $\xi$ are constants. In the limit of large $n_i$,

$$\zeta \to \alpha, \; \eta \to \beta \text{ and } \xi/n_i \to 0.$$

Equations (5.3) and (5.4) may be rewritten in the following manner:

$$n_i = \exp(-\alpha - \beta\epsilon_i) = f_0 \qquad (5.7)$$

$$n_i = f_0 \exp[-(\zeta-\alpha)-(\eta-\beta)\epsilon_i - \xi/n_i] = f. \qquad (5.8)$$

The error term, $X$, in (5.1) referred to by Pople, corresponds to

$$f_0\{\exp[-(\zeta-\alpha)-(\eta-\beta)\epsilon_i - \xi/n_i] - 1\}.$$

Pople's objection may be stated thus: in the calculation of $\langle \boldsymbol{\mu}_i \cdot \boldsymbol{\mu}_j \rangle^{\circ}_{\text{vac}}$ (§ 3), $f_0$ has been used to determine the distribution function, and the factor (eqn. (5.8))

$$\exp[-(\zeta-\alpha)-(\eta-\beta)\epsilon_i - \xi/n_i]$$

has been assumed to be equal to unity. However, if the error in setting this factor equal to unity were appreciable we would then expect that the quantity obtained for $\langle \boldsymbol{\mu}_i \cdot \boldsymbol{\mu}_j \rangle^{\circ}_{\text{vac}}$ would depend upon the value of $N$, the total number of particles of the system. It will be seen that, in the expansion obtained for $\langle \boldsymbol{\mu}_i \cdot \boldsymbol{\mu}_j \rangle^{\circ}_{\text{vac}}$, the only term which is affected by the magnitude of $N$ is that involving the summation $\sum\limits_{k(\neq i)}^{N} R_{ik}^{-6}$. It is of course necessary that $N$ should be sufficiently large so that this sum should approach its limiting value. $\sum\limits_{k(\neq i)}^{N} R_{ik}^{-6}$ will not have exactly the same value at every lattice point, but, because of the rapid convergence, the value of the summation will be very nearly equal for all lattice sites except those near the surface of the specimen. The error arising from the assumption that $\sum\limits_{k(\neq i)}^{N} R_{ik}^{-6}$ is the same for all lattice sites of the specimen may be made vanishingly small by taking $N$ sufficiently large.

By similar reasoning it would seem that Pople's second objection can also be answered. It will be seen in § 3 that $\langle \boldsymbol{\mu}_i \cdot \boldsymbol{\mu}_j \rangle^{\circ}_{\text{vac}}$ only depends upon $R_{ij}$, that is on the relative positions of $\boldsymbol{\mu}_i$ and $\boldsymbol{\mu}_j$, and not on their positions relative to the surface of the specimen. This result arises from the symmetry of the lattice and the symmetry of the shape of the specimen.

The fact that the expansion for $(\epsilon-1)$ does not depend upon $N$ implies that the dielectric constant of a macroscopic body does not depend on its volume. Further, the fact that $\langle \boldsymbol{\mu}_i \cdot \boldsymbol{\mu}_j \rangle^{\circ}_{\text{vac}}$ depends only on the relative positions of $\boldsymbol{\mu}_i$ and $\boldsymbol{\mu}_j$ and is very nearly the same for all $i$ and $j$ means that the body may be considered as homogeneous from a macroscopic point of view. In their paper, Rosenberg and Lax (1953) have shown that the factors in the expansion for $(\epsilon-1)$ which depend upon shape cancel out explicitly.

Therefore it would seem that (3.3) is valid for macroscopic bodies.

## § 6. CONCLUSIONS

It is concluded that Pople's attempt to calculate $\langle \mathbf{M}^2 \rangle^{\circ}$ was unsuccessful, and that the result he obtained was in fact equal to $\langle \mathbf{M}^2 \rangle^{\circ}_{\text{vac}}$. He ignored the fact that the relation (2.5) (eqn. (1.2) in Pople's paper) was obtained on the basis that the surroundings of the sphere are to be treated as a continuum of dielectric constant $\epsilon$.

The relation

$$[(\epsilon-1)(2\epsilon+1)/3\epsilon]=\psi[1+(2/9)\psi^2-B\psi^2+\ldots] \qquad . \quad . \quad (4.7)$$

to the approximation considered in this paper, differs from Onsager's relation,

$$[(\epsilon-1)(2\epsilon+1)/3\epsilon]=\psi \qquad . \quad . \quad . \quad . \quad . \quad . \quad . \quad (6.1)$$

(Onsager 1936) by the terms $[(2/9)\psi^2-B\psi^2]$.

Kirkwood (1939) has developed a theory of the dielectric constant which yields the formula

$$[(\epsilon-1)(2\epsilon+1)/3\epsilon]=g\psi \qquad . \quad . \quad . \quad . \quad . \quad . \quad . \quad (6.2)$$

where $g$, known as the correlation parameter, is a factor which takes into account the effect of short-range non-dipolar forces. Kirkwood expressed the opinion that $g$ would be equal to unity for pure dipole–dipole interaction. But, although only dipole–dipole interaction has been considered in this paper, one finds that

$$g=[1+(2/9)\psi^2-B\psi^2+\ldots]. \quad . \quad . \quad . \quad . \quad . \quad . \quad . \quad (6.3)$$

Thus $g$ may differ from unity even in the absence of non-dipolar short-range interaction. Attention has already been drawn to this point (Frenkel 1946), nevertheless it seems desirable to emphasize the fact that $g$ does depend upon dipole–dipole interaction.

Finally, it must be stated that the conditions necessary for the convergence of (3.15) are not known, but presumably the expansion will hold for sufficiently small values of $\psi$.

## ACKNOWLEDGMENT

The author wishes to thank Dr. P. N. Daykin for his helpful criticism of an earlier draft of this paper.

## REFERENCES

FRENKEL, J., 1946, *Kinetic Theory of Liquids* (Oxford : Clarendon Press).
FRÖHLICH, H., 1949, *Theory of Dielectrics* (Oxford : Clarendon Press).
KIRKWOOD, J. G., 1939, *J. Chem. Phys.*, **7,** 911.
ONSAGER, L., 1936, *J. Amer. Chem. Soc.*, **58,** 1486.
POPLE, J., 1953, *Phil. Mag.*, **44,** 1276.
ROSENBERG, R. and LAX, M., 1953, *J. Chem. Phys.*, **21,** 424.
TOLMAN, R. C., 1938, *Statistical Mechanics* (Oxford : Clarendon Press).
VAN VLECK, J. H., 1937, *J. Chem. Phys.*, **5,** 320, 556 ; 1940, *Ann. New York Acad. Sci.*, **40,** 293.

# CIII. *Electron Transport in Copper and Dilute Alloys at Low Temperature*

## *III : Solid Solutions of Iron in Copper*

By W. B. Pearson
Division of Physics, National Research Council, Ottawa*

[Received March 12, 1955]

## Abstract

Systematic measurements of thermoelectric force and electrical resistivity of dilute alloys of iron in copper have been made at close intervals of temperature between 4·2°K and ∼ 50°K. These show that iron gives rise to particularly large anomalous thermoelectric effects and minima in the resistance when dissolved in copper. The anomalous resistive component calculated by methods described in this paper does not follow an exponential or power law dependence on temperature, but, within certain limits, follows an empirical law dependent on a characteristic temperature. Taken at its face value this would suggest that the resistance minimum, in this case at least, is the result of some transition phenomenon.

The size of the resistance minimum in these alloys is notable ; for instance, the anomalous increase in resistivity between 27° and 4·2°K in an alloy containing 0·044 atomic % Fe is equal to the thermal scattering component found in pure copper at about 50°K.

## § 1. Introduction

It has been known for some time (Borelius, Keesom, Johansson, Linde 1930, 1932) and confirmed recently by us that as little as 0·004 atomic % Fe in solid solution profoundly modifies the thermoelectric power of copper at low temperatures. We have also found that this quantity of iron modifies the electrical resistivity of copper at low temperatures, giving rise to a resistance minimum of considerable size. It was, therefore, of interest to continue our work on the electrical properties of dilute copper alloys (MacDonald 1952, MacDonald and Pearson 1952, 1953, 1954 a, 1955 a, b—I and II of the present series, Pearson 1954, 1955) by examining in more detail the behaviour of very dilute alloys of iron in copper.

The equilibrium solid solubility of iron in copper decreases very rapidly with temperature, being ∼ 0·6% by weight at 800°C, 0·1% at 600°C and negligibly small at room temperature (Bauer and Hansen 1934). In order to avoid the possibility of effects due to coherently precipitated iron (Reekie, Hutchison and Hetherington 1953) we have examined only alloys which appear to lie in the homogeneous solid solution range at the annealing temperature. It is, however, interesting to note that iron, lead and bismuth, all of which have a rather small solid solubility in copper, show effects on the electrical properties of copper qualitatively somewhat different to those of Ga, In, Si, Ge and Sn, where the solid solubility is much larger (greater than 5 atomic % at the annealing temperature of 530°C).

---

* Communicated by the Author.

## § 2. EXPERIMENTAL METHOD

As in earlier work we have prepared alloys from a source of copper known as 'JTH', which had the lowest residual resistance of any polycrystalline copper which we had examined. This copper contained ~0·002 % by weight Fe (*present as an oxide*), some oxygen which exceeded the solubility limit (~ 0·0015% at 500°C), and traces of Ca.

A range of alloys was prepared from a basic alloy containing ~ 6% Fe and JTH copper by melting in alumina crucibles under hydrogen which was pumped off before the alloys solidified. In this way, the oxygen present was removed and all of the added iron entered into solid solution in the copper. The alloys were cold-worked and homogenized at 1050°C to 1065°C for a few hours or more. After cold-rolling and cutting into strips 2 mm × 0·1 mm, the specimens were annealed for a minimum of 14 hours at 530°C and quenched. The electrical properties were measured by methods previously described (MacDonald 1947, MacDonald and Pearson 1953, 1954 b).

The iron content of the alloys has been determined by chemical analysis and checked by spectroscopic analysis but, as we have already pointed out elsewhere, when very small additions of specific solutes are made the most satisfactory method of determining the amount in solid solution is by measurement of the residual resistivity of the alloy.

## § 3. MEASUREMENTS OF THERMOELECTRIC FORCE AND ELECTRICAL RESISTIVITY

The absolute thermoelectric power ($S=dE/dT$) of pure copper is very small up to 10°K after which it grows with *positive* sign. We find that even the smallest additions of iron (~ 0·002 wt. %) make the absolute thermoelectric power *negative*, increasing in magnitude very rapidly with temperature at first, becoming constant in the region of 20°K and at high temperatures decreasing again slowly in magnitude. This agrees with the findings of Borelius *et al.* (1932), although at 15°K, say, where $S$ is relatively constant for a given alloy and thermal scattering is still small, our values of $S_{15^\circ\mathrm{K}}$ are a little larger. Figure 1 shows how $S_{15^\circ\mathrm{K}}$ increases to a maximum at 0·05 to 0·07 atomic % Fe and then decreases again slowly. As the residual resistance of alloys increases linearly with added iron content up to ~ 0·05 at. % Fe (fig. 2), the flattening-off of the $S_{15^\circ\mathrm{K}}$ versus $r_{\mathrm{res}}$ curve before this concentration cannot be the result of precipitation from solid solution in our alloys annealed at 530°c, and *a fortiori* it cannot be the case with the alloys investigated by Borelius *et al.* which were quenched from 800°c.

Fig. 1

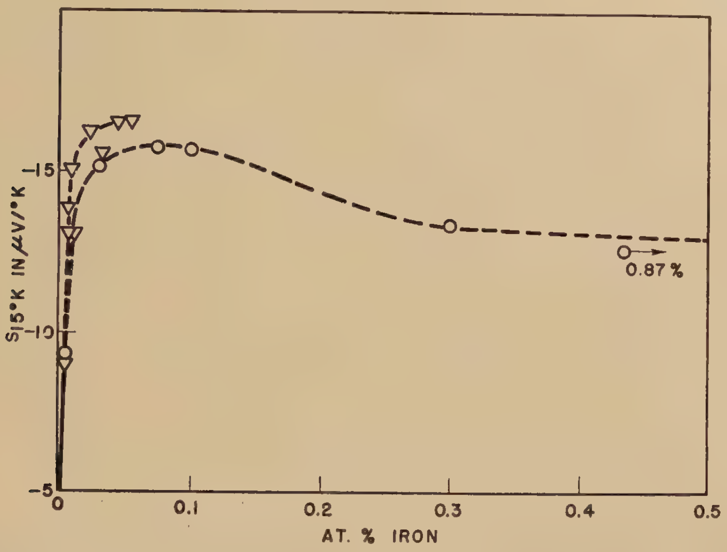

Variation of absolute thermoelectric power at 15°K with iron content of dilute Cu–Fe alloys.
▽ present work ; alloys quenched from 530°C.
○ Borelius *et al.* (1932) ; alloys quenched from 800°c.

Figure 2 shows the variation of residual resistance with analysed iron content of the alloys. The analyses of these very dilute alloys are uncertain to ±20%. We find that the increase of residual resistivity of copper per atomic % of Fe dissolved in solid solution is ~ $10{\cdot}4\times10^{-6}$ ohm cm which compares with the value of $9{\cdot}3\times10^{-6}$ ohm cm obtained by

Fig. 2

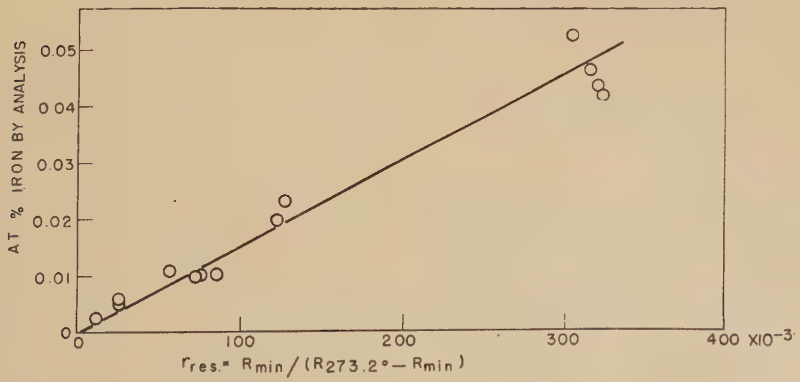

Variation of residual resistance, $r_{res}$, with analysed iron content of alloys. The analyses are reliable generally to ±20%.

Linde (1932) from measurements of the resistivity of alloys down to 78°K. Iron, therefore, has a scattering cross section of $1{\cdot}8 \times 10^{-15}$ cm$^2$ in copper, which, it should be noticed, is a rather large scattering cross section.

Fig. 3

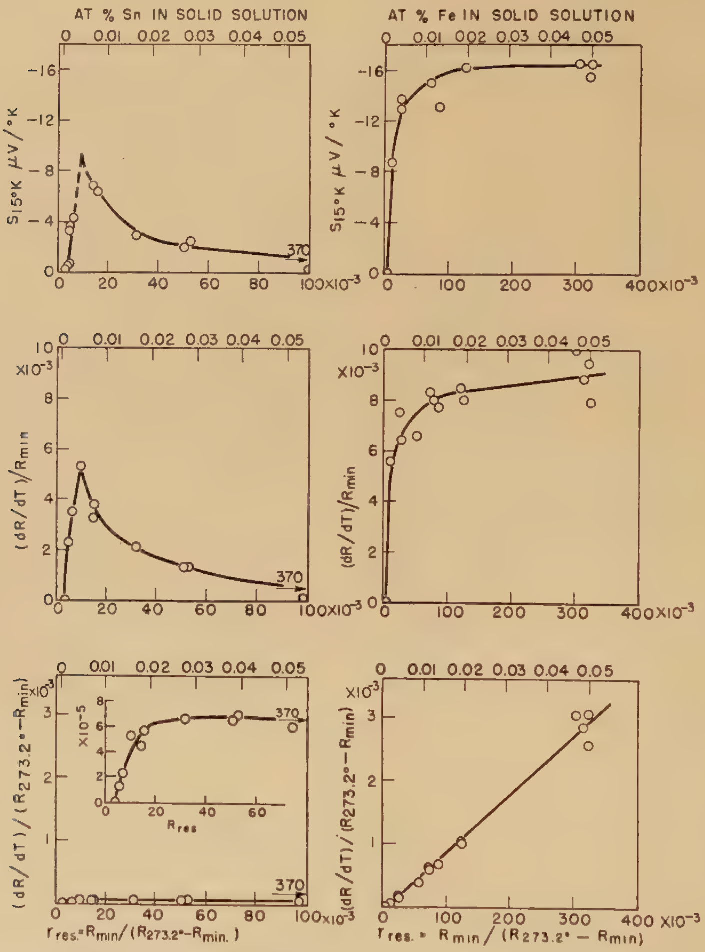

Comparison of the behaviour of dilute Cu–Sn and Cu–Fe alloys.

*Top :* Variation with residual resistance of absolute thermoelectric power at 15°K.

*Middle :* Variation with residual resistance of relative rate of resistance increase below the resistance minimum.

*Bottom :* Variation with residual resistance of the ‘ absolute ’ rate of resistance increase below the resistance minimum.

We have taken the slope, $dR/dT$, somewhat above 4°K, where it is relatively constant, as a measure of the rate of increase. This parameter may also be regarded as a measure of the ‘ size ’ of the resistance minimum.

The size of the resistance minimum found in these alloys is particularly notable. White (1955) has examined the resistivity of the alloy shown in fig. 5 (Cu+0·044 atomic % Fe) between 4·2 and ~ 0·1°K. Combining these measurements with ours, we find that the anomalous increase in resistivity between $T_{\min}$ and 0·1°K is greater than 16% of the resistivity of the alloy at $T_{\min}$.

In order to compare the behaviour of iron as solute in copper with that, say, of tin, we show in fig. 3 the absolute thermoelectric power at 15°K, the relative value of the resistance minimum and the 'absolute' size of the resistance minimum as functions of the residual resistance (solute concentration) of the alloy.* The absence of the sharp cusp such as is found at 0·005 to 0·01 wt. % solute for alloys of Sn, Ge, In and Ga in copper is notable. The data shown in fig. 3 were obtained from measurements of thermoelectric force and resistivity of the alloys continuously between 4·2 and ~ 50°K.

## § 4. Discussion

In considering the resistance minimum in these alloys, our best approach seems to be to separate the total resistivity into four parts, such that $r_{\text{total}}=r_T+r_P+r_C+r_A$, where $r_T$ is the thermal scattering which would presumably be the only resistance in an ideally pure copper sample, $r_P$ is scattering due to various physical and residual chemical imperfections, $r_C$ is the *normal* scattering due to the specific added chemical component causing the minimum and $r_A$ is the *anomalous* scattering due to this component. $r_P$ and $r_C$ are usually considered together as $r_{\text{impurity}}$ and are presumed to be temperature-independent. They may, however, be separated if $r_P$ is taken as the residual resistivity of pure copper which does not show a resistance minimum above 4°K. We may obtain $(r_P+r_C)+r_A$ for a copper–iron alloy by subtracting $r_T$ as determined from pure copper.

In figs. 4 and 5, which show the resistance–temperature variation of two Cu–Fe alloys, $r_T$ at any temperature is given by ordinates within the region ABC and values of $(r_P+r_C)+r_A$ are given by the curve DEF.†

---

* We have actually taken the resistance gradient a little above 4°K (in which region it is relatively constant for a particular alloy) as a measure of the size of the anomalous rise of resistance, as this parameter does not appear to be directly influenced by variation of the position of the minimum ($T_{\min}$).

† We assume that Matthiessen's rule would hold for copper–iron alloys in relation to pure copper if there were no *anomalous* scattering component present at low temperatures. Slight variations do in fact occur which are all in the same sense relative to pure Cu. Similar deviations have previously been reported for copper alloys by van den Berg (1938) and by Grüneisen (1933). These variations have the effect in general of making the curve for the anomalous component DE (figs. 4 and 5) apparently rise again beyond E. They will also affect the apparent position of E but we shall not consider this question further here as any changes produced generally lie within the overall accuracies attributed to the measurements.

As $(r_P+r_C)$ is postulated as temperature independent it is reasonable to assume that the anomalous component $r_A$ is given at any temperature by ordinates within the region DEG, i.e. $r_A=r_{\text{total}}-r_T-(r_P+r_C)$. Examining the temperature dependence of the anomalous component $r_A$ we find that it does *not* follow a simple exponential or power law of the type $r_A=f_1(r_C)\exp(W_A/RT)$ or $r_A=f_2(r_C)(\theta/T)^n$ (fig. 6). It does, however, appear to be represented surprisingly well by the relationship

$$r_A=f(r_C)(\theta-T)^n$$

between $\theta$ and 4·2°K* (fig. 6) where $f(r_C)$ is constant in any particular

Fig. 4

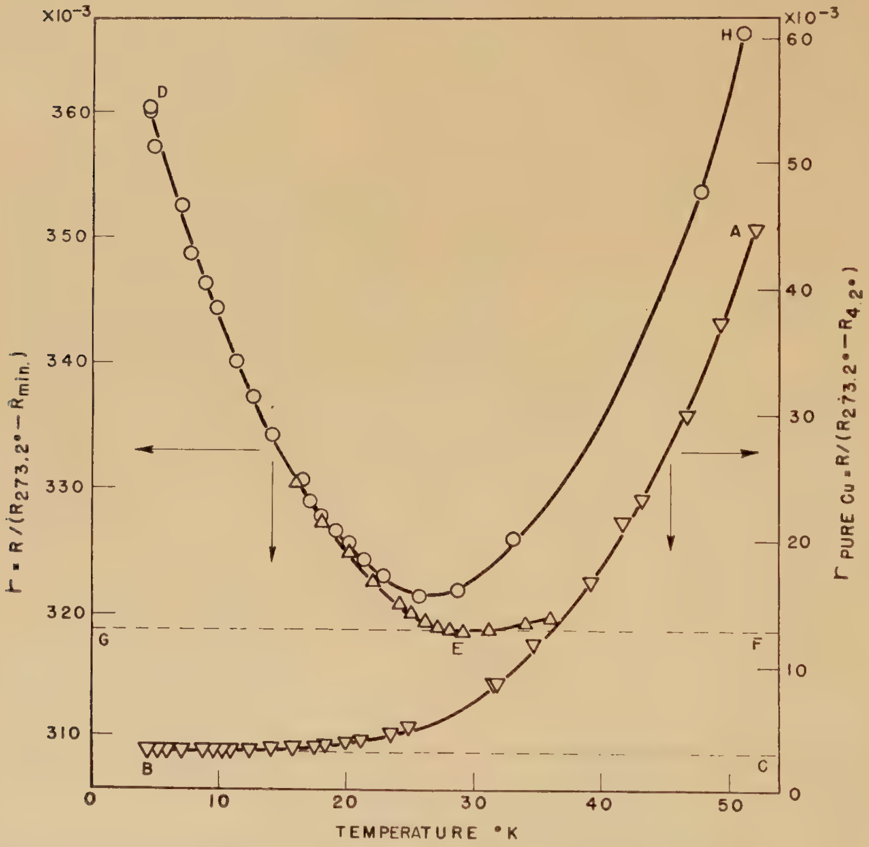

The resistance minimum in an alloy containing ∼ 0·044 atomic % Fe.

○, *Curve* DH : The resistance of this alloy as a function of temperature.

▽, *Curve* BA : The resistance of two 'pure' copper samples as a function of temperature.

△, *Curve* DE : Variation with temperature of the anomalous resistive component, as deduced in the text.

---

* It appears that this relationship is not obeyed at lower temperatures since White's (*loc. cit.*) results show a marked flattening of the resistance below ∼2°K, becoming practically temperature-independent below 1°K.

alloy, $T$ is the absolute temperature, $\theta$ is the temperature at which $r_A$ apparently becomes zero (point E, figs. 4 and 5), $\theta$ being a function of the iron content of the alloys, and $n$ is approximately 2 for alloys containing between ~ 0·005 and ~ 0·05 atomic % Fe. Although it would be of interest to proceed further by examining in some detail the variation of $\theta$ and $f(r_C)$ with $r_C$, we do not believe the accuracy of the present data justifies this step. $f(r_C)$, however, does appear to be more or less a linear function of $r_C$.

Fig. 5

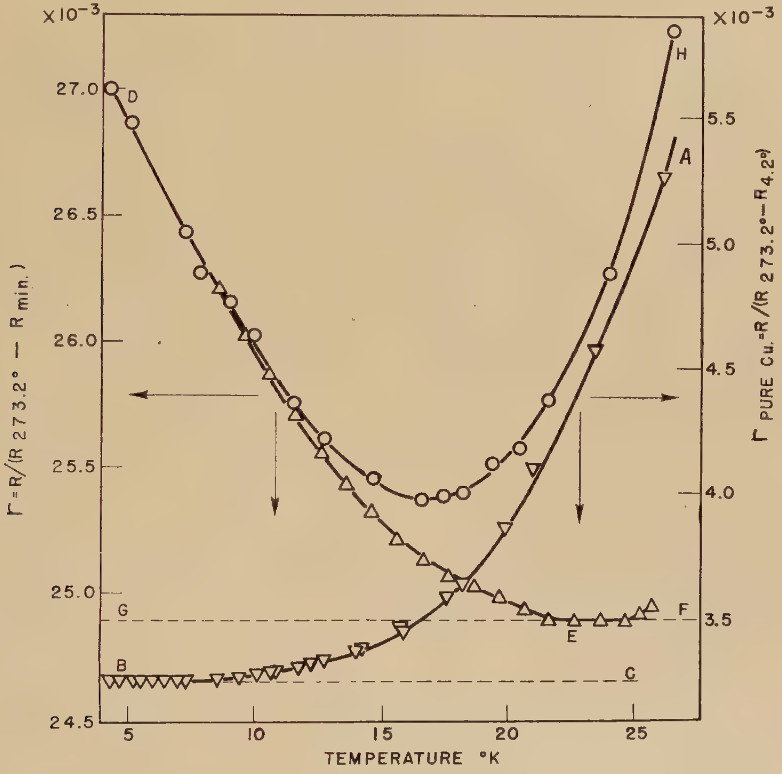

The resistance minimum in an alloy containing ~ 0·005 atomic % Fe.

| | |
|---|---|
| ⊙, *Curve* DH : | The resistance of this alloy as a function of temperature. |
| ▽, *Curve* BA : | The resistance of two ‘ pure ’ copper samples as a function of temperature. |
| △, *Curve* DE : | Variation with temperature of the anomalous resistive component, as deduced in the text. |

We can provide no specific theoretical interpretation for such a relationship at present. However, if one were to accept the expression at its face value, then we should be forced to recognize the anomalous resistance as some kind of transition phenomenon setting in at a definite temperature, $\theta$. Established phenomenon of this kind (e.g. ferromagnetism, superconductivity, the liquid helium I–II transition) always involve some cooperative behaviour in the assembly, and the ‘ phase ’ changes are generally regarded as being of the second order. The thermoelectric power, because of the Thomson relationships, should be a particularly valuable parameter for examining further the validity of such an interpretation. For a second order process one might expect a discontinuity in the derivative $dS/dT=\sigma/T$ where $\sigma$ is the Thomson heat. Experimentally, however, it is difficult to gain any precise information by this means, for $S$ is itself already the derivative of an experimentally measured

Fig. 6

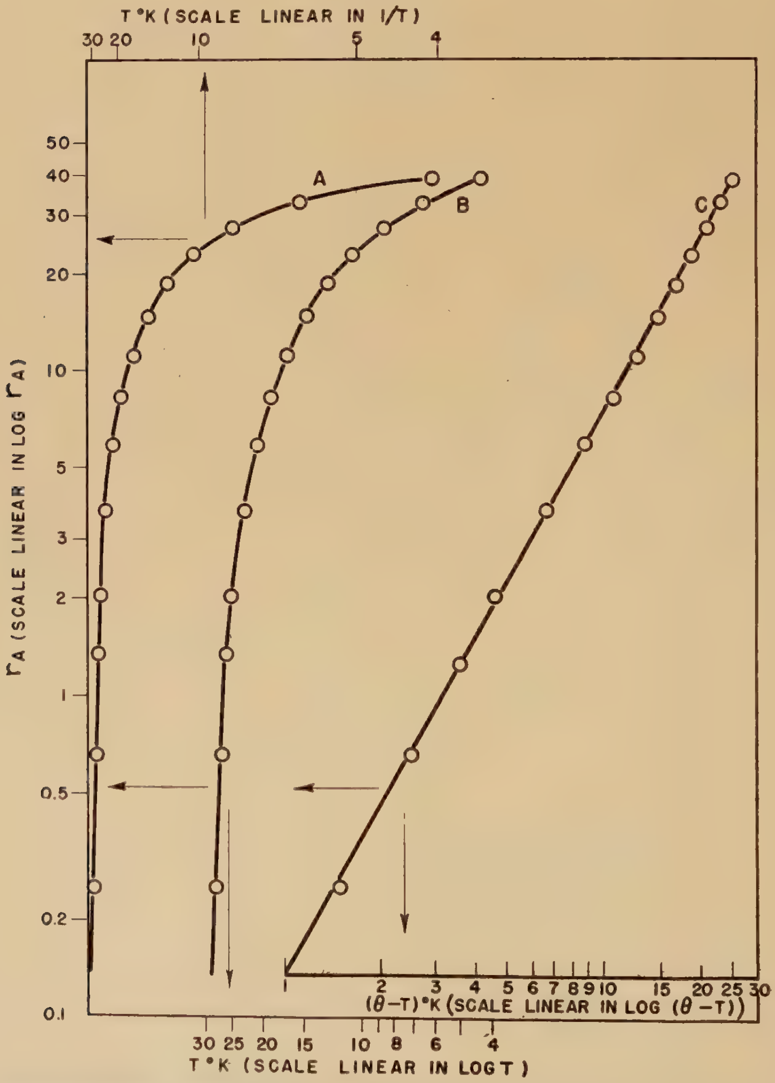

The anomalous component of resistance as a function of temperature.

A. To test the validity of $r_A=f_2(r_C)\ (\theta/T)^n$.

B. To test the validity of $r_A=f_1(r_C)\ \exp\ (W_A/RT)$.

C. Showing the validity of $r_A=f(r_C)\ (\theta-T)^n$.

e.m.f. Inspection of the values of the absolute thermoelectric power of alloys, Cu+0·004 atomic % Fe and Cu+0·03 atomic % Fe obtained from Borelius' measurements (adjusted for the *S* values of the 'silver normal' against which measurements were made) shows that a discontinuous change in $dS/dT$ would not be impossible at the characteristic temperature expected from our measurements or a few degrees below it, but it does not appear possible to analyse the available data more critically.

In conclusion let us reiterate that the anomalous scattering of very small quantities of iron in copper appears to be the most remarkable yet observed by us both as regards size and position of resistance minimum and variation of thermoelectric power. The size of the anomalous component at 4°K in the alloy containing 0·044 atomic % Fe is equal to the thermal scattering in pure copper at ∼ 48°K (fig. 4). That the effects are not due only to the presence of a transition metal which may have unfilled holes in the d shell is shown by Cu–Ni alloys in which no such striking effects are found, even though magnetic susceptibility measurements indicate that the 'holes' in the d shell of nickel are not filled in dilute alloys of nickel in copper. In addition, lead and bismuth in copper give anomalous effects which approach in magnitude those due to iron and with these solutes there can be no question of 'holes' in the d shell. We look forward with lively interest to the results of investigations of the magnetic susceptibility of these alloys at low temperatures which are being undertaken in our laboratory to throw more light on this problem.

## ACKNOWLEDGMENTS

I wish to thank Dr. D. K. C. MacDonald for his continued interest and assistance with this subject, Dr. R. G. Chambers for discussion of the manuscript, also Miss D. M. Pester who prepared and heat-treated the alloys, and Mr. W. Stockdale who carried out the spectroscopic and chemical analysis.

## REFERENCES

BAUER, O., and HANSEN, M., 1934, *Z. Metallk.*, **26,** 121.

VAN DEN BERG, G. J., 1938, *De Electrische Weerstand Van Zuivere Metalen Bij Lage En Zeer Lage Temperaturen* (Amsterdam).

BORELIUS, G., KEESOM, W. H., JOHANSSON, C. H., and LINDE, J. O., 1930, *Proc. Roy. Acad., Amsterdam*, **33** (1), 32 ; 1932, *Ibid.*, **35** (1), 25.

GRÜNEISEN, E., 1933, *Ann. Phys.* (5), **16**, 530.

LINDE, J. O., 1932, *Ann. Phys.* (5), **15,** 219.

MACDONALD, D. K. C., 1947, *J. Sci. Inst.*, **24,** 232 ; 1952, *Phys. Rev.*, **88,** 148.

MACDONALD, D. K. C., and PEARSON, W. B., 1952, *Phys. Rev.*, **88,** 149 ; 1953, *Proc. Roy. Soc.* A, **219,** 373 ; 1954 a, *Phil. Mag.*, **45,** 491 ; 1954 b, *Proc. Roy. Soc.* A, **221,** 534 ; 1955 a, *Acta Met.* (in the press) ; 1955 b, *Ibid.*

PEARSON, W. B., 1954, *Phil. Mag.*, **45,** 1087 ; 1955, *Phys. Rev.*, **97,** 666.

REEKIE, J., HUTCHISON, T. S., and HETHERINGTON, F. E., 1953, *Proc. Phys. Soc.* B, **66,** 1101.

WHITE, G. K., 1955, *Canad. J. Phys.*, **33,** 119.

# CIV. *Electron Transport in Copper and Dilute Alloys at Low Temperature*

## *IV : Resistance Minimum : Temperature of Occurrence as a Function of Solute Concentration*

By W. B. Pearson

Division of Physics, National Research Council, Ottawa*

[Received March 12, 1955]

### Abstract

We have determined the temperature ($T_{\mathrm{min}}$) at which the resistance minimum occurs for a large number of dilute copper alloys containing Fe, Ga, In, Si, Ge, Sn, Pb and Bi as solutes. Data on the absolute thermoelectric power and size of the resistance minimum of these alloys have previously been published. For alloys of Fe, Bi and Pb, we find that $(T_{\mathrm{min}})^n \propto r_C$ where $n \sim 5$ and $r_C$ is the normal residual resistivity increase due to the added solute. The variation of $T_{\mathrm{min}}$ with solute concentration is much smaller for Ga, In, Ge and Sn as solutes than for Fe, Bi and Pb.

### § 1. Introduction

The earliest investigations of $T_{\mathrm{min}}$, the position at which the resistance minimum occurs, in relation to impurity content or residual resistivity ($r_{\mathrm{res}}$) were confined to gold (cf. de Haas and van den Berg 1936, 1937, Giauque, Stout and Clark 1937, Stout and Barieau 1939, MacDonald and Templeton 1951, MacDonald 1951). More recently the scope has been broadened to include in particular copper, silver and magnesium, as parent metals (cf. Gerritsen and Linde 1951, 1952, MacDonald 1952, Herlin 1953). These investigations have shown generally that $T_{\mathrm{min}}$ is a function of the specific impurity atom and its concentration.

We have already examined the variation of the size of the resistance minimum with solute concentration in a series of dilute copper alloys with various solutes (MacDonald and Pearson 1955 a, b, Pearson 1955). In the present note, we give data on the temperature at which the resistance minimum occurs in these alloys. The methods of preparing and examining very dilute alloys of Fe, Ga, In, Si, Ge, Sn, Pb and Bi in copper have already been fully discussed. In the present work, when the minimum is of small size, it is often not possible to fix its position to better than ±1·5°K.

---

* Communicated by the Author.

## § 2. Experimental Results and Discussion

The variation in position of the resistance minimum in Cu–Fe alloys as a function of iron concentration, shown in fig. 1, is the most striking which we have found in a series of alloys. It changes from 13·5°K for 0·002 atomic % Fe to $\sim$ 28°K for 0·05 atomic % Fe in solid solution and

Fig. 1

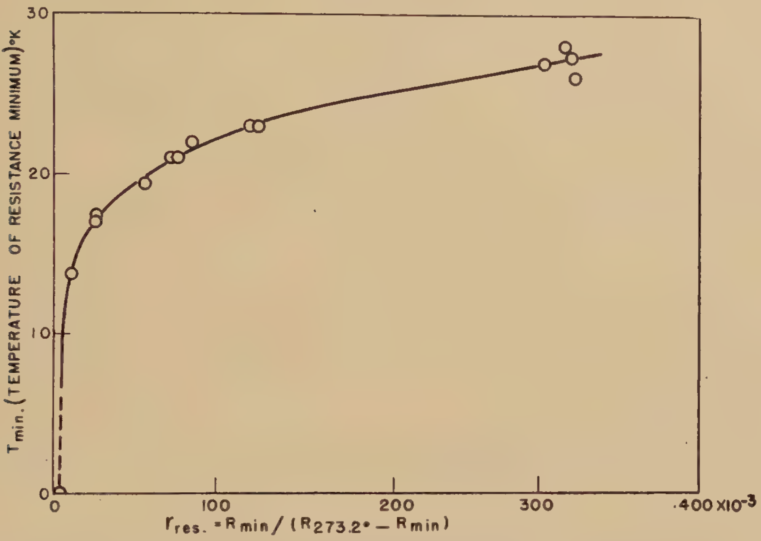

The temperature at which the resistance minimum occurs in dilute Cu–Fe alloys as a function of the residual resistance of the alloys.

Fig. 2

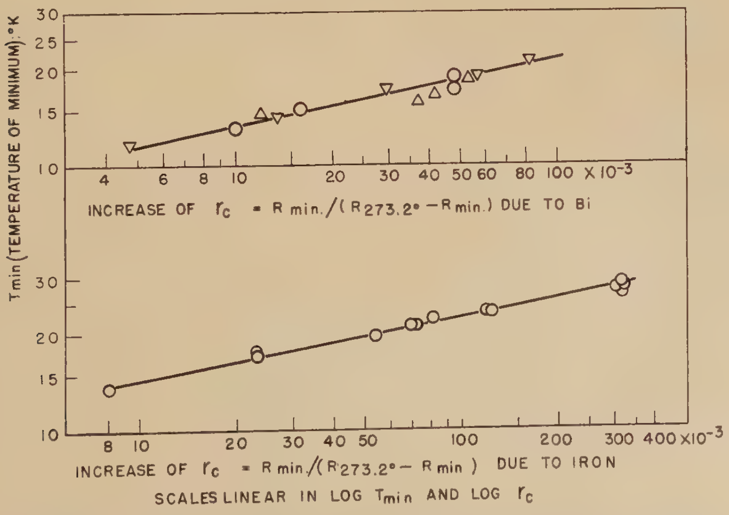

The temperature at which the resistance minimum occurs as a function of $r_C$, (the increase of residual resistance due to the 'normal' scattering caused by (1) bismuth, (2) iron in solid solution) showing $r_C \propto (T_{\min})^n$.

obeys rather exactly the law $r_C = C(T_{\min})^n$ where $n \sim 5{\cdot}2$ (fig.2) and $r_C$ is the 'normal' impurity scattering due to the component which gives rise to the resistance minimum. The behaviour of lead and bismuth as solutes is similar to that of iron (e.g. see fig. 3). In the case of bismuth we find $r_C = C(T_{\min})^n$ where $n \sim 4{\cdot}8$ (fig. 2).

Fig. 3

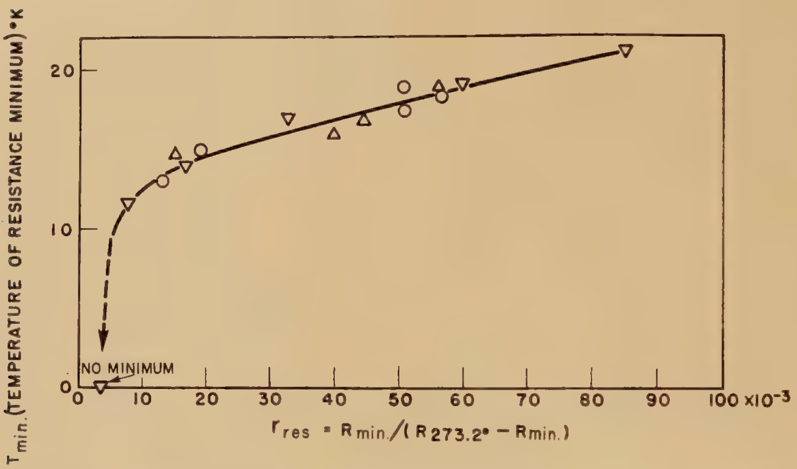

The temperature at which the resistance minimum occurs in dilute Cu–Bi alloys as a function of the residual resistance of the alloys.

In alloys having Ga, In, Ge and Sn as solutes we find that $T_{\min}$ increases rapidly from ~ 10·5°K for ~ 0·002 atomic % solute to a constant or very slowly rising value between 13° and 15°K in alloys containing up to ~ 0·5 atomic % solute. The solute concentration at which $T_{\min}$ becomes approximately constant coincides with the concentration at which the actual size of the minimum saturates.

In the more dilute alloys containing Ga, In, Ge and Sn as solutes prepared *under reducing conditions*, the small amount of iron entering solid solution (~ 0·002 wt. % present originally in the copper as an oxide) appears to control the position of the minimum which then lies generally between 13·5° and 15°K (over 90% of the measurements lie in this range).

The data shown above for alloys of iron and bismuth in copper now make it possible to examine critically a suggestion by MacDonald (1949, 1951) that it might be possible to treat the resistance minimum formally in somewhat the same way as an applied magnetic field is introduced in the theory of magneto-resistance by writing

$$r = r_T + r_0 + \frac{B^2 \, r_0^{\,2}}{r_T + r_0}$$

where $r_T$ is the resistive component due to ideal thermal scattering and $r_0$ is the resistive component due to 'normal' impurity scattering.

This led to the prediction that $r_{\min} \propto (T_{\min})^n$ where $n$ has the value $\sim 5$, given by the expression for thermal scattering of ideally pure copper ($r = A \cdot T^n$). We see that this prediction is rather well obeyed for bismuth and iron as solutes in copper where $r_{\min}$ changes by a factor of 30. The model, however, does not lead quantitatively to the observed temperature dependence of the anomalous increase of resistivity of these alloys below $T_{\min}$ (cf. the previous paper) and it does not appear possible to attain agreement by any simple modification of the above expression.

## ACKNOWLEDGMENTS

I wish to thank Dr. D. K. C. MacDonald for helpful discussions and suggestions, and Miss L. T. Towle for assistance with calculations.

## REFERENCES

GERRITSEN, A. W., and LINDE, J. O., 1951, *Physica*, **17**, 573 ; 1952, *Ibid.*, **18**, 877.

GIAUQUE, W. F., STOUT, J. W., and CLARKE, C. W., 1937, *Phys. Rev.*, **51**, 1108.

DE HAAS, W. J., and VAN DEN BERG, G. J., 1936, *Physica*, **3**, 440 ; 1937, *Ibid.*, **4**, 683.

HERLIN, M. A., 1953, *Third International Conference on Low Temperature Physics and Chemistry* (Houston), p. 49.

MACDONALD, D. K. C., 1949, *Anomalous Electrical and Thermal Properties of Substances at Low Temperatures, Thesis* (Oxford : University Press) ; 1951, *Proc. Internat. Conf. Low Temp. Physics* (Oxford), p. 58 ; 1952, *Phys. Rev.*, **88**, 148.

MACDONALD, D. K. C., and PEARSON, W. B., 1955 a, *Acta Met.* (in the press) ; 1955 b, *Ibid.*

MACDONALD, D. K. C., and TEMPLETON, I. M., 1951, *Phil. Mag.*, **42**, 432.

PEARSON, W. B., 1955, *Phil. Mag.*, **46**, 911.

STOUT, J. W., and BARIEAU, R. E., 1939, *J. Amer. Chem. Soc.*, **61**, 238.

# CV. CORRESPONDENCE

## *Gamma-rays from Inelastic Scattering of D–T Neutrons from Carbon* 12 *and Oxygen* 16

By L. E. Beghian, D. Hicks and B. Milman
Clarendon Laboratory, Oxford

[Received July 1, 1955]

The gamma-ray spectra resulting from the inelastic scattering of D–T neutrons by $^{12}$C and $^{16}$O have been investigated. Simple spectra consisting of strong ground state transitions from the 4·43 Mev level in $^{12}$C (Thompson and Risser 1954, Battat and Graves 1955) and the 6·13 Mev level in $^{16}$O (Thompson and Risser 1954) have been reported previously. More complex spectra were however obtained by Scherrer *et al.* (1953). The aim of the present investigation was to search for weaker radiations from the higher excited states and in particular to establish the energy of the second excited state of $^{12}$C which has an astrophysical interest (Öpic 1952, Hoyle 1954). In fact, for both $^{12}$C and $^{16}$O, only a single line was observed and an upper limit is placed on the intensity of radiation from the second excited state of $^{12}$C.

### Experimental Arrangement

14 Mev neutrons were produced by bombarding a zirconium tritide target with 300 kev deuterons. Since gamma radiation is produced by the neutrons in the target assembly itself this was constructed as lightly as possible. It consisted of a thin aluminium can supported by a glass tube and cooling was provided by an air blast.

A large scale ring geometry was employed in these experiments. The gamma radiation was observed in a direction perpendicular to the motion of the primary neutrons entering the scatterer thus eliminating the effects of Doppler shift (see fig. 1).

The gamma radiation was detected with a 1 in. cube NaI(Tl) crystal and a Dumont 6292 photomultiplier, and the resulting pulse height distribution was analysed with a 25 channel kicksorter.

### Experimental Technique

Pulse height distributions were recorded with and without the scatterer and were normalized to the same total neutron emission from the source. From these measurements the difference $D$ was calculated.

$$D=\left\{\begin{array}{l}\text{(Counts per channel with scatterer)} - \\ \text{(Counts per channel without scatterer)}\end{array}\right\}$$

Fig. 1

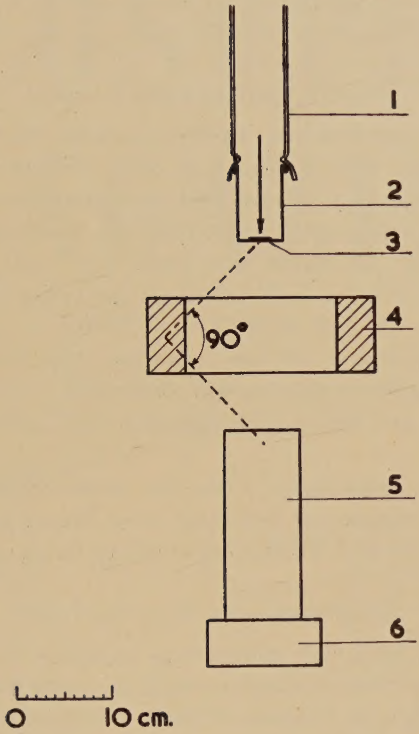

Experimental arrangement.

(1) Glass tube. (2) Aluminium can. (3) Zirconium tritide target. (4) Scattering annulus. (5) Photomultiplier case. (6) Preamplifier.

Fig. 2

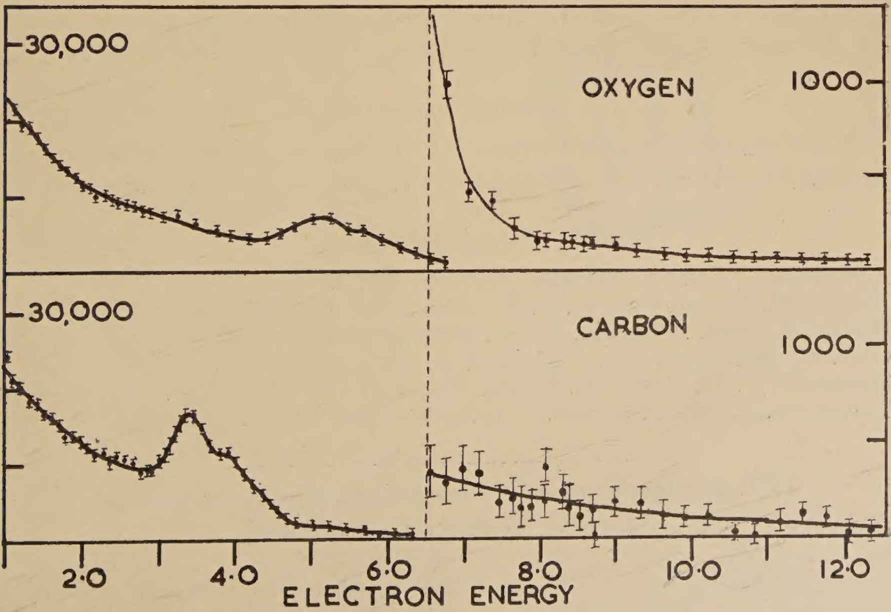

Gamma-ray spectra from oxygen and carbon.

A plot of the difference $D$ will give the spectrum of the gamma-rays associated with inelastic scattering superimposed on a general background due to the scattered neutrons.

### MEASUREMENTS WITH CARBON

A solid graphite annullus was used as scatterer in the $^{12}C$ experiment. The spectrum shows the presence of only one gamma-ray of energy 4·4 MeV, leading to the typical one and two quantum escape pair peaks. This corresponds to the excitation of the first level in $^{12}C$ (see Ajzenberg and Lauritsen 1955). A search was made for a gamma-ray of 3·1 MeV which would result from a 7·65 MeV level decaying by cascade through the 4·43 MeV state.

However in this region of the spectrum the background is rising sharply, and a weak line might escape detection. An upper limit to the intensity of the 3·1 MeV line can be placed at 10% of the intensity of the 4·4 MeV gamma-ray.

These results are consistent with the measurement of Battat and Graves (1955). However no evidence was found for the presence of gamma-rays of 2·8, 6·0 and 7·0 MeV reported by Scherrer, Theus and Faust (1953).

### MEASUREMENTS WITH OXYGEN

Water, contained in a thin aluminium annullus was used as the $^{16}O$ scatterer. The spectrum obtained reveals the presence of a strong line of 6·1 MeV energy. This is consistent with a transition from the second level in $^{16}O$ (6·13 MeV) to the ground state (see Ajzenberg and Lauritsen 1955). No gamma transition is to be expected from the first level (6·05 MeV) to the ground state since this is a forbidden transition. However the resolution is not sufficient to exclude the possibility of some contribution to the observed peak by radiation from 6·9 and 7·1 MeV states which may also be excited. No evidence was found for gamma-rays of 3·0, 3·8, and 5·2 MeV reported by Scherrer, Theus and Faust (1953).

### ACKNOWLEDGMENTS

We would like to thank Professor H. Halban for helpful discussions and Professor Lord Cherwell for extending to us the facilities of this laboratory.

### REFERENCES

AJZENBERG, F., and LAURITSEN, T., 1955, *Rev. Mod. Phys.*, **27**, 77.
BATTAT, M. E., and GRAVES, E. R., 1955, *Phys. Rev.*, **97**, 1266.
HOYLE, F., 1954, *Astrophys. Journ.*, Supple. 1, 121.
ÖPIC, F., 1952, *Proc. Roy. Irish Acad.* A, **54**, 49.
SCHERRER, V. E., THEUS, R. B., and FAUST, W. R., 1953, *Phys. Rev.*, **91**, 1476.
THOMPSON, L. C., and RISSER, J. R., 1954, *Phys. Rev.*, **94**, 941.

---

[*The Editors do not hold themselves responsible for the views expressed by their correspondents.*]